Polarization Analysis of X-Ray Resonant Exchange Scattering and X-Ray Magnetic Kerr Effect

Koichi Mori

Doctor of Philosophy

Department of Synchrotron Radiation Science
School of Mathematical and Physical Science
The Graduate University for Advanced Studies

1991

CONTENT

Introduction

As a first experiment of magnetic X-ray diffraction, two superlattice X-ray diffraction peaks of a NiO single crystal using CuKα radiation were observed by de Bergevin and Brunel in 1972.[1] Because those intensities were 4×10^{-8} smaller than normal Bragg peak intensities, its application to measuring magnetic properties has long been practically impossible as far as the radiation from conventional X-ray tubes is used. Since the advent of synchrotron radiation(SR) in the X-ray region, many sciences have been highly developed owing to its excellent properties such as its high intensity, high brilliance, continuous wavelength distribution and controllable polarization, and scattering amplitude dependence on polarization states. Magnetic scattering has become also a useful experimental tool for study of magnetism.

In 1985, X-ray resonance magnetic scattering(XRMS) at the Ni K-absorption edge was first observed by Namikawa et al.[2] This phenomenon originates from an interference between an electric transition and a magnetic transition. In 1988, X-ray resonant exchange scattering(XRES) was first observed for Ho single crystal by Gibbs et al.[3] This phenomenon originates from electric-multipole-transitions which take place from the spin-orbit interacting initial state to the exchange splitting intermediate state. The intensity of XRES is larger by an order of $mc^2/h\nu$ than that of the XRMS. However, the contribution of XRES is smaller than that of the XRMS at K or L_1-absorption edge. Both scattering give the information on the spin polarization in the intermediate state. X-ray magnetic resonant scattering is applicable to the investigation of spin polarized unoccupied density-of-states.

One way to observe such magnetic scattering is to apply the magnetic field on the sample to measure its "flipping ratio".[2,4] However, to alternate the magnetic field in ferromagnetic materials having high coercive force is undesirable because of its technical difficulty in switching the high magnetic field. Moreover, it is uncertain whether the alternation of the magnetic field makes symmetric behavior because of its magneto striction and the magnetic after effect.

On the other hand, rotation of the major axis in the reflected light is called " magnetic Kerr effect ". Valence electrons are excited by the linearly polarized incident light. The amount of the rotation of the major axis is proportional to the difference of the joint-density-of-state between up spin and down spin.

In the wavelength region longer than ultraviolet, this rotation phenomenon has been widely applied to study of the magnetism. In the resonance magnetic scattering, the phase of the scattering amplitude differs by $\pi/2$ from that of the normal electric one. Polarization of the incident X rays is changed from linear to elliptical after scattering. The major axis is rotated from the plane of polarization of the electric scattering. This behavior can be observed in an X-ray magnetic Faraday effect[5] and " X-ray magnetic Kerr effect ".[6] Change of the polarization state due to the magnetic scattering can be separated from that of the electric one by measuring the orientation of the major axis of the scattered X rays under fixed magnetic field instead of measuring the flipping ratio.

In order to realize such a measurement we have made a polarization analyzing system which can measure the " X-ray magnetic Kerr rotation ". A purpose of this work is to observe the X-ray

magnetic Kerr rotation, which is also applicable to studies magnetism. In the following will be described a theory of X-ray magnetic Kerr effect, instrumentation of the system and experiments on X-ray magnetic Kerr rotation. A brief discussion will be further given.

Theory of the X-ray Magnetic Kerr Effect[6]

(1) X-ray scattering amplitudes

Total X-ray scattering amplitude f can be written in the following way [15]

$$f = f_0 + f_a^{(r)} + if_a^{(i)} + if_m + f_{rm}^{(r)} + if_{rm}^{(i)} \quad , \qquad (1)$$

where

f_0 ··normal electric scattering amplitude(the electric form factor),

$f_a^{(r)}$ ··real part of the anomalous scattering amplitude,

$f_a^{(i)}$ ··imaginary part of the anomalous scattering amplitude,

f_m ··normal magnetic scattering amplitude(the magnetic form factor),

$f_{rm}^{(r)}$ ··real part of the resonant magnetic scattering amplitude, and

$f_{rm}^{(i)}$ ··imaginary part of the resonant magnetic scattering amplitude.

The dependence on the polarization states of f_a and f_0 is described as follows,[7]

$$f_0 = f_0(\mathbf{e}_f \cdot \mathbf{e}_0) \quad , \qquad (2)$$

and $$f_a = f_1(\mathbf{e}_f \cdot \mathbf{e}_0) - if_2(\mathbf{e}_f \times \mathbf{e}_0) \cdot \mathbf{z}_J \quad , \qquad (3)$$

where $\mathbf{e}_0$ and $\mathbf{e}_f$ are the polarization unit vector of the incident and scattered X rays, respectively. The real f_0 and the complex of f_1 and f_2 are independent on the polarization state of the X rays. $\mathbf{z}_J$ is the unit vector of the magnetic moment. The definition of polarization vector used in this paper is shown in Fig.1. The unit vectors $\mathbf{k}_0$ and $\mathbf{k}_f$ are the incident and the scattered wavevectors, respectively. $\mathbf{e}_{(0,f)\perp}$ and $\mathbf{e}_{(0,f)\parallel}$

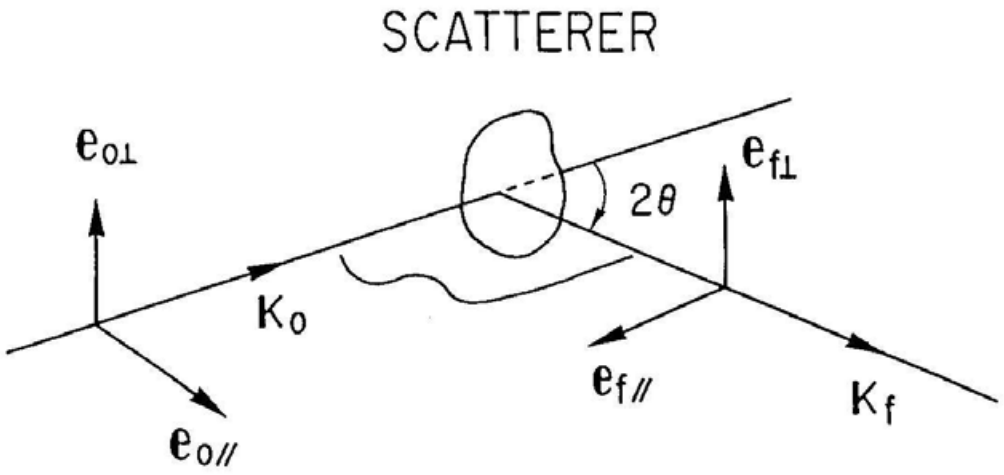

Fig.1 $\mathbf{k}_0$ and $\mathbf{k}_f$ are the incident and scattered wavevectors. $\mathbf{e}_{(0,f)\perp}$ and $\mathbf{e}_{(0,f)\parallel}$ are the unit vector components of the polarization perpendicular and parallel to the diffraction plane of incidence which is formed by $\mathbf{k}_0$ and $\mathbf{k}_f$.

are the unit vector components of the polarization perpendicular and parallel to the plane of incidence(spanned by $\mathbf{k}_0$ and $\mathbf{k}_f$), respectively. In equation (3), only electric dipole transitions are considered.

It is convenient to express the polarization dependence of the anomalous scattering as 2×2 matrix expression as follows,

$$f_a = f_1 \begin{pmatrix} \mathbf{e}_{f\perp} \cdot \mathbf{e}_{0\perp} & \mathbf{e}_{f\parallel} \cdot \mathbf{e}_{0\perp} \\ \mathbf{e}_{f\perp} \cdot \mathbf{e}_{0\parallel} & \mathbf{e}_{f\parallel} \cdot \mathbf{e}_{0\parallel} \end{pmatrix} - if_2 \begin{pmatrix} (\mathbf{e}_{f\perp} \times \mathbf{e}_{0\perp}) \cdot \mathbf{z}_J & (\mathbf{e}_{f\parallel} \times \mathbf{e}_{0\perp}) \cdot \mathbf{z}_J \\ (\mathbf{e}_{f\perp} \times \mathbf{e}_{0\parallel}) \cdot \mathbf{z}_J & (\mathbf{e}_{f\parallel} \times \mathbf{e}_{0\parallel}) \cdot \mathbf{z}_J \end{pmatrix},$$

$$= f_1 \begin{pmatrix} 1 & 0 \\ 0 & \cos 2\theta \end{pmatrix} - if_2 \begin{pmatrix} 0 & 0 \\ 0 & \sin 2\theta \end{pmatrix}, \qquad (4)$$

where 2θ is the scattering angle at the sample crystal and the direction of the magnetic moment is normal to the plane of incidence and parallel to $(\mathbf{k}_f \times \mathbf{k}_0)$. In the first term, the diagonal element (1,1) means the transition from the polarization state $\mathbf{e}_{0\perp}$ to $\mathbf{e}_{f\perp}$, which means that the amplitude of the scattered X-ray is same as that of the incident one. The diagonal element (2,2) means the transition from the polarization state $\mathbf{e}_{0\parallel}$ to $\mathbf{e}_{f\parallel}$. The amplitude of the scattered X-ray is smaller than that of the incident one by a factor of $\cos 2\theta$. In the second term, the diagonal element (2,2) means the transition from the polarization state $\mathbf{e}_{0\parallel}$ to $\mathbf{e}_{f\parallel}$, where the amplitude of the scattered X-ray is smaller than that of the incident one by a factor of $\sin 2\theta$. In the case of the electric scattering, the second term vanishes.

(2) Rotation of the major axis

Linearly polarized light(**E**) can be resolved into right circularly polarized light($\mathbf{E}_+$) and left circularly polarized light($\mathbf{E}_-$), as follows,

$$\mathbf{E} = \mathbf{E}_+ + \mathbf{E}_- \quad ,$$

$$\mathbf{E}_+ = E_+ e^{i\phi_+}(\varepsilon_1 - i\varepsilon_2)e^{i(\mathbf{K}\cdot\mathbf{r}-\omega t)} \quad ,$$

and

$$\mathbf{E}_- = E_- e^{i\phi_-}(\varepsilon_1 + i\varepsilon_2)e^{i(\mathbf{K}\cdot\mathbf{r}-\omega t)} \quad , \qquad (5)$$

where ε_1 and ε_2 are the unit vector in the angular co-ordinates. E_+ (E_-) is an amplitude of the right circularly polarized light (left circularly polarized light) and ϕ_+ (ϕ_-) is the phases.

In the XRES at L-absorption edge, neglecting the effects of the magnetic scattering and the resonant magnetic scattering, the total X-ray scattering amplitude(1) is approximated as follows,

$$f = f_0 + f_a^{(r)} + if_a^{(i)} + if_m + f_{rm}^{(r)} + if_{rm}^{(i)} \quad ,$$

$$\cong f_0 + f_1 - if_2 \quad ,$$

$$= f_0 + f' + if'' - i\,(f_m' + if_m'') \quad ,$$

and

$$= f_0 + f' + if'' + f_m'' - if_m' \quad , \qquad (6)$$

where f' , f'' , f_m' and f_m'' are real. ($f' + if''$) correspond to the complex f_1 while ($f_m' + if_m''$) correspond to the the complex f_2. The real part f'

is related to dispersive processes and the imaginary part f″ to absorptive processes. In magnetically sensitive part, the real part f_m'' means dispersive processes and the imaginary part ($-f_m'$) means absorptive processes.

From equations (2), (3) and (6), it is seen that the vertical amplitude of the scattered X-ray is proportional to $f_0 + f' + if''$ and the horizontal amplitude of the scattered X-ray is proportional to $(f_0 + f' + if'') \cos 2\theta - i (f_m' + if_m'') \sin 2\theta$. In equation (4), in spite of the zero off-diagonal elements which means no transition from the vertical amplitude to the horizontal one or from the horizontal amplitude to the vertical one, the plane of polarization and the major axis is rotated if the incident beam is 45 degrees linearly polarized from the plane of incidence. The condition is shown in Fig.2(a) and (b).

In the electric scattering, the complex amplitude of $E_+e^{i\phi_+}$ and $E_-e^{i\phi_-}$ are expressed as follows,

$$E_+^0 = \frac{1}{2}\gamma\sqrt{\{(f_0 + f')\cos 2\theta - f''\}^2 + (f_0 + f' + f''\cos 2\theta)^2} \quad ,$$

$$\phi_+^0 = \tan^{-1}\left(\frac{f_0 + f' + f''\cos 2\theta}{(f_0 + f')\cos 2\theta - f''}\right) \quad , \qquad (7)$$

$$E_-^0 = \frac{1}{2}\gamma\sqrt{\{(f_0 + f')\cos 2\theta + f''\}^2 + (f_0 + f' - f''\cos 2\theta)^2} \quad ,$$

and

$$\phi_-^0 = \tan^{-1}\left(-\frac{f_0 + f' - f''\cos 2\theta}{(f_0 + f')\cos 2\theta + f''}\right) \quad , \qquad (8)$$

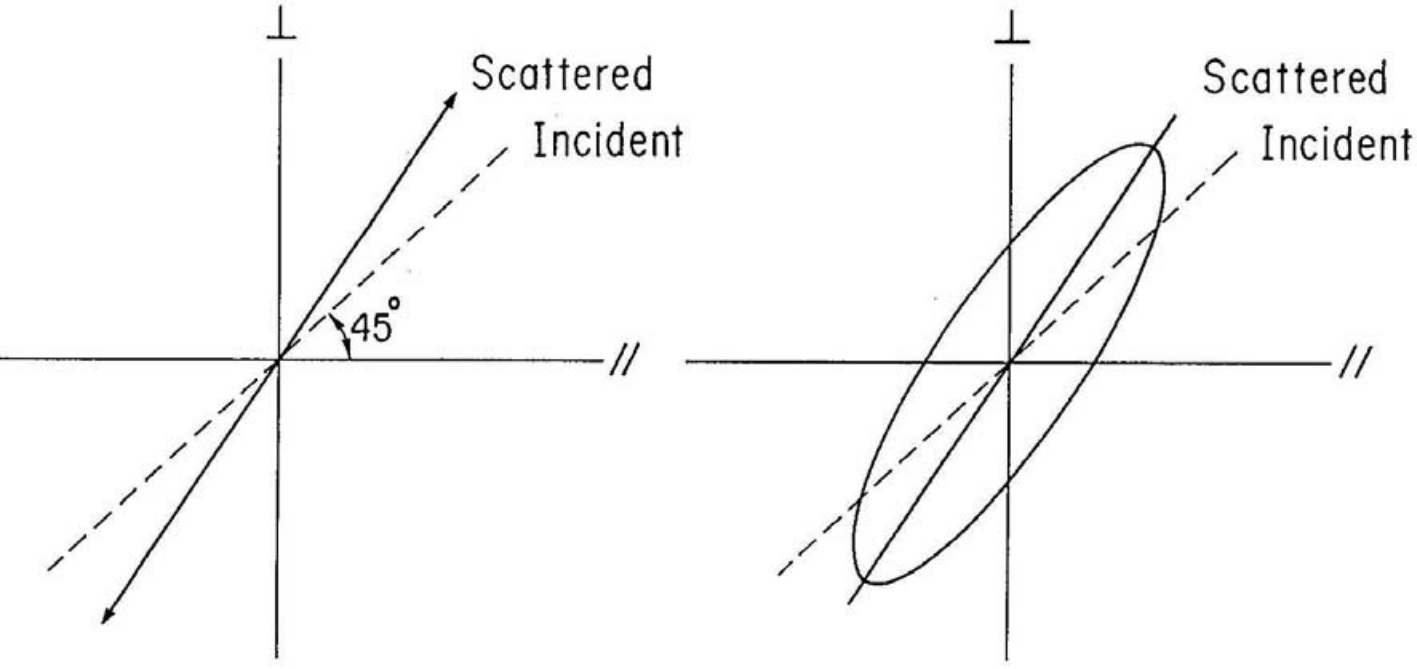

Fig.2 (a) The case of the electric scattering. The scattered X-ray is linearly polaried with the plane of the polarization rotated from 45°. (b) The case of the resonant magnetic scattering. The scattered X-ray is elliptically polaried with the major axis of the polarization ellipse rotated.

where γ is a constant, which makes a connection between E_+^0 (E_-^0) and the scattering amplitudes.

For the resonant exchange scattering, the complex amplitude of $E_+e^{i\phi_+}$ and $E_-e^{i\phi_-}$ are expressed as follows,

$$E_+^{\uparrow\downarrow}=\frac{1}{2}\gamma\sqrt{\{(f_0+f')\cos2\theta - f'' \pm f_m''\sin2\theta\}^2+(f_0+f'+f''\cos2\theta \mp f_m'\sin2\theta)^2} \ ,$$

$$\phi_+^{\uparrow\downarrow}= \tan^{-1}\left(\frac{f_0+ f' + f''\cos2\theta \mp f_m'\sin2\theta}{(f_0+ f')\cos2\theta - f'' \pm f_m''\sin2\theta}\right) \ , \qquad (9)$$

$$E_-^{\uparrow\downarrow}=\frac{1}{2}\gamma\sqrt{\{(f_0+f')\cos2\theta+f'' \pm f_m''\sin2\theta\}^2+(f_0+f'-f''\cos2\theta \pm f_m'\sin2\theta)^2} \ ,$$

and

$$\phi_-^{\uparrow\downarrow}= \tan^{-1}\left(-\frac{f_0+ f' -f''\cos2\theta \pm f_m'\sin2\theta}{(f_0+ f')\cos2\theta + f'' \pm f_m''\sin2\theta}\right) \ , \qquad (10)$$

where γ is a constant, which makes a connection between $E_+^{\uparrow\downarrow}$($E_-^{\uparrow\downarrow}$) and the scattering amplitudes. The sign + or - in the brackets corresponds to the sense of the direction of the magnetic field, either parallel($\uparrow$) or anti-parallel($\downarrow$) to ($\mathbf{k}_f \times \mathbf{k}_0$), respectively.

The rotation of the major axis for the magnetic field ($\uparrow$) is expressed as follows,

$$\Delta\alpha^{\uparrow} = \frac{1}{2}\{(\phi_+^{\uparrow} - \phi_-^{\uparrow}) - (\phi_+^{0} - \phi_-^{0})\} \ , \qquad (11)$$

The rotation of the major axis for the magnetic field (↓) is expressed as follows,

$$\Delta\alpha^{\downarrow} = \frac{1}{2}\{(\phi_{+}^{\downarrow} - \phi_{-}^{\downarrow}) - (\phi_{+}^{0} - \phi_{-}^{0})\} \quad , \tag{12}$$

We use an approximate relation $\tan^{-1}(x+h) \cong \tan^{-1}(x) + h(1/1+x^2)$ and ignore f_m'' in the denominator in equations (9) and (10). Then the rotation $\Delta\alpha^{\uparrow}$ and $\Delta\alpha^{\downarrow}$ are approximated as follows,

$$\Delta\alpha^{\uparrow} \cong 2\frac{f'' f_m'}{(f_0 + f')^2 + f''^2}\frac{\sin 2\theta}{1+\cos^2 2\theta} \quad , \tag{13}$$

$$\cong 2\frac{f''}{f_0^2} f_m' \frac{\sin 2\theta}{1+\cos^2 2\theta} \quad ,$$

$$\Delta\alpha^{\downarrow} \cong -2\frac{f''}{f_0^2} f_m' \frac{\sin 2\theta}{1+\cos^2 2\theta} \quad , \tag{14}$$

The magnitude of the rotation $|\Delta\alpha^{\uparrow}|$ and $|\Delta\alpha^{\downarrow}|$ is almost the same. The rotation of the major axis $\Delta\alpha$, which is the difference of the orientation between the magnetic field up and down, is expressed as follows,

$$\Delta\alpha = \Delta\alpha^{\uparrow} - \Delta\alpha^{\downarrow} \quad ,$$

$$\cong 4\frac{f''}{f_0^2} f_m' \frac{\sin 2\theta}{1+\cos^2 2\theta} \quad ,$$

$$\propto f'' f_m' \quad , \tag{15}$$

and also

$$f_m' \propto \frac{d\Delta\rho}{d\omega} \quad , \quad \Delta\rho = \rho(\uparrow) - \rho(\downarrow) \quad , \tag{16}$$

$$f'' \propto \rho \quad , \text{ and } \quad \rho = \rho(\uparrow) + \rho(\downarrow) \quad , \tag{17}$$

where, $\rho(\uparrow)$ means the density-of-state for the up spin, $\rho(\downarrow)$ means the density-of-state for the case down spin. Therefore, the rotation $\Delta\alpha$ is a function of the product, $\rho \times \{d(\Delta\rho)/d\omega\}$. Under the dipole approximation, the value $\{d(\Delta\rho)/d\omega\}$ is proportional to the value $\{d(Ra) / d\omega\}$, where Ra means the flipping ratio.

Method of Measurement

(1) Estimation of the polarization state of SR X rays[8]

This experiment has been performed at the beamline 15B at the Photon Factory, where the accelerating energy is 2.5GeV and the initial stored current is 350mA. The photon flux is estimated to be about 6×10^{12} photons/sec/0.1%b.w. The source size estimated is 0.39mm in the x-direction and 0.11mm in the z-direction at the energy range between 5.0keV and 10.0keV. From calculation, the SR X ray beams emitted from the bending magnet contain 96.7% linearly polarized and 3.3% non-polarized components, and 94.1% linearly polarized and 5.9% non-polarized components when the beam divergence is 7.1×10^{-6} rad (the beam size is about 0.5mm × 0.5mm) and 5.7×10^{-5} rad (the beam size is about 4mm × 4mm) off the orbital plane, respectively.

(2) Generation of 45 degrees linearly polarized X rays[9]

The SR X rays from the bending magnet are predominantly linearly polarized within the plane of the electron or positron orbit of the storage ring. The horizontally linearly polarized X-ray is changed into 45 degrees linearly polarized one by the crystal polarizer whose Bragg angle is nearly equal to 45 degrees in such a way that the ratio of the π-component to the σ-component of the electric vector is equal to one and there is no phase difference between them. The calculated ratio of the π-component to the σ–component is shown in Fig.3. The abscissa denotes the azimuthal angle of the polarizer crystal and the ordinate denotes the ratio. An approximate relation between the azimuthal angle χ (deg.) and the parameter κ is expressed as follows,

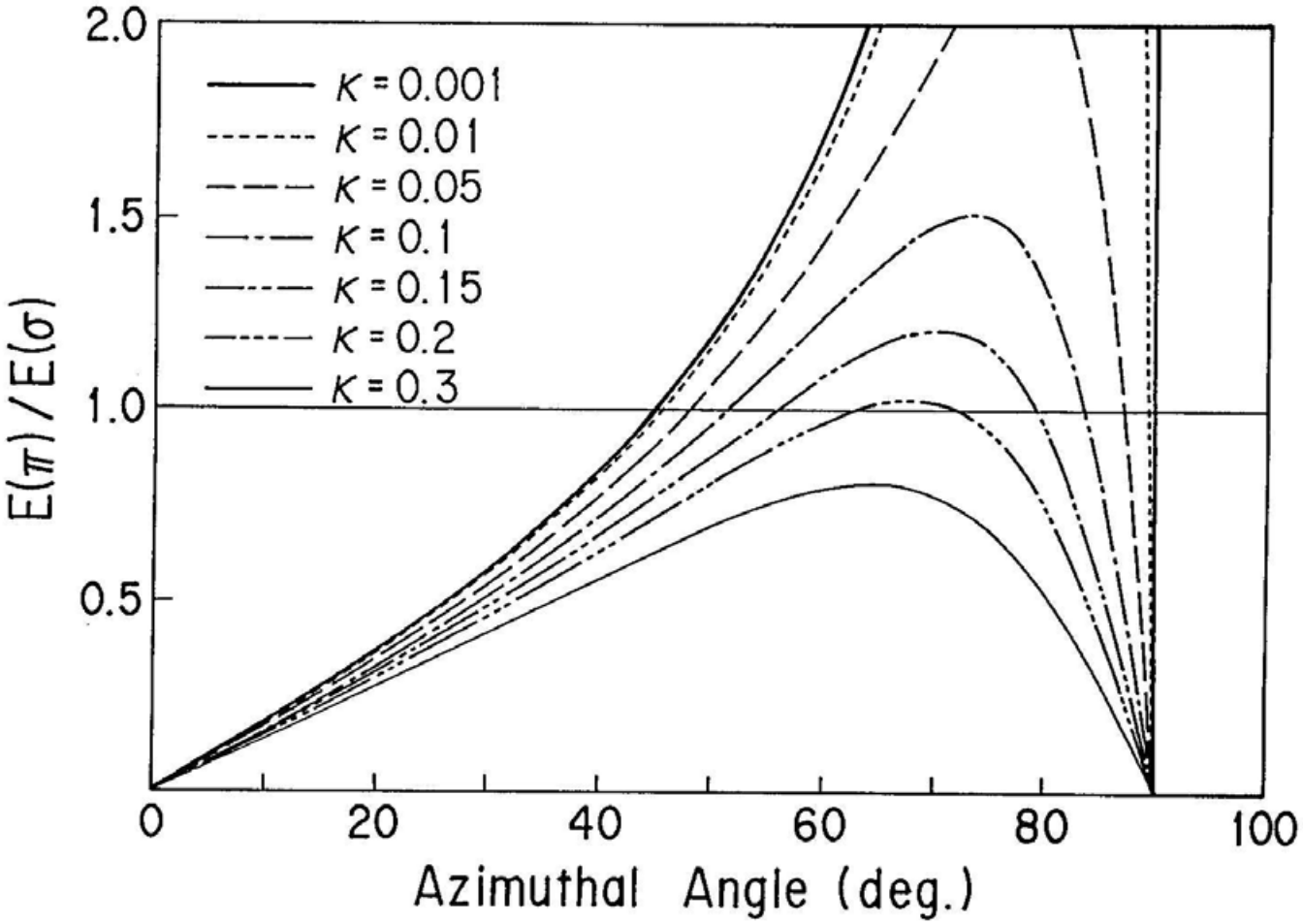

Fig.3 The calculated ratio of the π-component to the σ–component. The relation $E(\pi)/E(\sigma) = 1$ means linearly polarized X rays under the condition $\kappa \ll 1$.

$$\cos\chi = \frac{\sqrt{2}}{2}(1 - \kappa) \quad , \tag{18}$$

where $\kappa = P/(1 - P)$ and $P \lesssim \cos^2 2\theta_B$. The condition $\kappa \ll 1$ is good for generating the 45 degrees linearly polarized X rays. $2\theta_B$ is the scattering angle at the polarizer crystal.

Non-polarized component changes into linearly polarized one at the scattering. The degree of linear polarization P_L is expressed as follows[10],

$$P_L = \frac{1-\cos^2 2\theta_B}{1+\cos^2 2\theta_B} \quad . \tag{19}$$

If the scattering angle is equal to 90 degrees, the non-polarized component changes into a completely linearly polarized component after the scattering.

(3) Rotation analysis of the major axis[6,11]

A principle of polarization analysis is the same as in the polarizer. When the Bragg angle at the analyzer crystal is nearly equal to 45 degrees, it is possible to detect the intensity of σ-component (parallel to the crystal surface) of the diffracted X rays. The polarization state can be analyzed by measuring the intensity variation of the scattered X rays for various azimuthal angles, χ, of the polarizer crystal. The theoretical intensity variation is expressed with the amplitudes of the circularly polarized X rays as follows,

$$I = |\mathbf{E}_+ + \mathbf{E}_-|^2$$

$$= 4\,|\mathbf{E}_+|\,|\mathbf{E}_-|\cos^2\{\chi - (\phi_+ - \phi_-)/2\} + (|\mathbf{E}_+| - |\mathbf{E}_-|)^2 \quad , \tag{20}$$

where the azimuthal angle χ is measured from the horizontal plane.

For linearly polarized X rays, from the equations (7),(8) and (20) the intensity I observed through the polarizer is expressed as follows,

$$I = 4 \, | \mathbf{E}_+^0 | \, | \mathbf{E}_-^0 | \cos^2(\chi - \alpha) \quad , \qquad (21)$$

with

$$\alpha = (\phi_+^0 - \phi_-^0)/2 = \tan^{-1} (1/ \cos 2\theta) \quad ,$$

where 2θ is the scattering angle at the sample. The azimuthal angle which gives the maximum value of the equation (21), that comes to $\chi = \alpha$, means the orientation of the plane of polarization. This case is shown in Fig.4(a).

For elliptically polarized X rays which is produced with the magnetic scattering (resonant exchange scattering), from the equations (9),(10) and (20), the intensity $I^{\uparrow}$ and $I^{\downarrow}$ observed through the polarizer are expressed as follows,

$$I^{\uparrow} = 4 \, |\mathbf{E}_+^{\uparrow}| \, |\mathbf{E}_-^{\uparrow}| \cos^2(\chi - \alpha - \Delta\alpha^{\uparrow}) + (|\mathbf{E}_+^{\uparrow}| - |\mathbf{E}_-^{\uparrow}|)^2 \quad , (22)$$

with

$$\Delta\alpha^{\uparrow} = (\phi_+^{\uparrow} - \phi_-^{\uparrow})/2 \; - \alpha \quad ,$$

and

$$I^{\downarrow} = 4 \, |\mathbf{E}_+^{\downarrow}| \, |\mathbf{E}_-^{\downarrow}| \cos^2(\chi - \alpha - \Delta\alpha^{\downarrow}) + (|\mathbf{E}_+^{\downarrow}| - |\mathbf{E}_-^{\downarrow}|)^2 \quad , (23)$$

with

$$\Delta\alpha^{\downarrow} = (\phi_+^{\downarrow} - \phi_-^{\downarrow})/2 \; - \alpha \quad .$$

The azimuthal angle which gives the maximum value of the equations (22) or (23) means the orientation of the major axis as shown in Fig.4(b). Therefore, it is possible to observe the rotation $\Delta\alpha$ from the measurement of the equations (22) and (23).

(4) Ellipticity analysis of the scattered beam

The ellipticity ratio R is expressed by a right circularly polarized X-ray $\mathbf{E}_+$ and a left circularly polarized X-ray $\mathbf{E}_-$ as follows,

$$R = \frac{|\mathbf{E}_+| - |\mathbf{E}_-|}{|\mathbf{E}_+| + |\mathbf{E}_-|} = \sqrt{\frac{I_{min}}{I_{max}}} \quad . \tag{24}$$

This quantity is the function of (ρ , $d(\Delta\rho)/ d\omega$) through the equations (9), (10), (16) and (17).

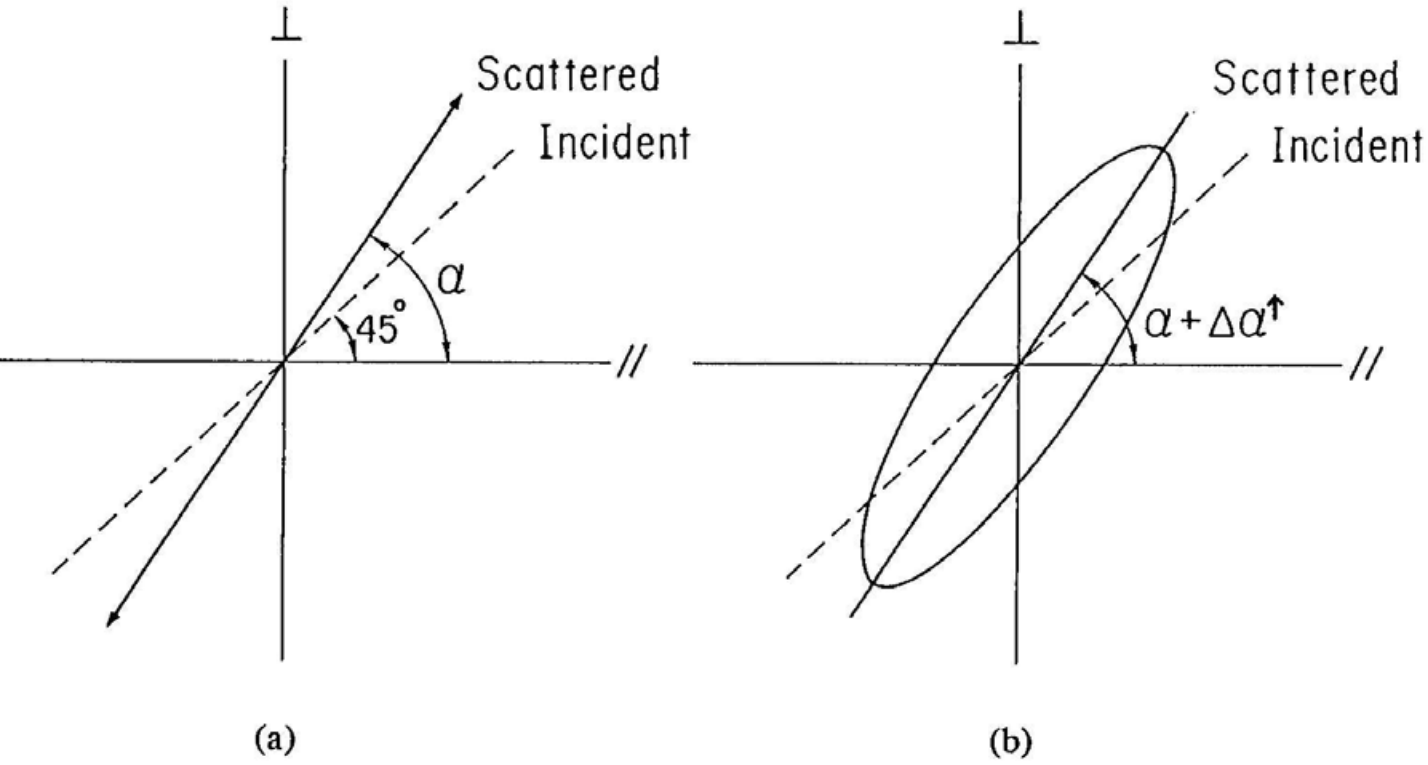

Fig.4 (a) The case of the electric scattering. The orientation of the plane of polarization is changed 45° to α { $\alpha = 1/2(\phi_+ - \phi_-)$ }. (b) The case of the magnetic scattering. When the magnetic field is parallel (antiparallel) to $(\mathbf{k}_f \times \mathbf{k}_0)$, the orientation of the major axis is changed 45° to $\alpha+\Delta\alpha^{\uparrow}$ ($\alpha+\Delta\alpha^{\downarrow}$), where $\Delta\alpha^{\uparrow}$ ($\Delta\alpha^{\downarrow}$) is defined as the rotation of the major axis from the plane of polarization of the electric scattering.

Instrumentation

(1) Outline of the polarization analyzing system

A schematic experimental arrangement illustrating the polarization analyzing system is shown in Fig.5. In order to take out the horizontally polarized component(in the x-y plane) of SR, a slit of the beamline was used. This is placed about 40m down from the source point. The beam size is adjusted by four micrometer-screws. The polarizer monochromator makes the incident SR X rays monochromatized to change the horizontal linear polarization to 45-degree linear polarization as shown in Fig.5 to the plane of incidence. The intensity of the incident beams were monitored by a nitrogen gas-filled ionization chamber after the second slit. A sample crystal is held between the magnet poles. To measure the polarization state of the scattered X-ray, an analyzer crystal was placed after the sample crystal.

The side view of the experimental apparatus, about 2m in length and about 1.5m in height, is shown in Fig.6 and Fig.7. It comprises a polarizer monochromator, a 2-axis diffractometer equipped with an electromagnet and a polarization analyzer. They have minimum number of horizontal stages to adjust each component easily.

(2) Polarizing device

The polarizing device is made from a monolithic silicon-rod which is manufactured by Shin-Etsu Handotai Co.,Ltd. in Japan.

Lot No.	3901804-501	Quantity	2,938 g
Diameter	76.00 mm	Carrier Type	N
Specifications	FZ-N-ROD		

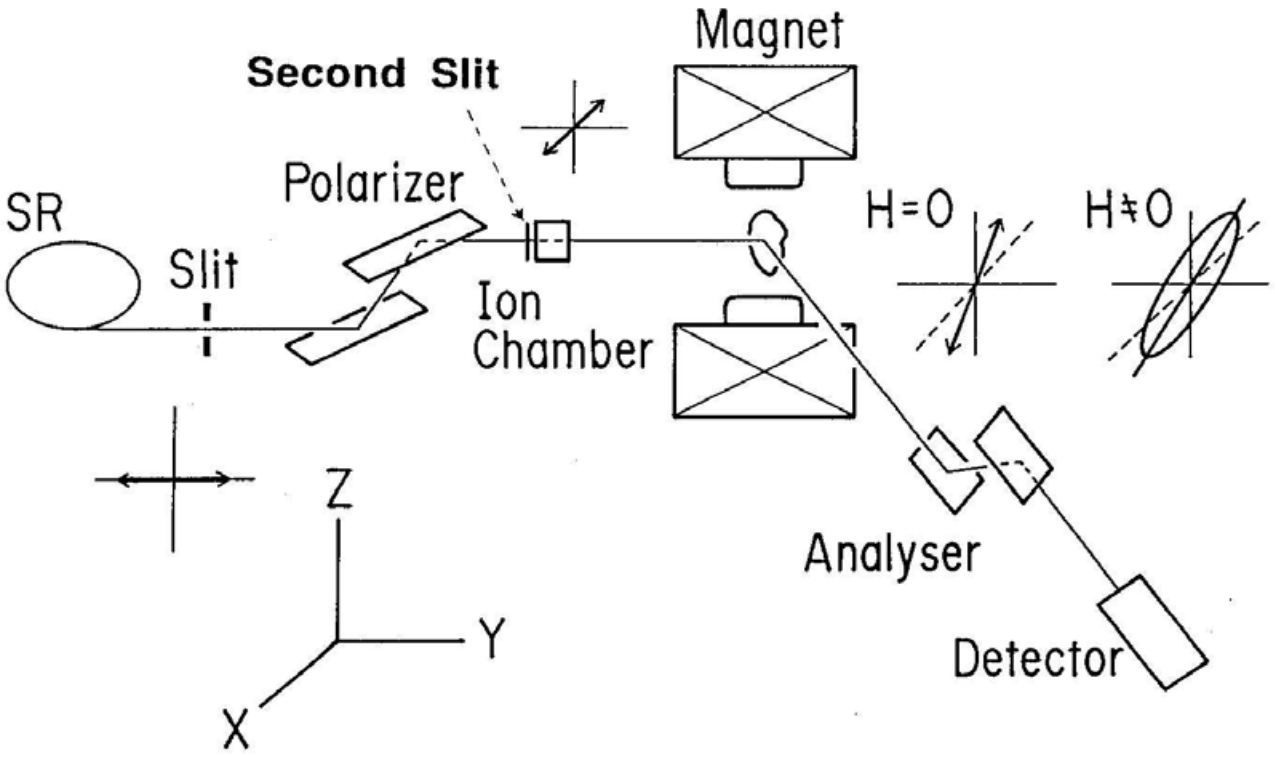

Fig.5 A schematic experimental arrangement of the polarization analyzing system. The SR X rays from the bending magnet is predominantly linearly polarized in the x-y plane of the electron orbit of the storage ring. The polarization state is changed into 45° linearly polarized X rays by the polarizer. The polarization state is measured by the analyzer placed after the sample.

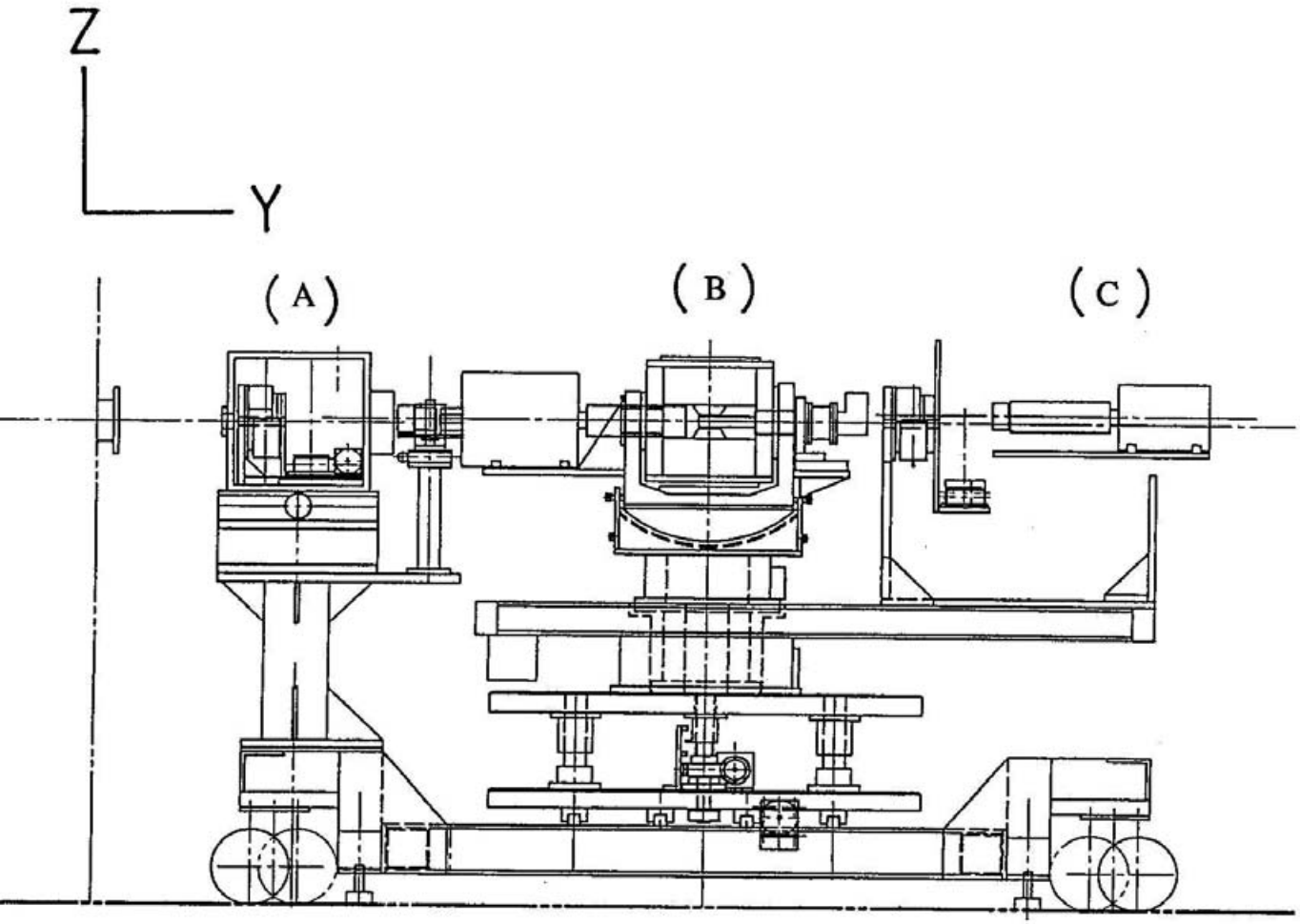

Fig.6 The side view of the experimental apparatus. (A) is a polarizer monochromator, (B) is a 2-axis diffractometer with a electromagnet and (C) is a polarization analyzer.

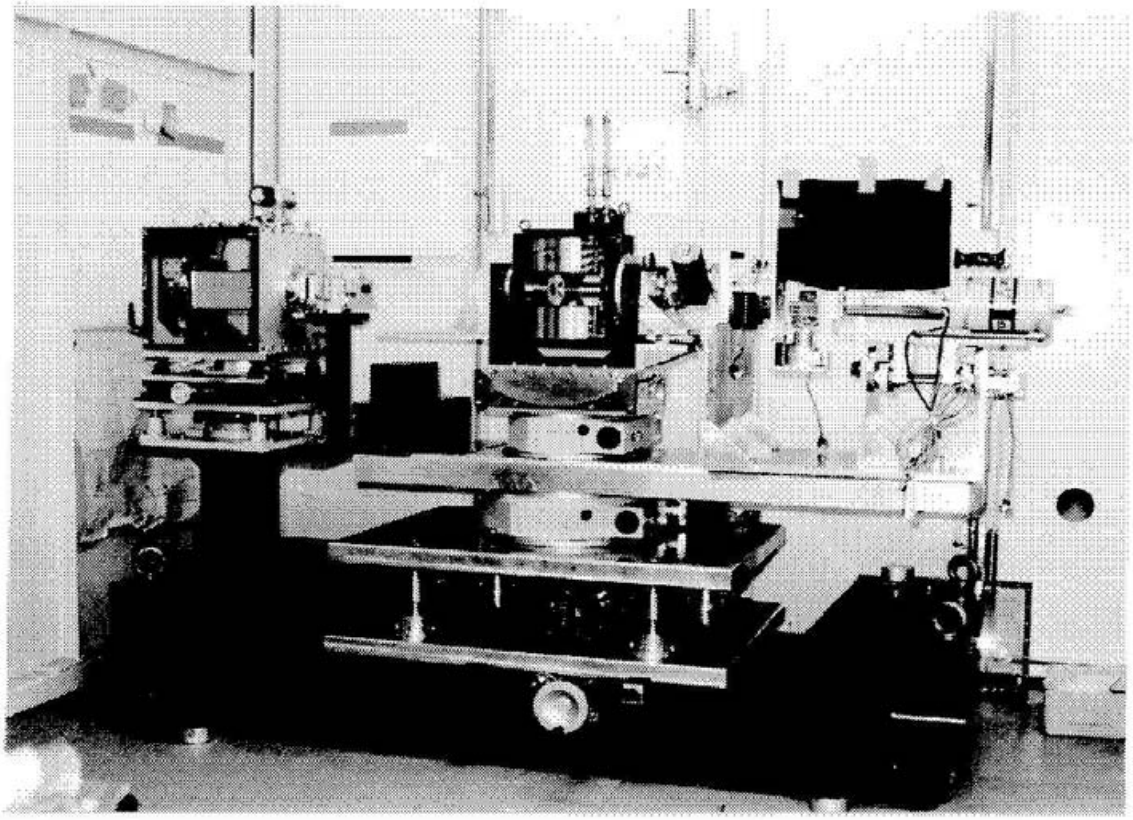

Fig.7 A photograph of the experimental apparatus.

The design of the polarizer crystal and the index of the surface is shown in Fig.8. The polarizing device is a channel-cut 422 crystal providing two consecutive Bragg reflections. The energy resolution is better than 1eV. The polarizer and analyzer was shaped by a diamond-cutter after the orientation of the reflection surfaces was searched with MoKα radiation. The whole surfaces were chemically etched by HNO_3 solution mixed with HF solution with the mixing ratio of 20:1 and soaked for 20min under 25°C. The Laue-photograph of the 110 and the 111 surfaces were detected by polaroid-films (ASA 3000), which are shown in Fig.9(a) and(b).

(3) Polarizer monochromator

The polarizer monochromator is located on a crossed goniometer (a). The goniometer (a) to define the Bragg angle of the crystal is fixed on the second goniometer (b) for driving the azimuthal angle as shown in Fig.10. The rotation axis of these goniometers meet at right angle with the precision of 20 arcseconds and intersect at the point (c) with the precision of 0.2mm. Both rotations are computer controlled by stepping motors. The angular resolution of these goniometers is 0.72 arcsec/pulse in case of a reducer gear of the ratio 1:10 while it is 0.36 arcsec/pulse in case of a reducer gear of the ratio 1:40.

The SR beam passes through the center hole of the goniometer (b) and the intersection point (c) of the both goniometers. These devices are mounted in an aluminum container the both sides of which are made of lead-containing acrylic windows to watch the inside. The equivalent lead thickness is 1.2 mm to suppress X-ray leakage. A 0.3 mm thick

(a) Polarizer crystal

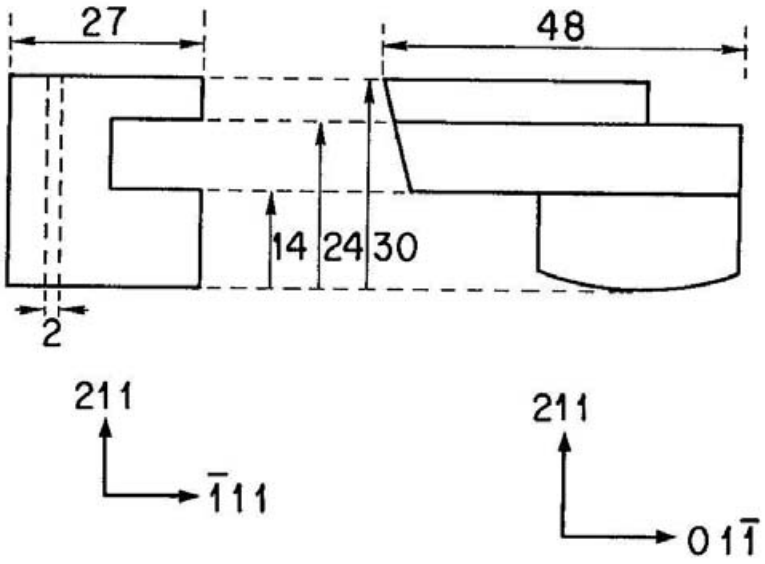

(b) Analyser crystal

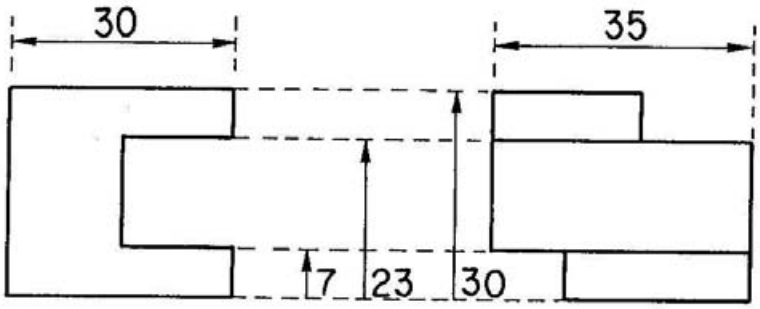

Fig.8 Design of (a) the polarizer and (b) the analyzer crystal.

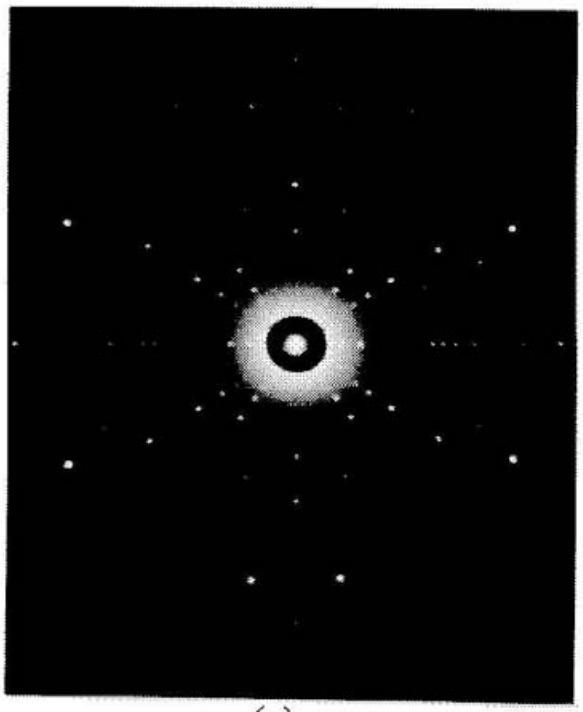

(a)

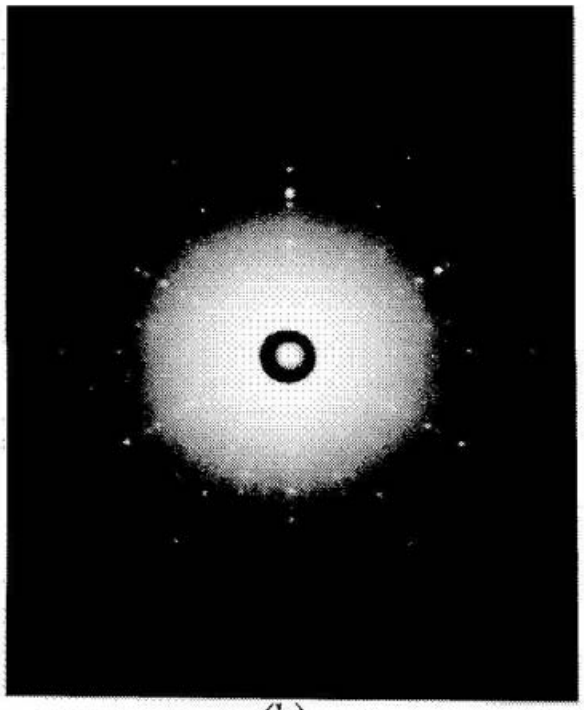

(b)

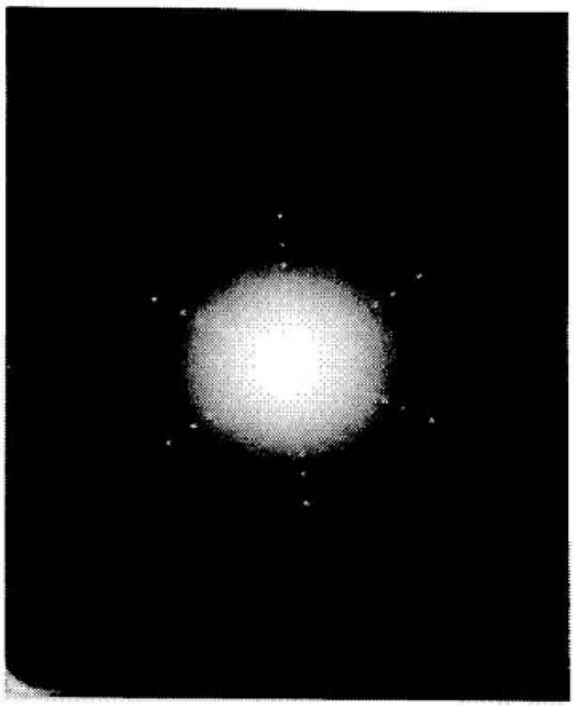

(c)

Fig.9 (a)The (110) Laue photograph of the polarizer(analyzer) device. (b)The (111) Laue photograph of the polarizer and the analyzer crystal. (c) The (001) Laue photograph of the sample crystal.

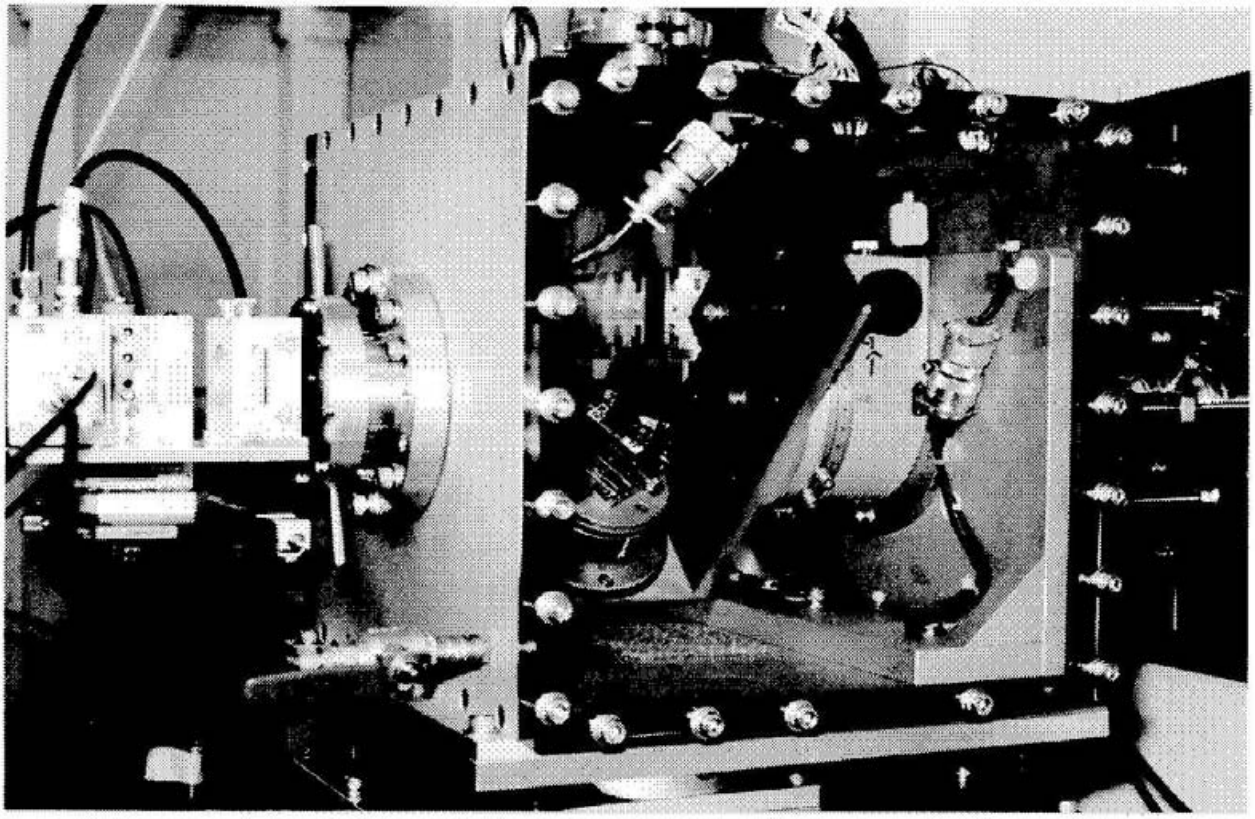

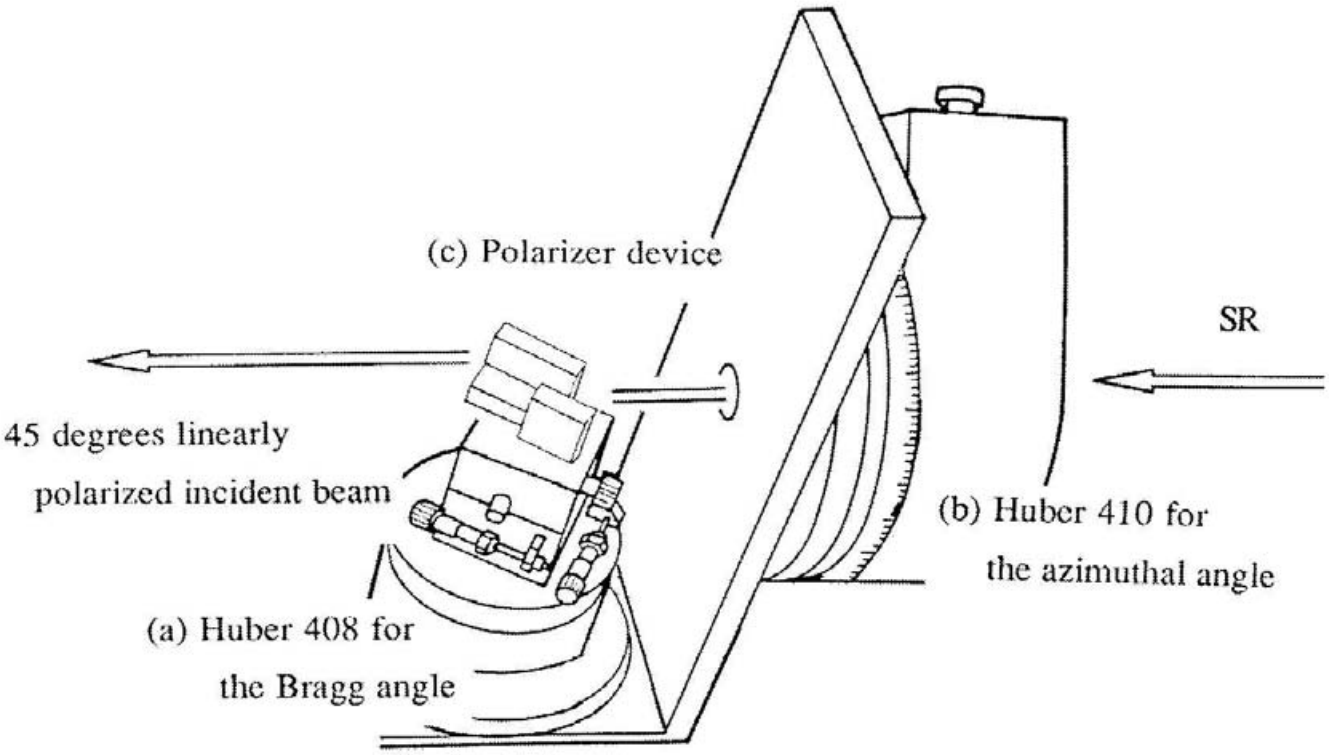

Fig.10 A photograph and an illustration of the polarizer monochromator.

beryllium window with the size of 25 mm in diameter is located at the entrance side of the container. To pursue the change of the exit beam position in every azimuthal angle of a polarizer crystal, a rotatable flange having 0.3 mm thick beryllium window with the size of 40 mm × 25 mm was put on the beam exitside. The vacuum valve fixed is to substitute the inner air with He(helium) gas effectively.

These apertures were aligned through the following procedures. The whole system was made horizontal using an accurate level gauge as shown in Fig.11. Then the arrangement of the x-y plane in Fig.5 and Fig.6 was finished. The y-z plane parallel to the SR beam has been established by comparison of the X-ray intensity at a specific absorption edge, while changing the Bragg angle of the polarizer crystal at two symmetrical positions of the azimuthal angle in the x-y plane. In order to measure the specific Bragg angle we use the K-absorption edge of some materials such as Cu and Fe. We put a thin foil whose K-absorption edge corresponding to the Bragg angle is far from 45 degrees of the polarizer crystal, in front of the ionization chamber of the beam monitor and measured the pulse-data of the K-absorption edge at the two symmetrical positions. By correcting the angle corresponding to the half quantity of the difference between the two pulse data, one can adjust the polarizer crystal parallel to the SR beam with the precision of 0.01°.

(4) Diffractometer equipped with an electromagnet

The diffractometer consists of two stages of goniometers the bottom of which has a 2θ arm for a analyzer and a detector. The rotation axes of these goniometers are adjusted parallel to system vertical

Fig.11 An accurate level gauge to make the system horizontal. Its slope inclination of the system is kept within 10 arcsec.

with the precision of 20 arcseconds. Both rotations of θ and 2θ are computer controlled by stepping motors. The angular resolution of these goniometers are 0.72 arcsec/pulse with a reducer gear of the ratio of 1:10. An electromagnet capable of generating the maximum magnetic flux of 5 kG with the current of 30A was mounted at the center of the upper goniometer. It has a cradle goniometer for adjusting the plane of incidence within 2.5° and -2.5°. The diffractometer is further equipped with a closed-cycle helium refrigerator for cooling a sample ($T > 20K$) and an intrinsic germanium solid state detector (SSD) with a magnetic shield cap. They were mounted on the magnet as shown in Fig.12. The SSD is used for measuring fluorescent X rays from the sample crystal. The magnetic shield cap can reduce the magnetic flux leakage down to about 1/500 at its middle position.

This apparatus is aligned by putting the rotation-axis of both goniometers into the center of the beams.

(5) Polarization analyzer

It also consists of two crossed goniometers with an analyzer crystal. One is for driving the Bragg angle and the other for driving the azimuthal angle of the analyzer crystal. The rotation axes of these goniometers meet at right angle with the precision of 20 arcseconds. All rotations are computer controlled by stepping motors. The resolutions of these goniometers are 0.144 arcsec/pulse with a reducer gear of the ratio 1:100 and 0.72 arcsec/pulse with a reducer gear of the ratio 1:10, respectively. The whole goniometer on the 2θ arm after the sample diffractometer, as shown in Fig.13. The diffracted X rays from the sample crystal pass through the center hole of the analyzer goniometer.

The X-ray intensity is measured by a small sized SSD on a table which can make a circular locus with a variable radius synchronizing with the exit beam position of the analyzed beams, so that the analyzer crystal and the SSD were rotated around the diffracted beams. This apparatus is adjusted with the same principle as the polarizer.

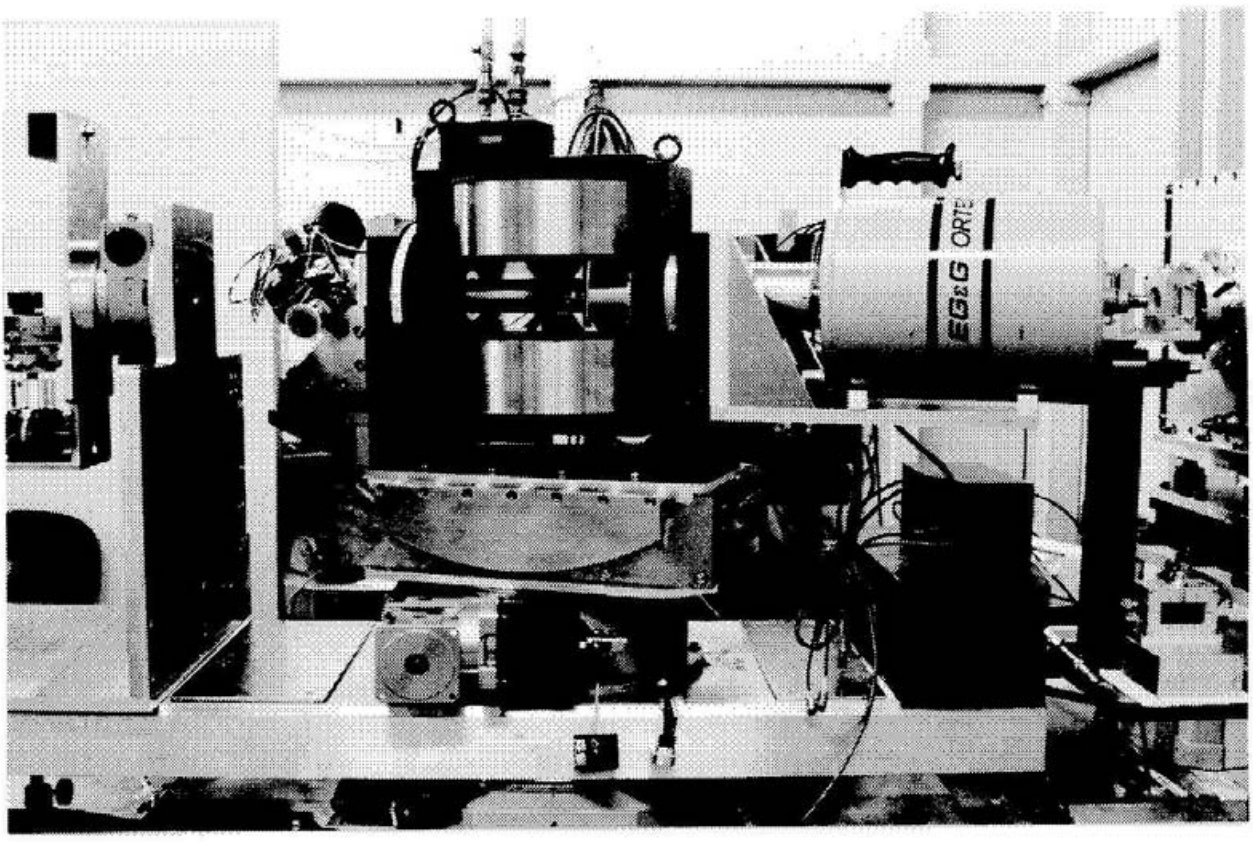

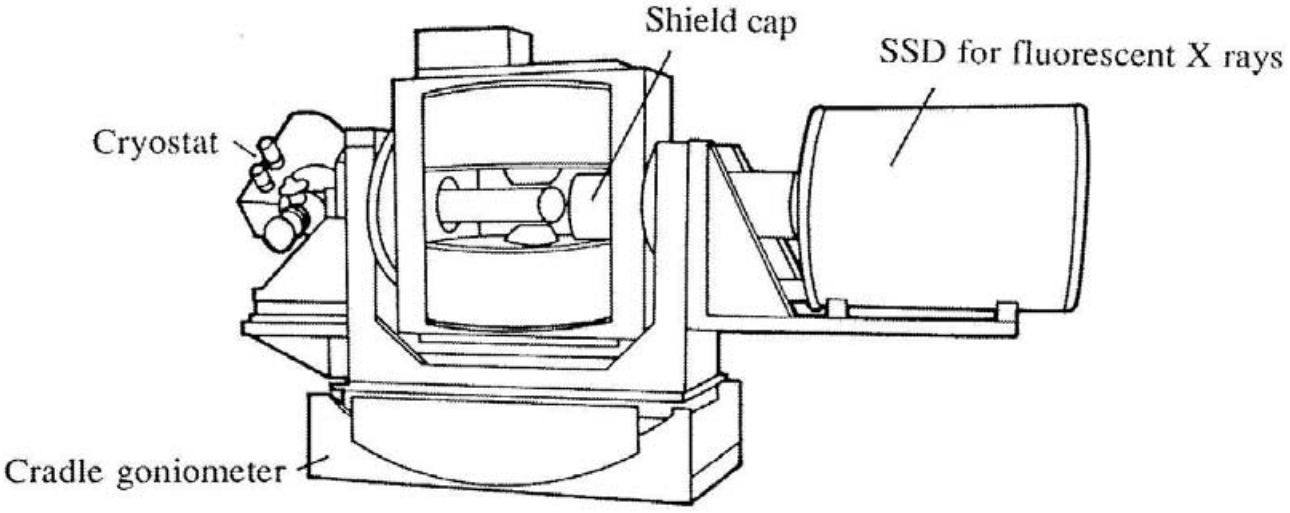

Fig.12 A photograph and an illustration of the magnet.

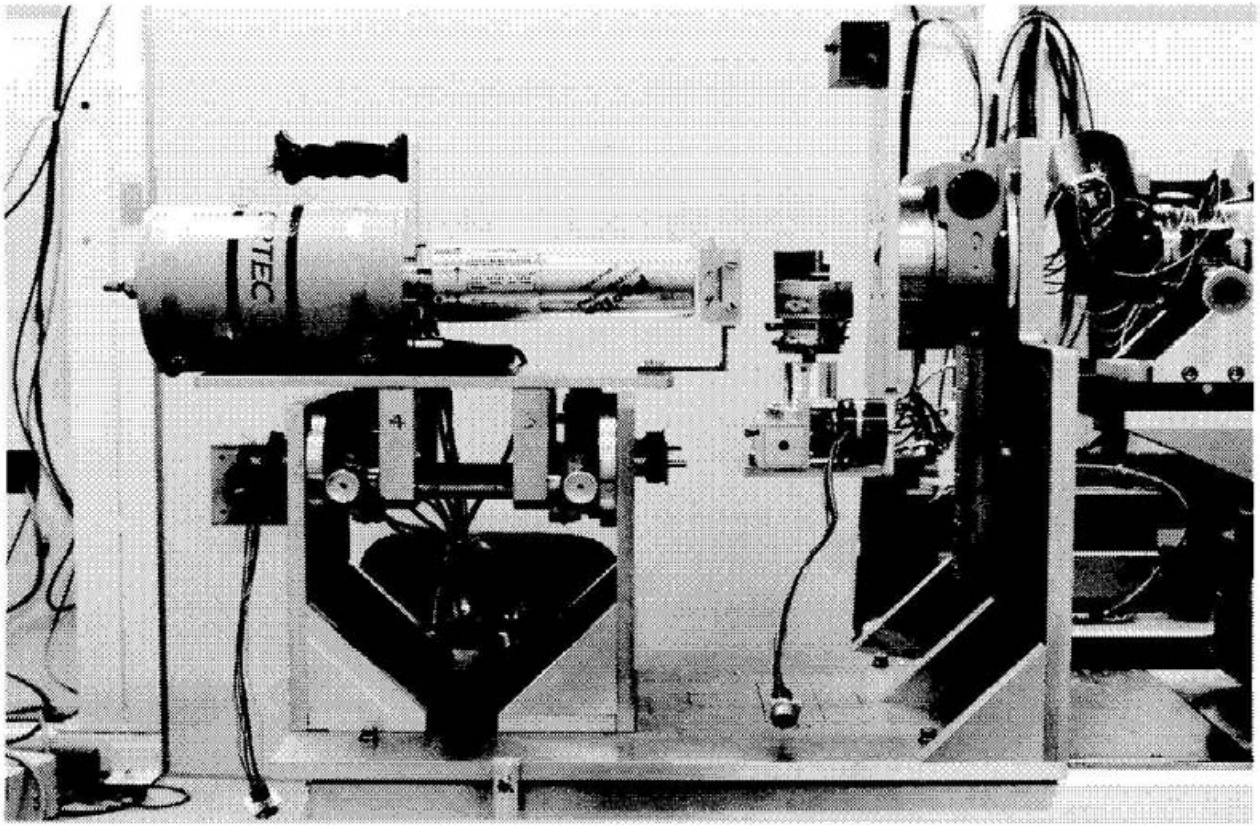

Fig.13 A photograph of the polarization analyzer placed on the 2θ-arm. The analyzer crystal and the detector are rotated around the diffracted X rays.

Experiments

The intensity of the incident X-ray was monitored by an ionization chamber. The ionization current from an ionization chamber was monitored in a preset-count mode. The magnitude of the ionization current is around 0.25nA with the high voltage of 300V at the ring current of 300mA. All X-ray beam path was filled with He(helium) gas. The purity of the incident beams examined by the analyzer is shown in Fig.14. The abscissa denotes the relative intensity and the ordinate denotes the energy of the beams. An impure component is mixed into the primary beams. Its energy is located about 50eV higher than that of the L_2 absorption edge. The intensity is about one third of the primary one. The higher harmonics and the other back ground noises were discriminated by a single channel analyzer(SCA). The electric circuit for this measurement is shown in Fig.15.

A sample is an oval shaped Gd (001) single crystal with the size of 8mm × 5mm and 1mm in thickness. The Laue photograph of the 001 surface is shown in Fig.9(c). The L_2 absorption edge occurs at 7.930keV, and is well separated from its L_3 and L_1 partners at 7.243keV and 8.376keV, respectively. The magnetic ordering temperature T_C is 293K. Since the mosaic width of this sample crystal is about 0.2°, the diffracted X rays are subject to the angular divergence at the sample. The impure component whose energy is close to the primary beam are scattered by this sample.

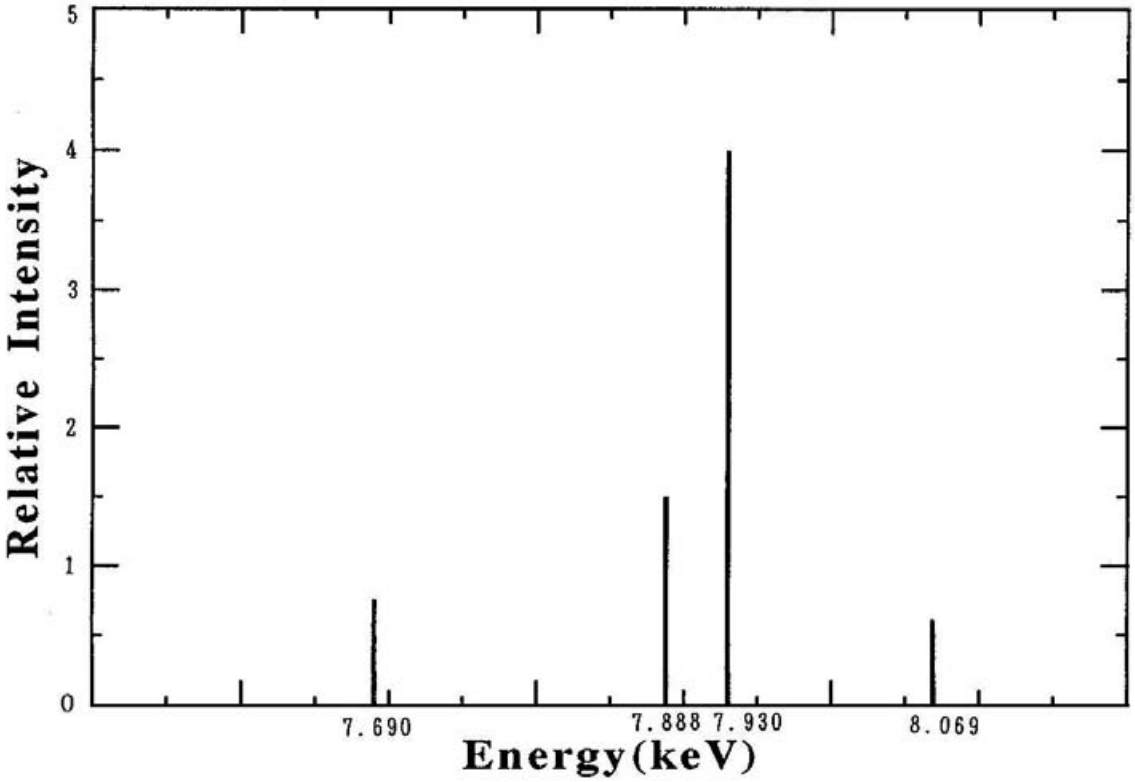

Fig.14 The purity of the incident beam. The size of the beam is about 0.5 mm × 0.5 mm. The abscissa denotes the energy of the X-ray. The strongest component is located at the energy 7.930keV. Three impure X rays of the energy 8.069keV, 7.888keV and 7.690eV are mixed into the primary beams. The intensity is measured by a SSD.

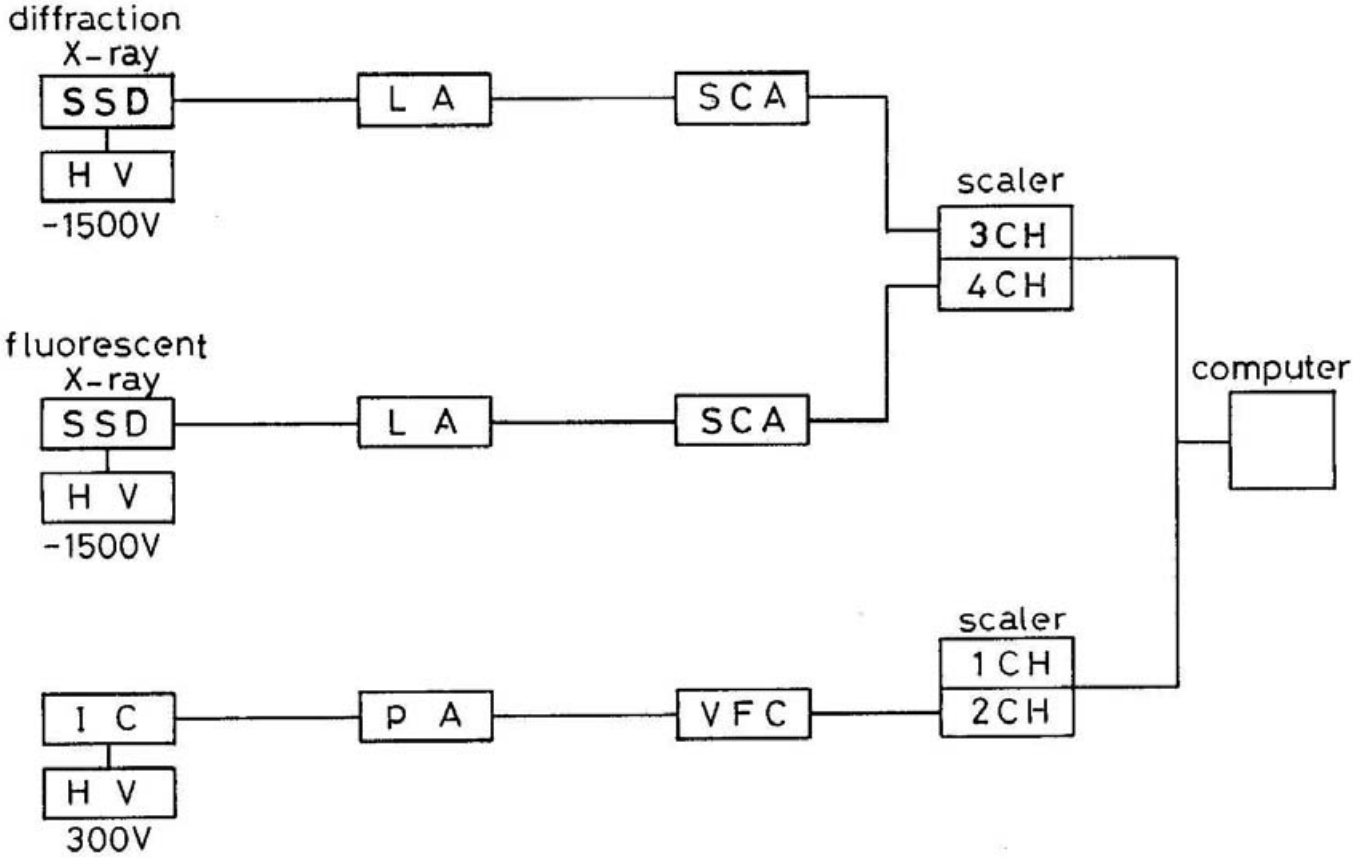

Fig.15 The electric circuit of the measurement. The input bias voltage for SSD is -1500V. L A , SCA, PA,VFC and IC correspond to a linear amplifier, a single channel analyzer, a current amplifier, a V-F converter and an ionization chamber, respectively.

(1) Polarization analysis of the incident X rays

The orientation of the plane of polarization was measured at the energy of L_3-edge. In this case, the monochromatic X-ray has been tuned to E = 7.243 keV using a Si 331 polarizer crystal(same type as the Si 422 polarizer crystal), whose Bragg angle is equal to 43.38°. Its polarization ratio (the intensity ratio of the π to σ) for two consecutive reflections comes up to 10^{-3}. To set the scattering angle $2\theta = 0°$ and with no sample, the incident beams with the size of about 0.5mm×0.5mm were analyzed. The analyzer device is same as the polarizer crystal. The theoretical value of full width at half maximum(FWHM) of Si 331 reflection curve is about 2.7 arcsec at this energy. The count rate is about 2.5×10^4 /sec at the azimuthal angle of 45° and about 1.0×10^5 /sec at the azimuthal angle of 225°. The intensities were integrated within 3 times of FWHM of the intensity distribution at each azimuthal position. Data were taken with 10° increments over the azimuthal position 0° to 360°(-90° to 270°). The measured intensity variation is shown in Fig.16. Abscissa denotes the azimuthal angle of the analyzer crystal and ordinate denotes the relative integrated intensity. The solid-line means the curve fitted profile. The fitted profile of the intensity variation of the scattered beam was obtained by a standard least squares method.

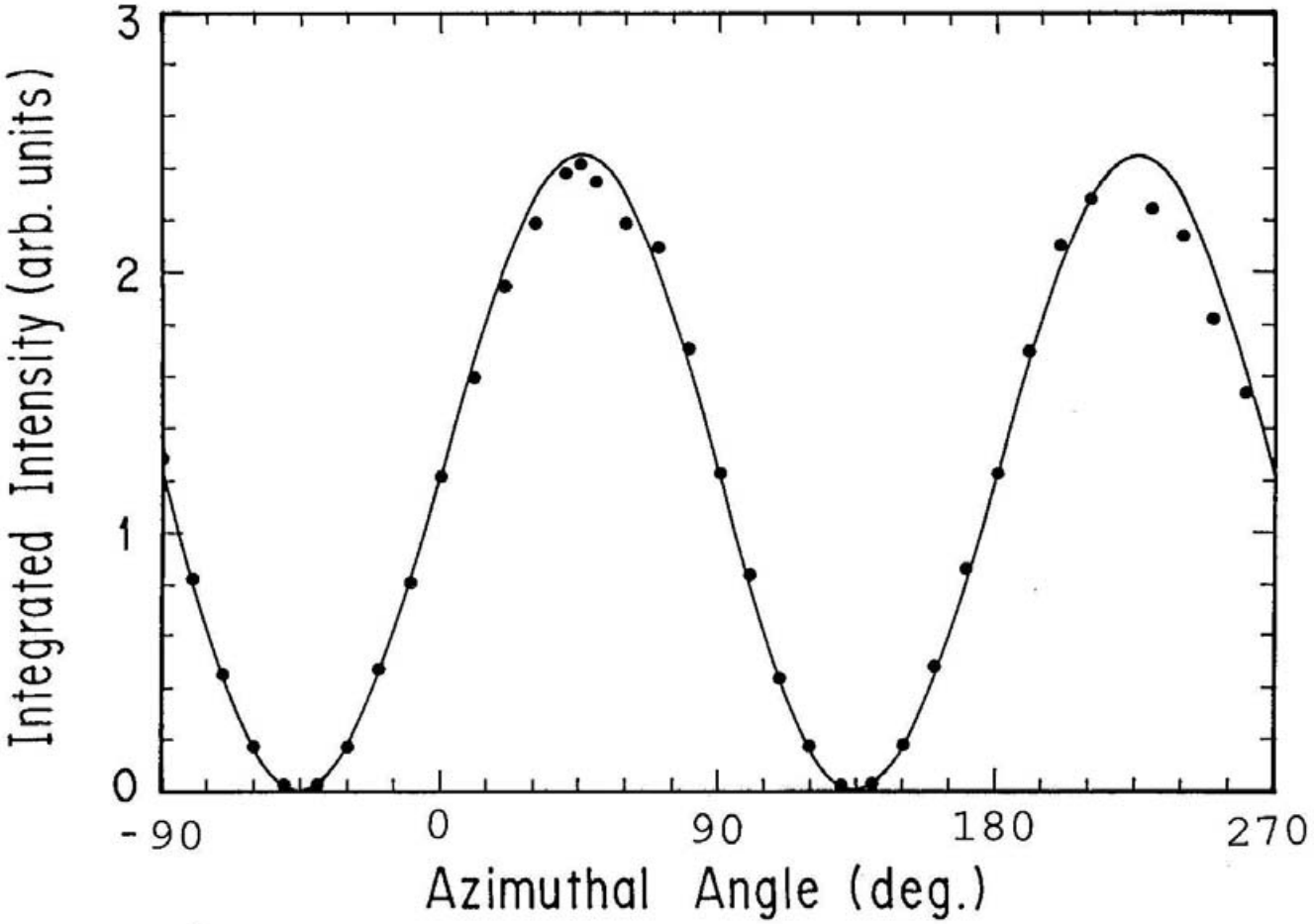

Fig.16 The intensity variation of the incident beam. The count rate is about 2.5×10^4 /sec at the azimuthal angle 45° and about 1.0×10^5 /sec at the azimuthal angle 225°.

(2) Polarization analysis of the diffracted X rays

The experimental arrangement is shown in Fig.17. We used a Si 422 channel-cut crystal as a polarizer device. The azimuthal angle of the polarizer device was fixed to 45 degrees for each energy E_1 (0.5eV above the edge), E_2(3.0 eV above the edge), and E_3 (1.5eV below the edge) near the L_2-absorption edge. The size of the incident beams are about 4mm $\times$ 4mm. The sample crystal was supported inside the refrigerator and the magnet was aligned so that the magnetic field is along the easy axis of magnetization of the sample crystal. At E_1 and E_2, the magnetic field applied are H=3 kG (parallel to $\mathbf{k}_f \times \mathbf{k}_0$) , H=0 kG , and H=-3 kG (anti-parallel to $\mathbf{k}_f \times \mathbf{k}_0$). At E_3, the magnetic field are H=3 kG and H=-3 kG. The temperature of the sample is 140K. Under these conditions the magnetization of the sample is nearly saturated.[12] The scattering angle of (004) beam is 72.62°. The analyzer crystal is same as that of the polarizer device. In this case, the intensity ratio of the π to σ at the polarizing device is estimated about 10^{-5}.

We measured the rocking curves for each azimuthal angle with a step of 5 degrees between 35° and 185° as illustrated in Fig.18. Abscissa denotes the azimuthal angle (10^4 pulse correspond to 0.2°) of the analyzer device and ordinate denotes the intensity. The maximum count rate takes place at the azimuthal angle where the FWHM of the intensity distribution becomes minimum. The peak of the intensity distribution is indistinct between 135° and 185°. Maximum count rate is about 100 counts/sec at 90°, where the FWHM is about 0.1°

At E_1 and E_3 the intensities were integrated over 3 times of FWHM of the intensity distribution, while at E_2 the intensities were integrated over 4 times of FWHM. The raw data of the integrated intensities is

shown in Table 1(a) to (h). The measured intensity variation is shown in Fig.19(a) to (h). Abscissa denotes the azimuthal angle of the analyzer device and ordinate denotes the integrated intensities. Full circles indicate the measured data. The Solid line indicates the curve fitted profile. The fitted profile of the intensity variation of the scattered beam was obtained also by a standard least squares method. If the azimuthal position coincides with the orientation of the minor axis, the output intensity becomes lower and the peak of the intensity distribution is not clear. Such data is excluded from the fitting. The experimental data also agrees well with the fitted profile. The counting time for each azimuthal angle is about 700 sec. Net counting time needed approximately 6 hours except for the access time of the measurement system.

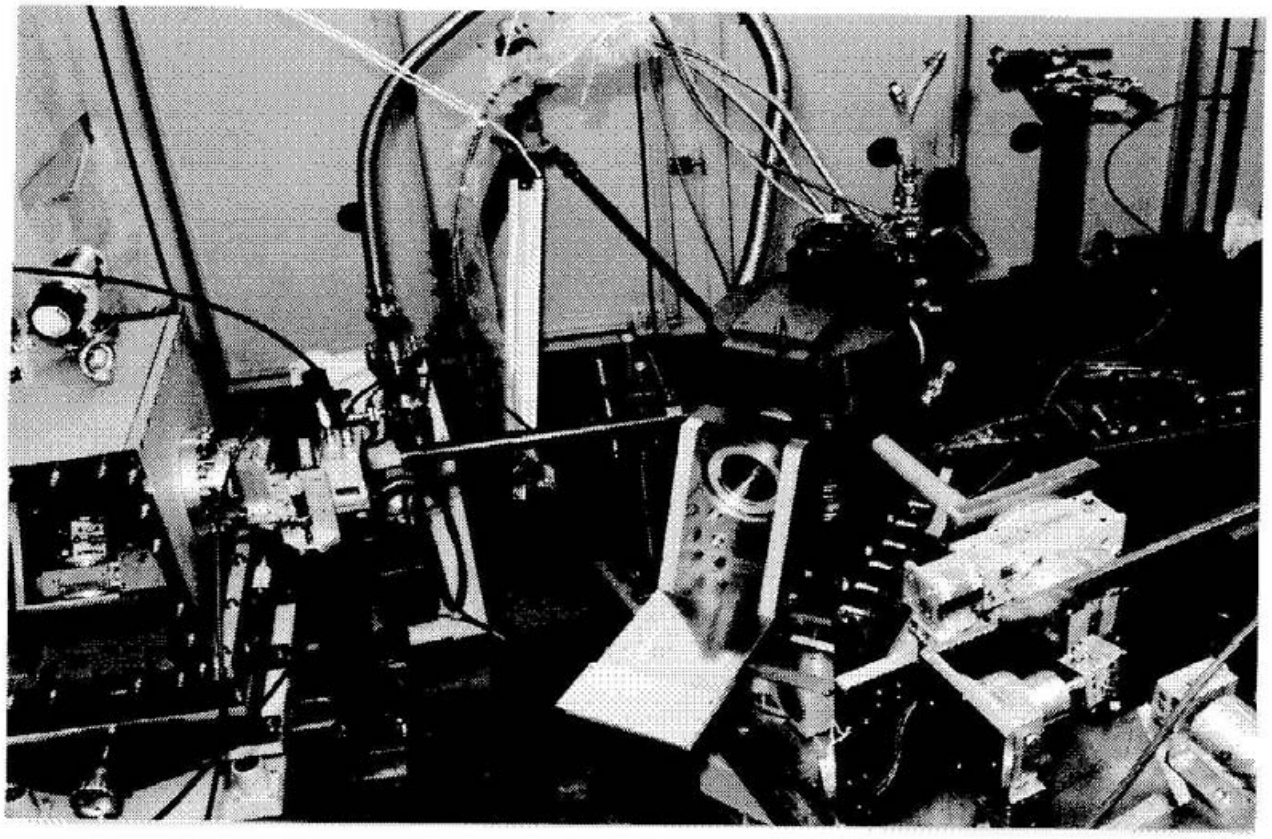

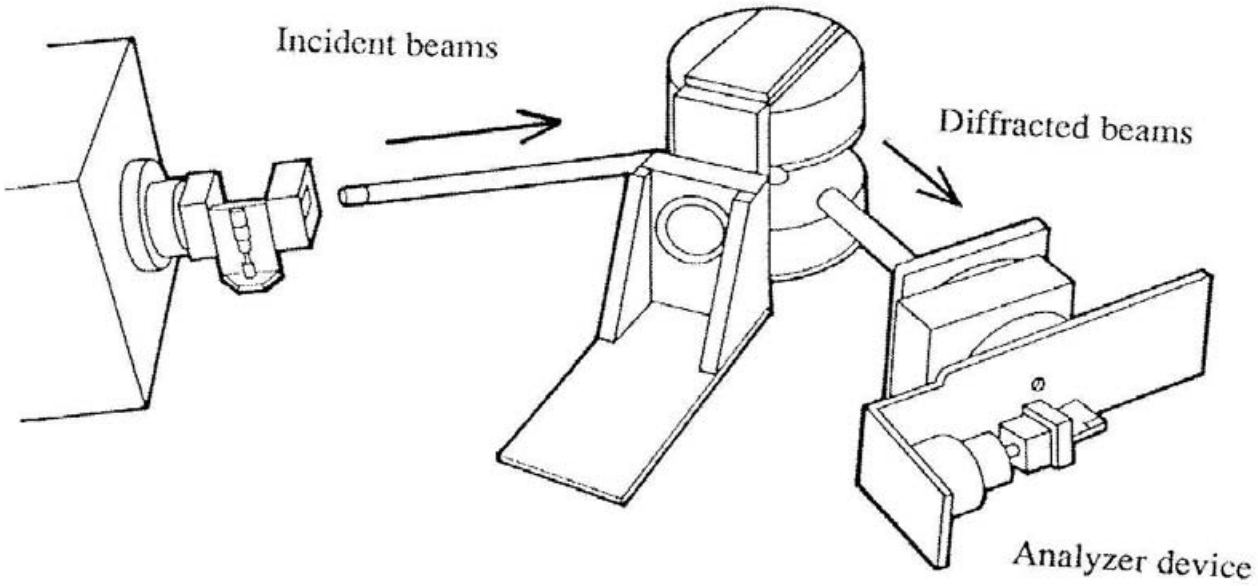

Fig.17 A photograph of the experimental arrangement.

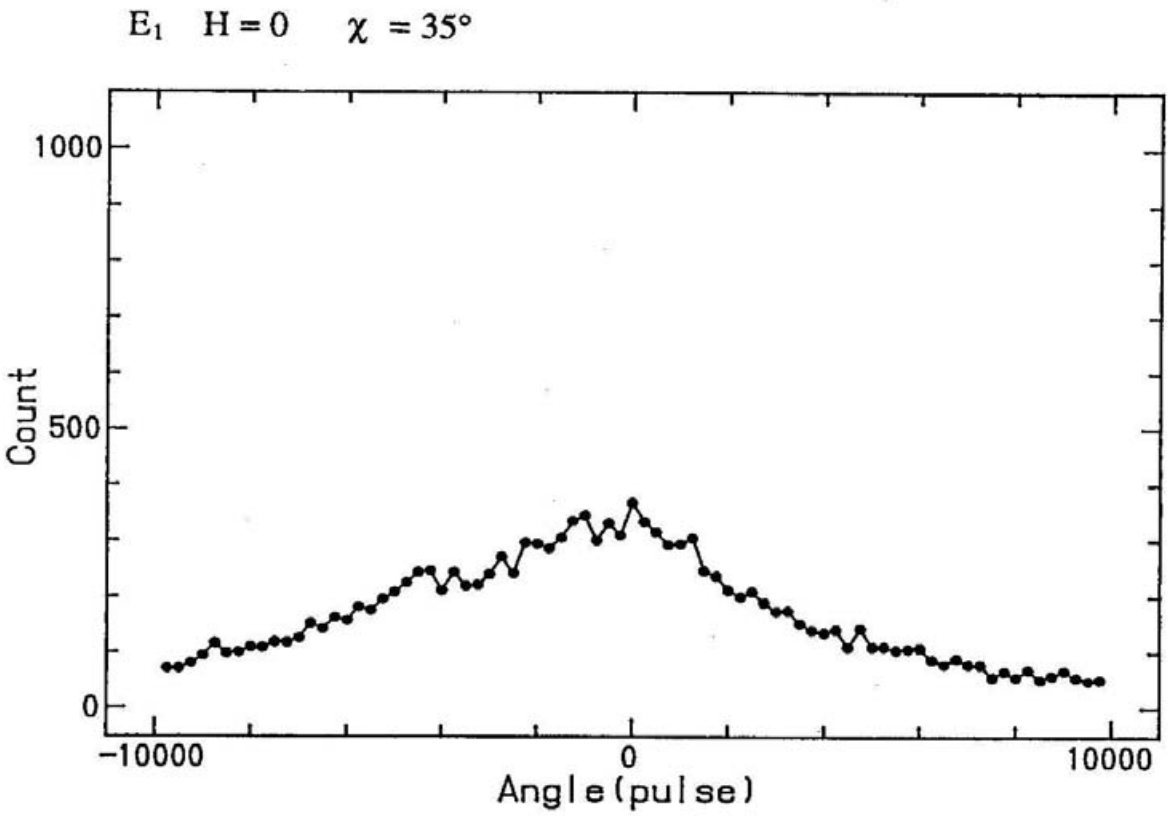

Fig.18 The intensity distributions of the scattered X rays at the azimuthal angle χ. The abscissa denotes the azimuthal angle of the analyzer crystal and the ordinate denotes the intensity. In the ordinate, 10000 pulses correspond to 0.2°.

E_1 H = 0 $\chi = 40°$

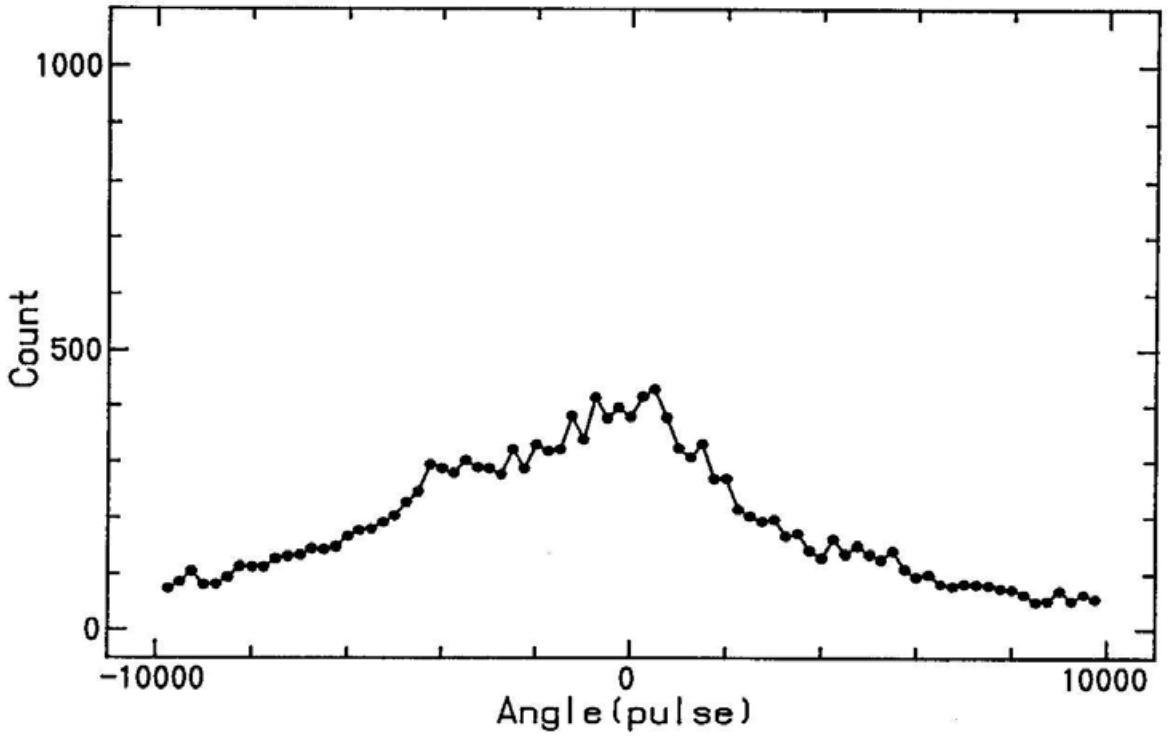

E_1 H = 0 $\chi = 45°$

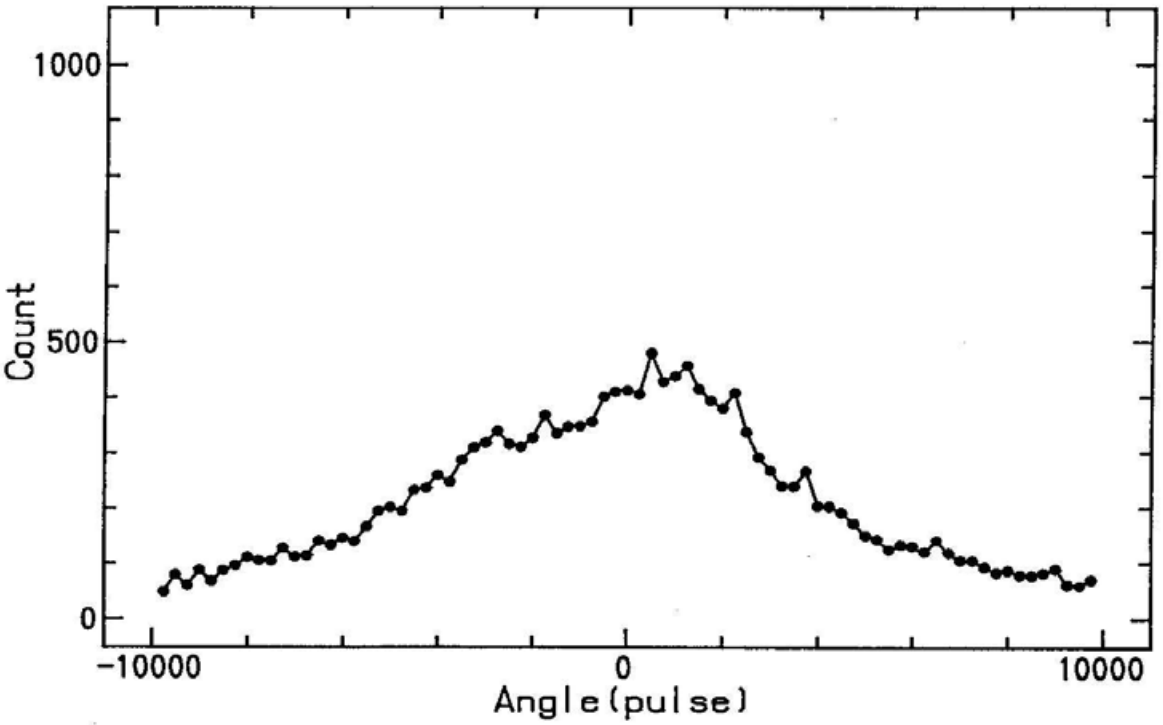

Fig-18

E_1 H = 0 $\chi = 50°$

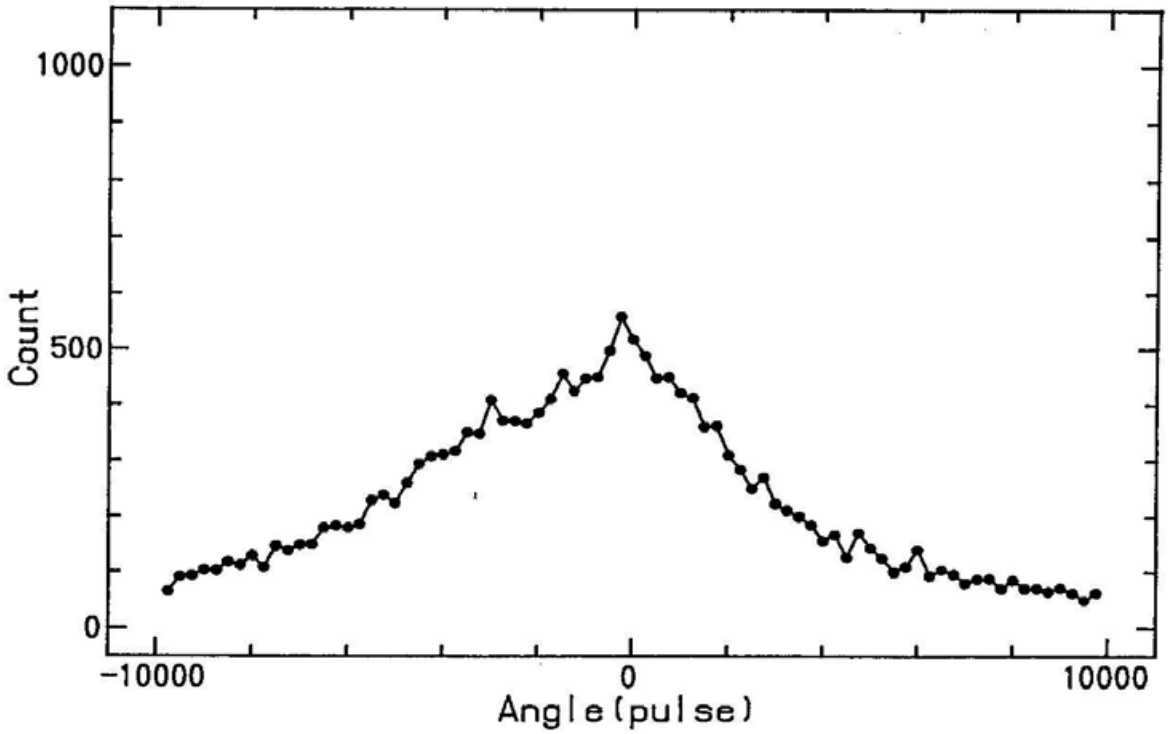

E_1 H = 0 $\chi = 55°$

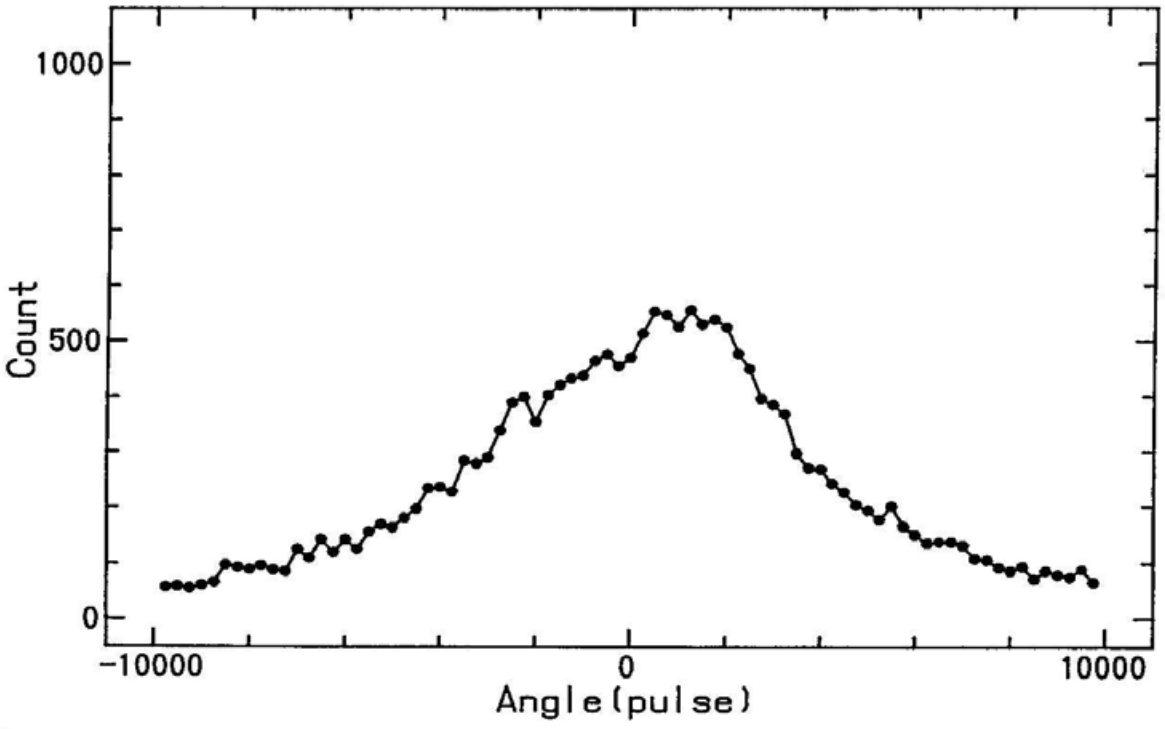

Fig-18

E_1 H = 0 χ = 60°

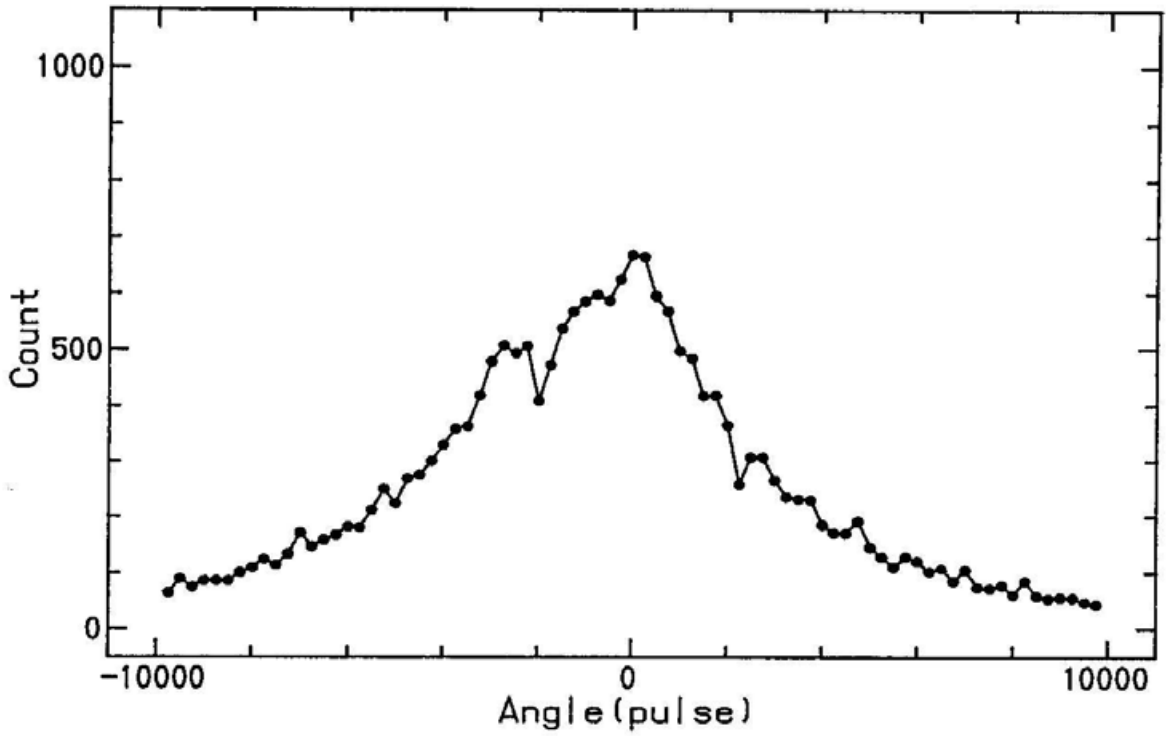

E_1 H = 0 χ = 65°

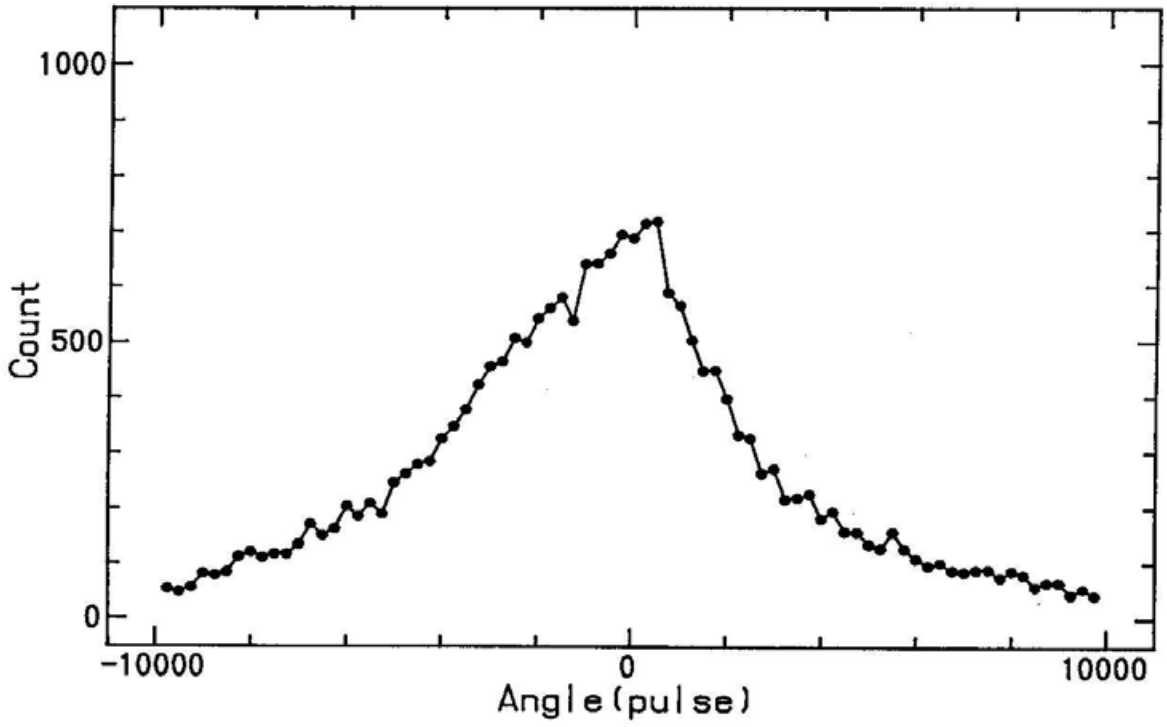

Fig-18

E_1 H = 0 χ = 70°

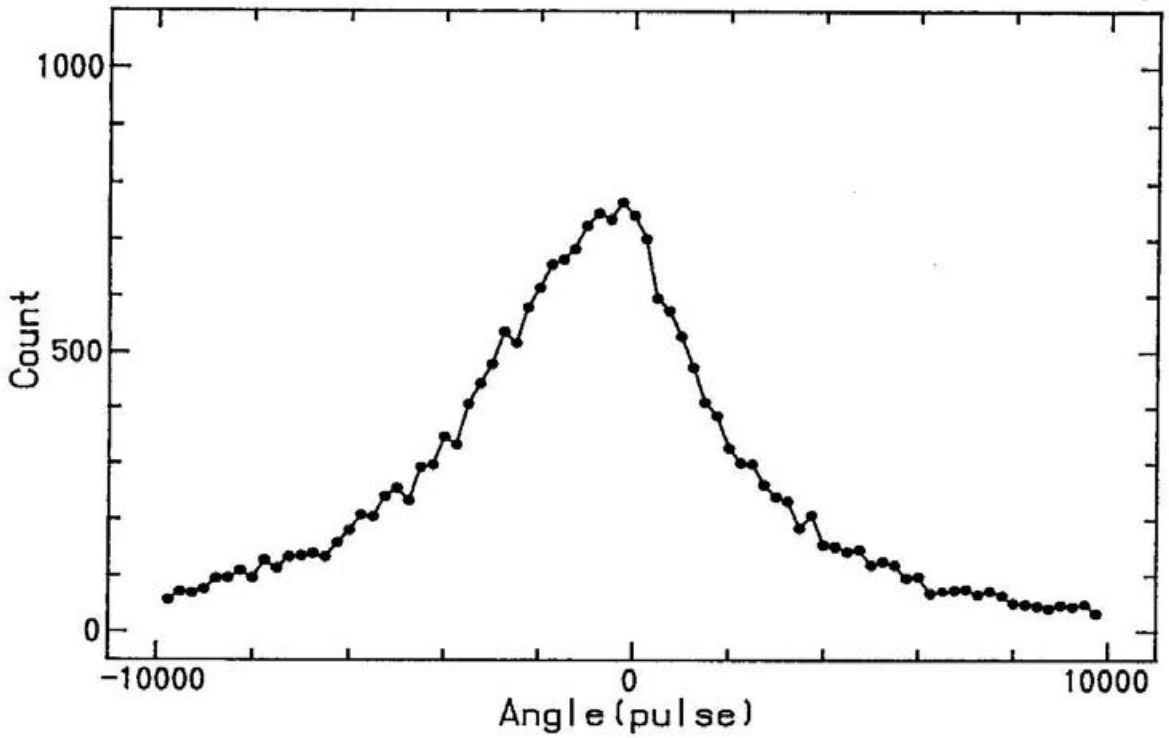

E_1 H = 0 χ = 75°

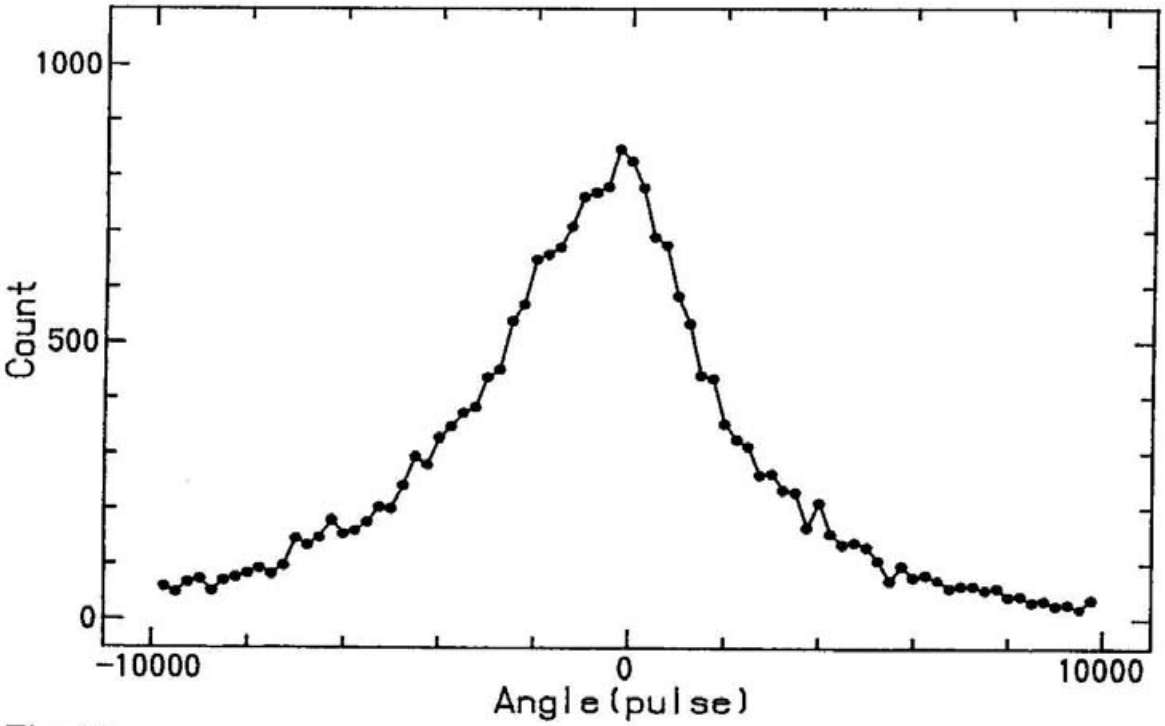

Fig-18

E_1 H = 0 $\chi = 80°$

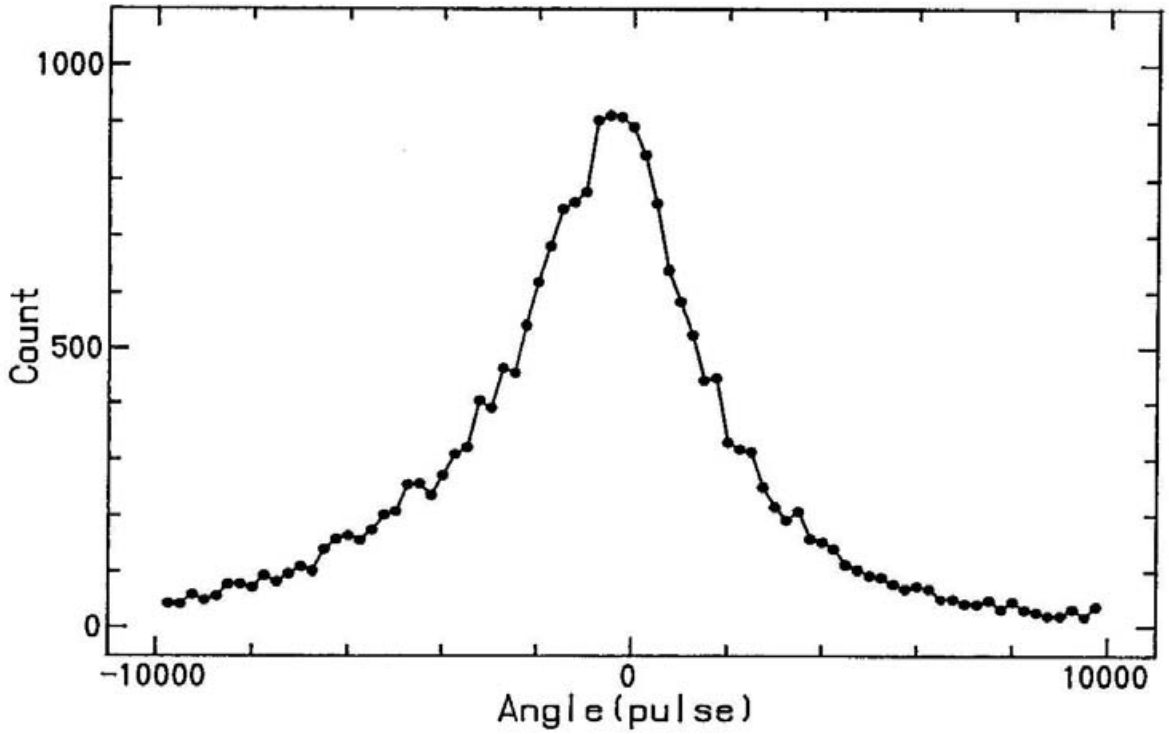

E_1 H = 0 $\chi = 85°$

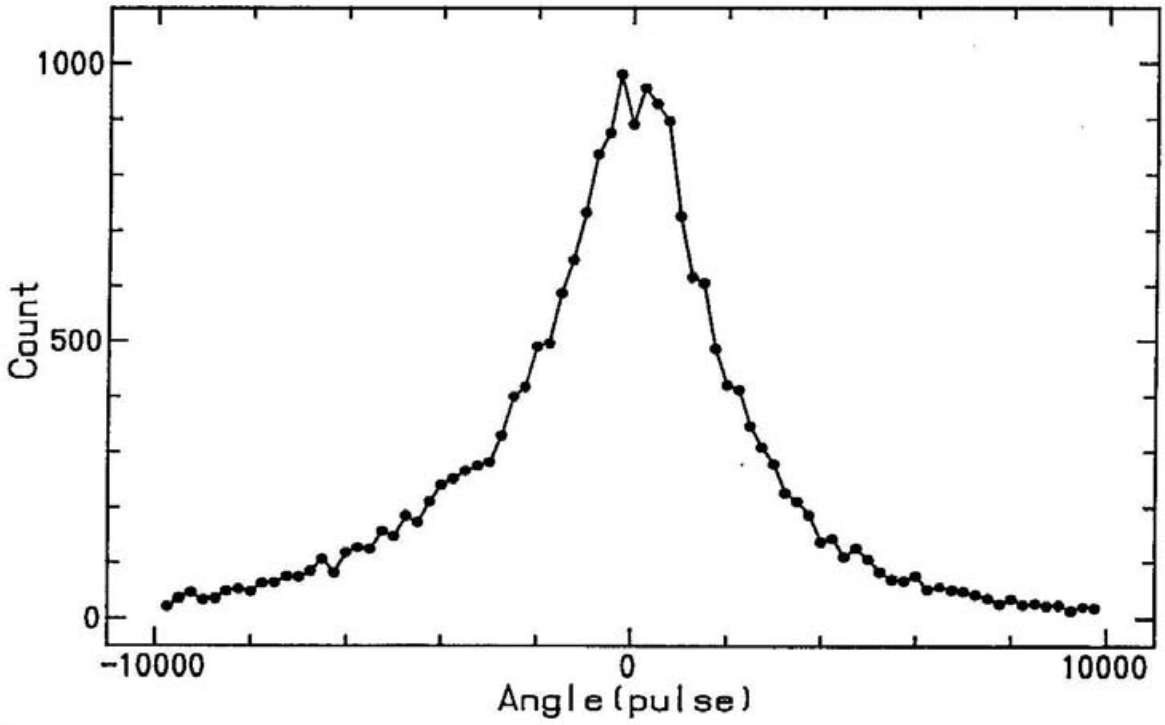

Fig-18

E_1 H = 0 $\chi = 90°$

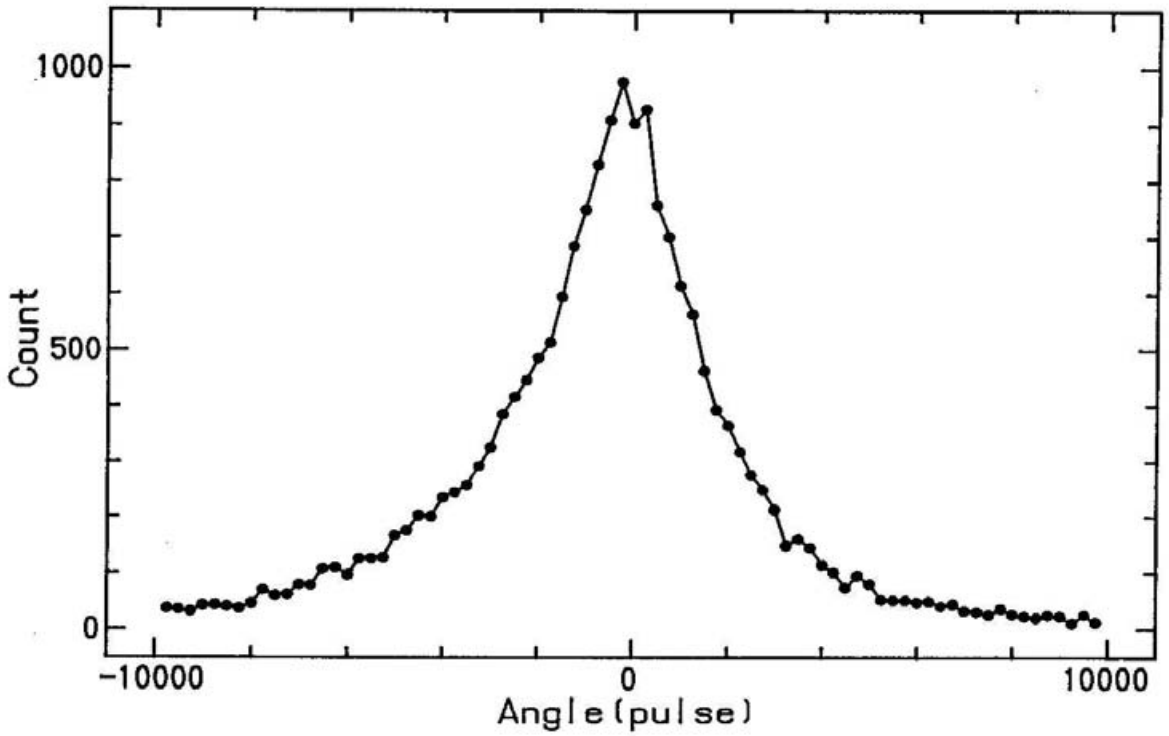

E_1 H = 0 $\chi = 95°$

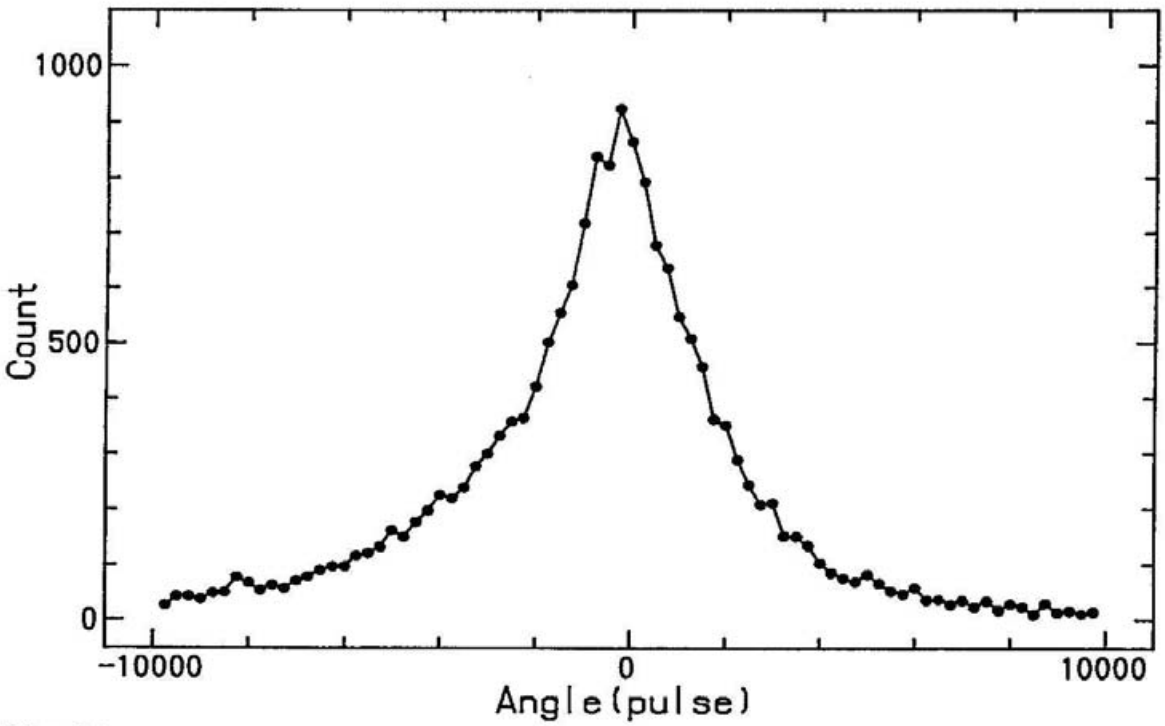

Fig-18

E_1 H = 0 χ = 100°

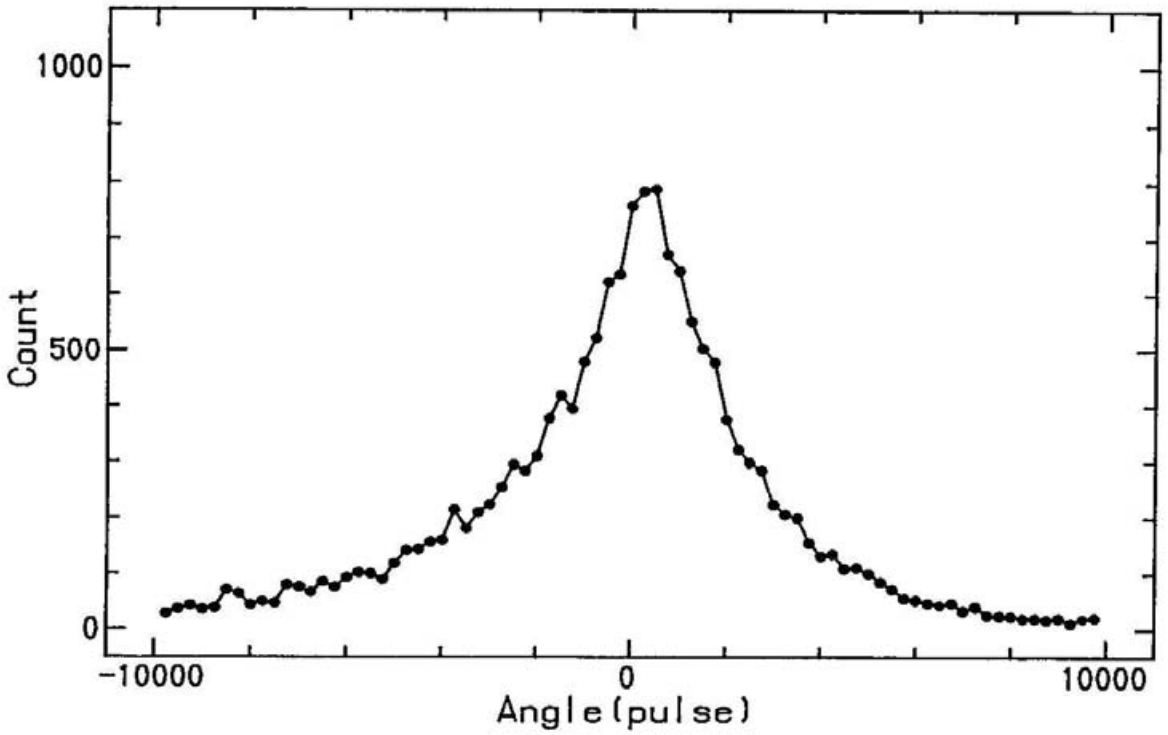

E_1 H = 0 χ = 105°

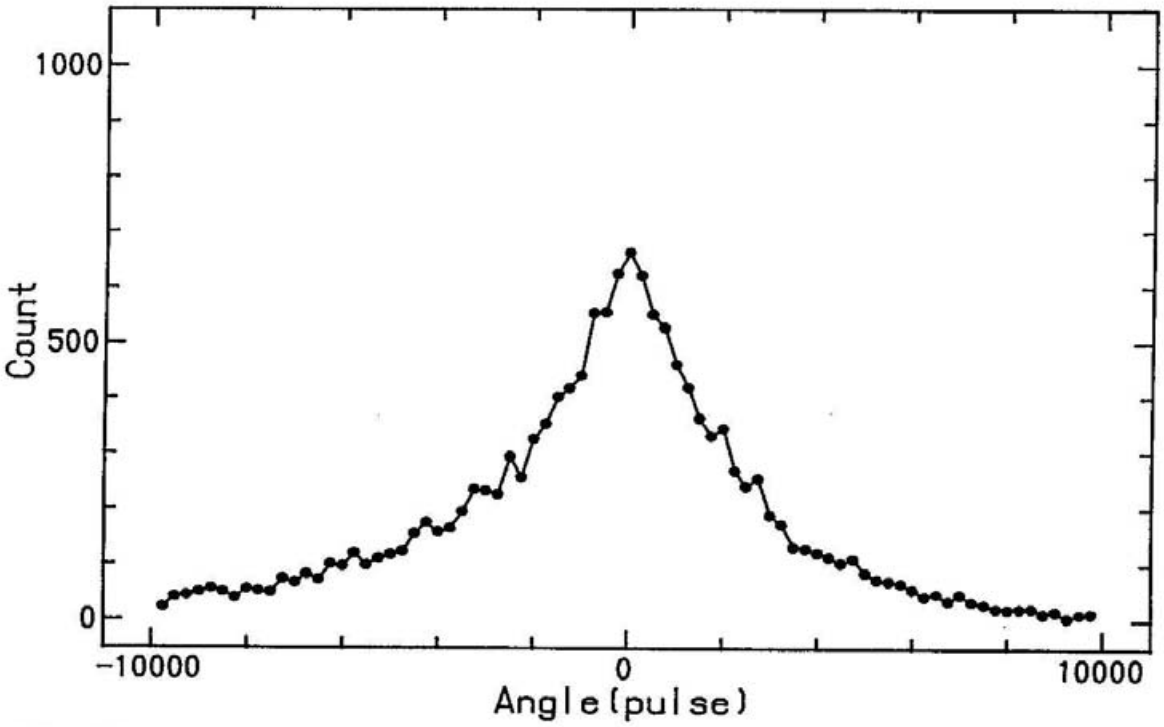

Fig-18

E_1 H = 0 χ = 110°

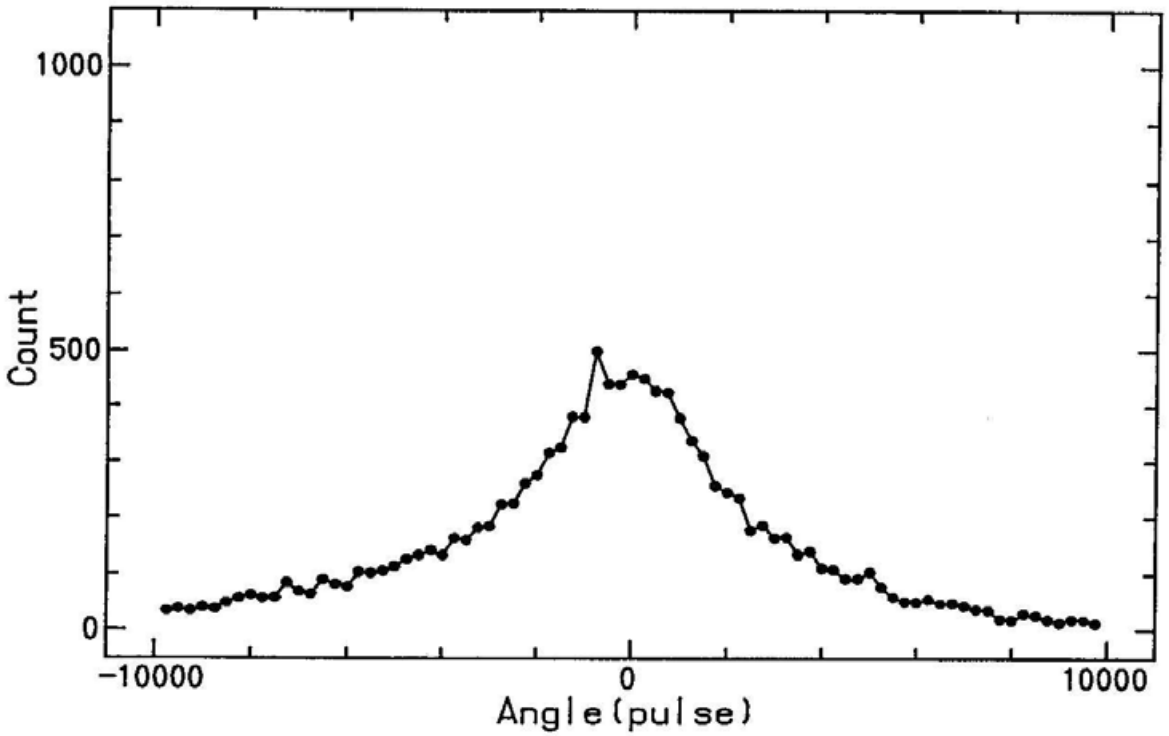

E_1 H = 0 χ = 115°

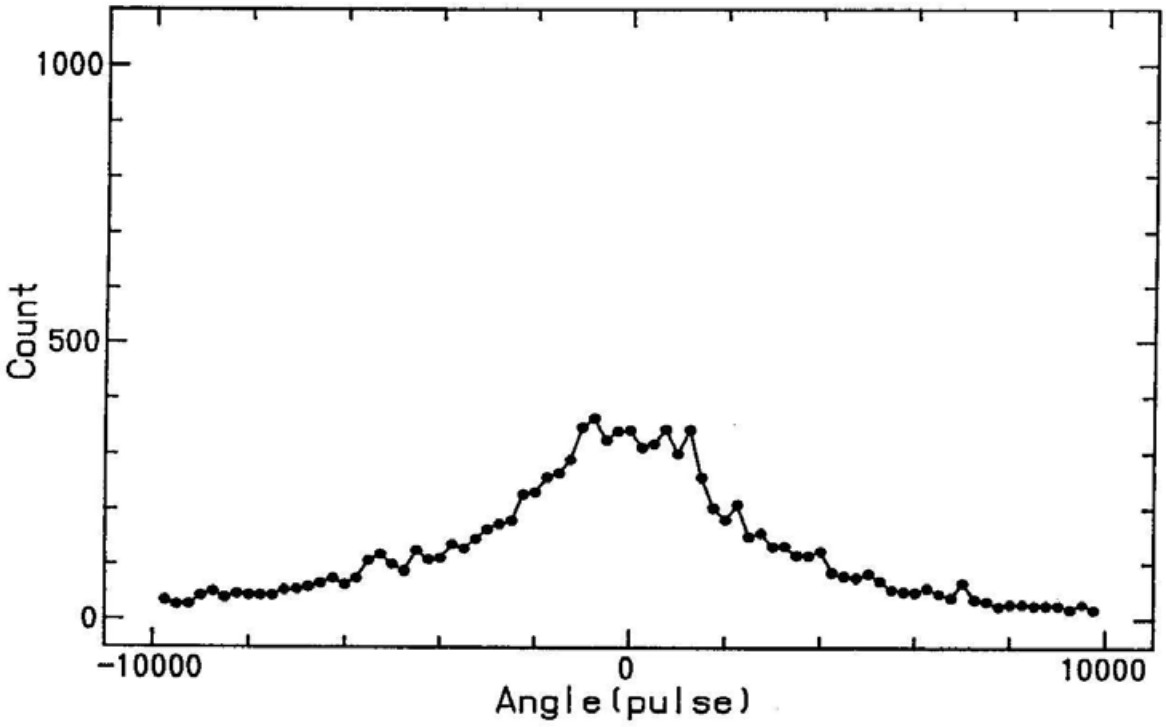

Fig-18

E_1 H = 0 $\chi = 120°$

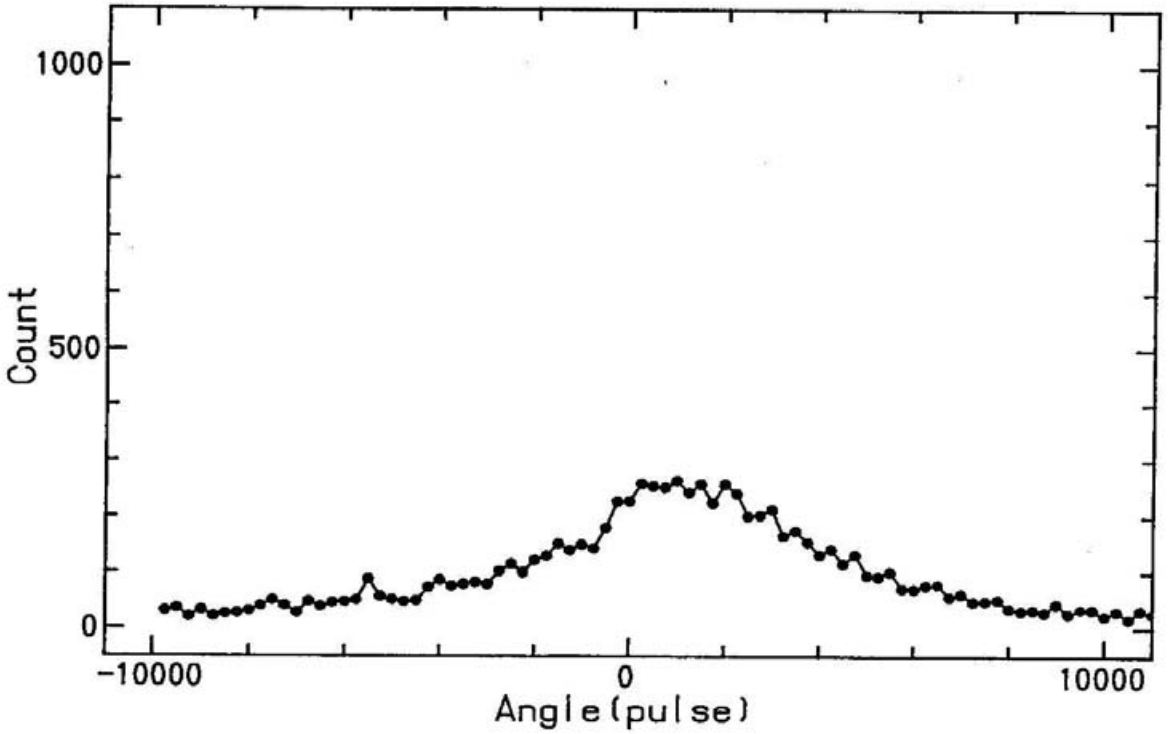

E_1 H = 0 $\chi = 125°$

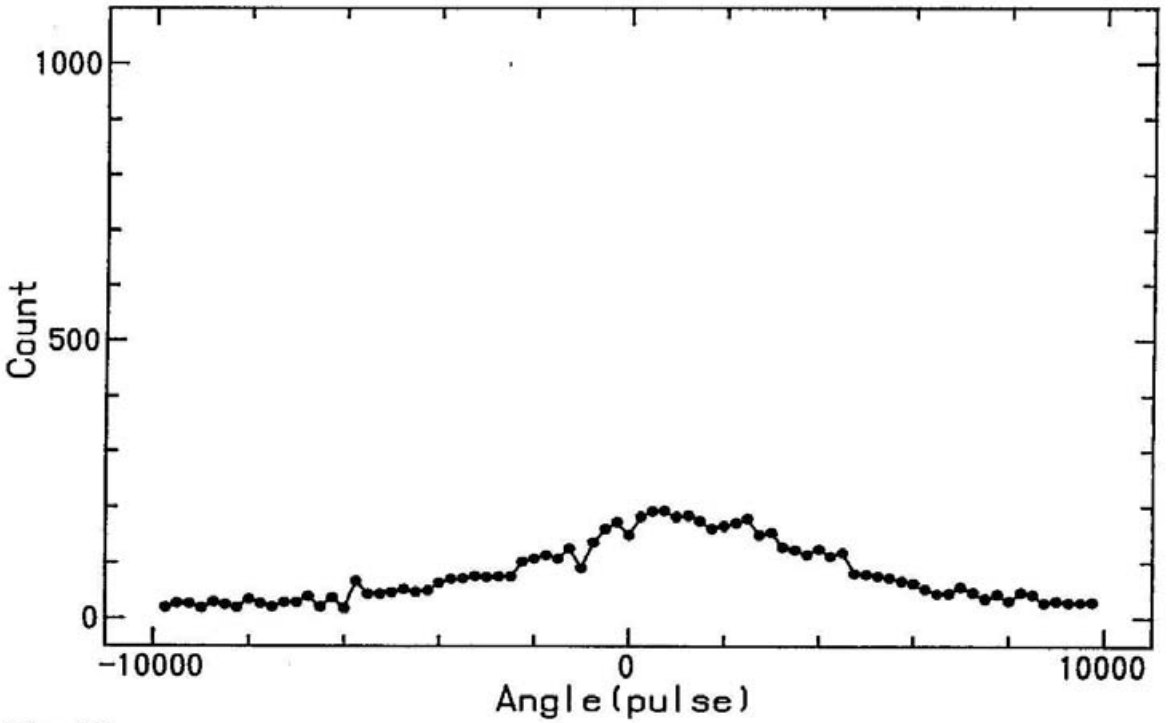

Fig-18

E_1 H = 0 $\chi = 130°$

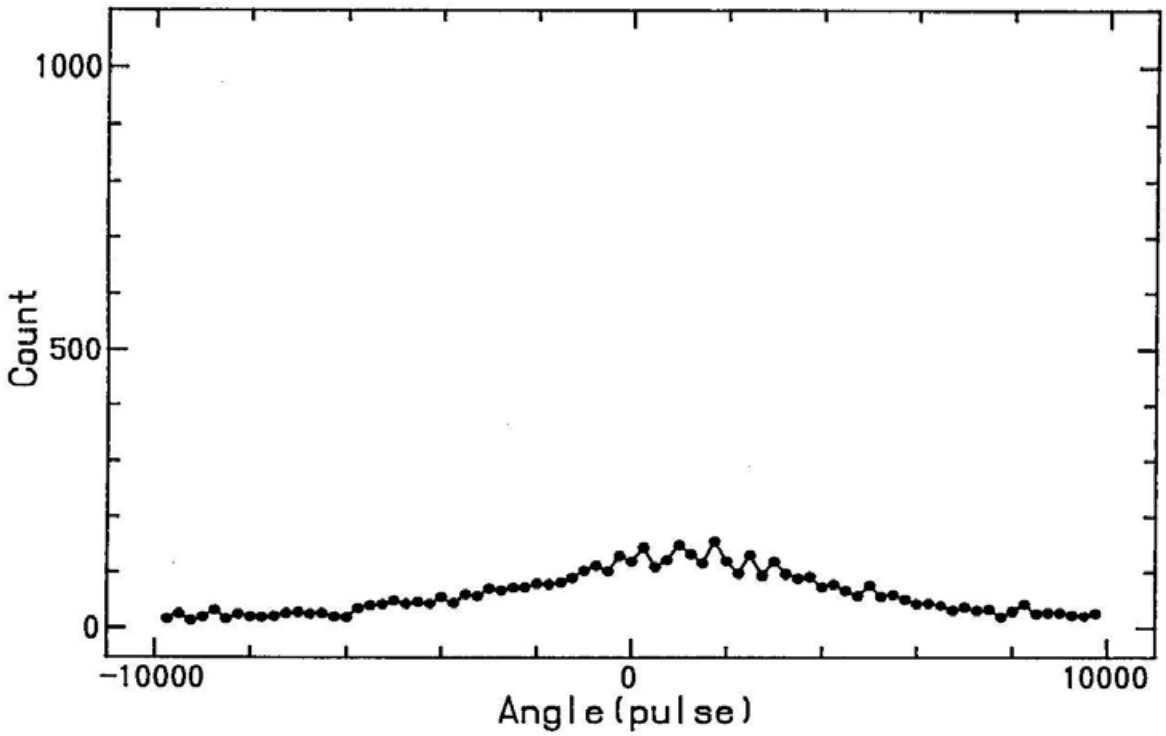

E_1 H = 0 $\chi = 135°$

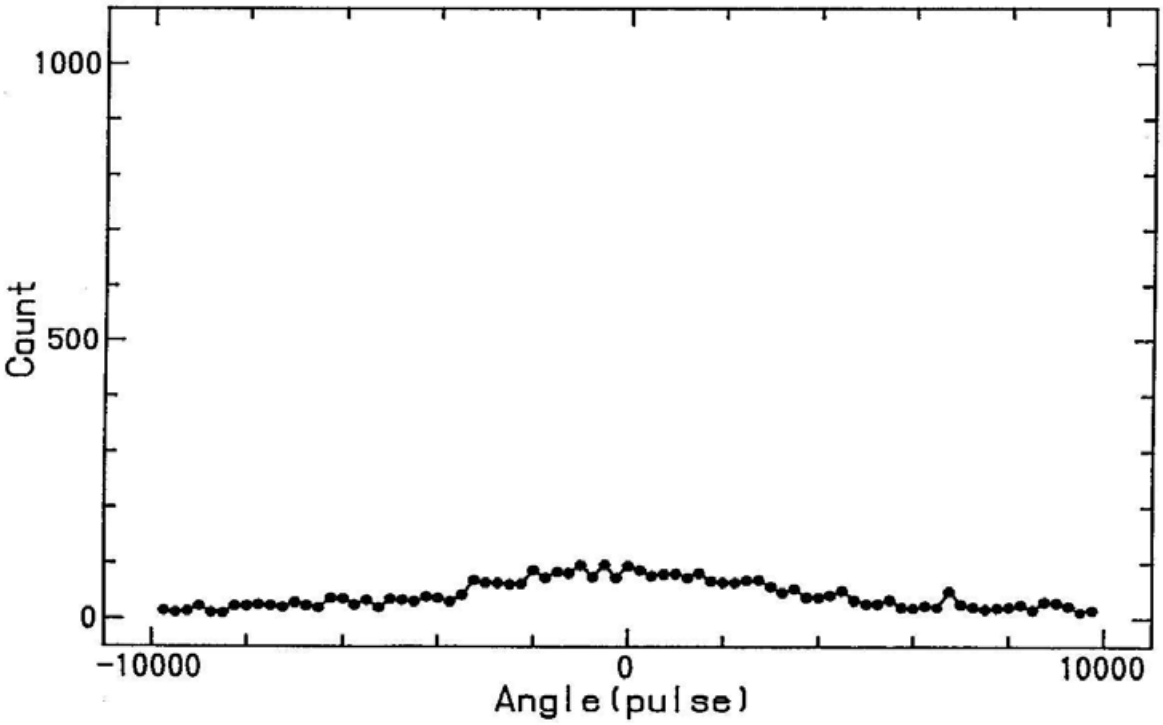

Fig-18

E_1 H = 0 χ = 140°

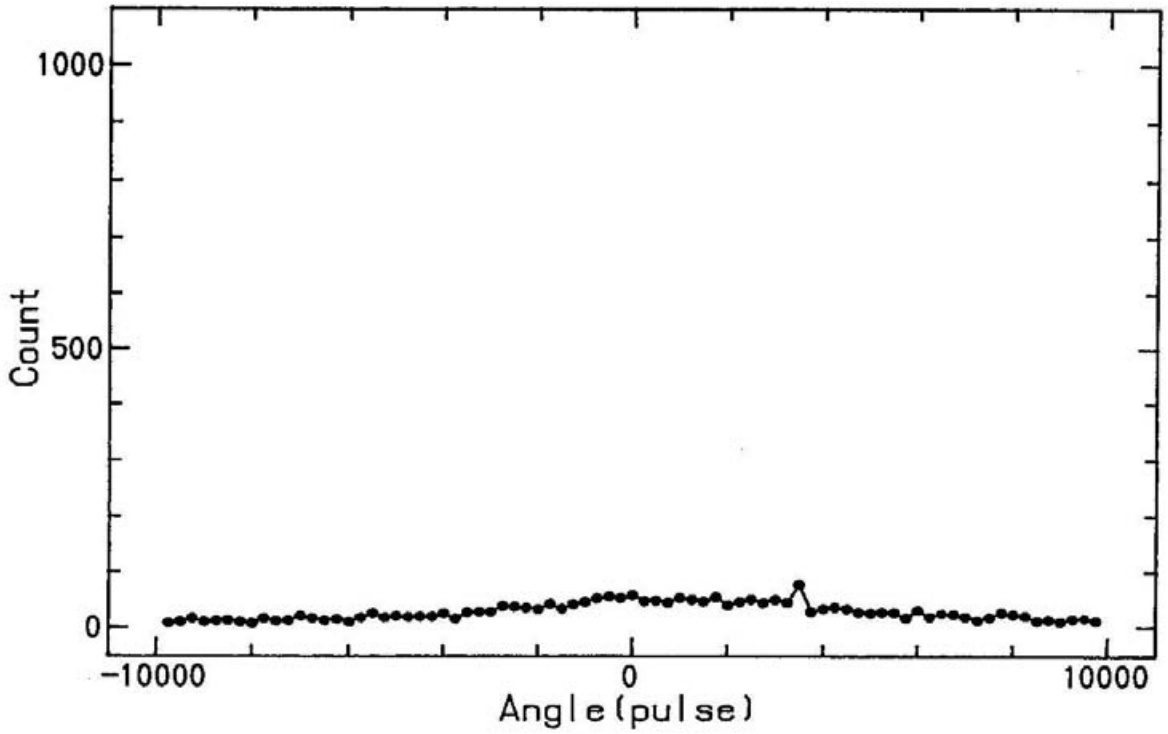

E_1 H = 0 χ = 145°

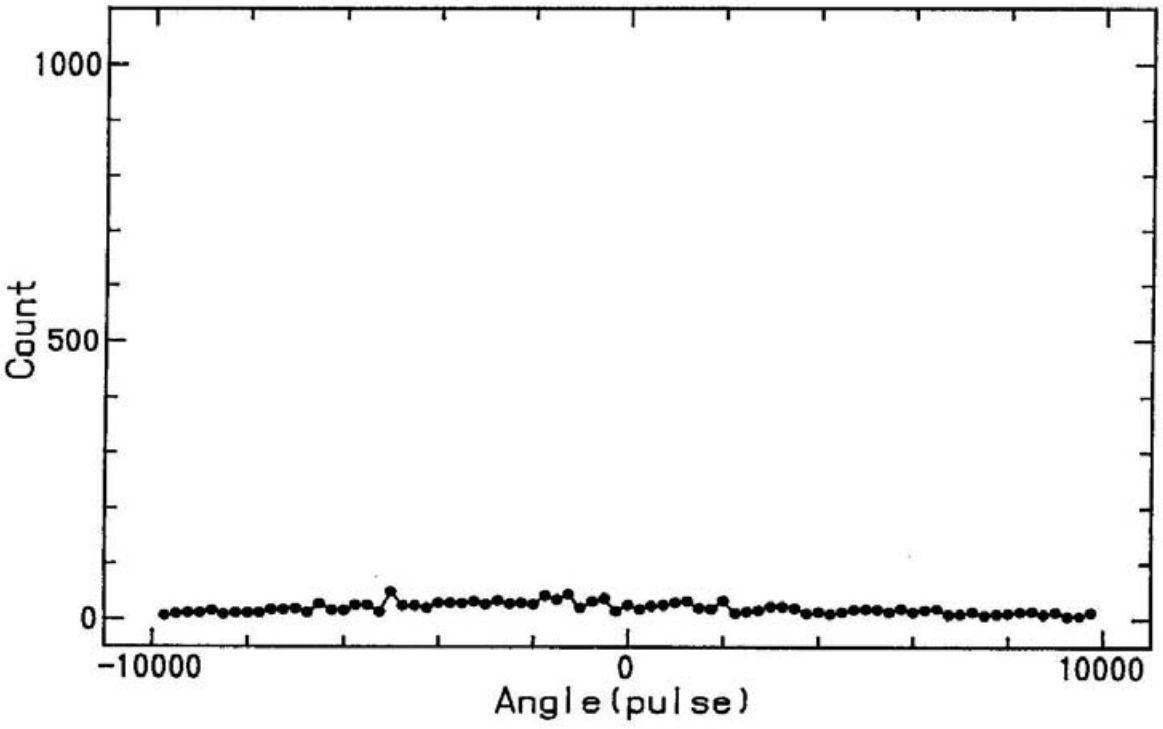

Fig-18

E_1 H = 0 χ = 150°

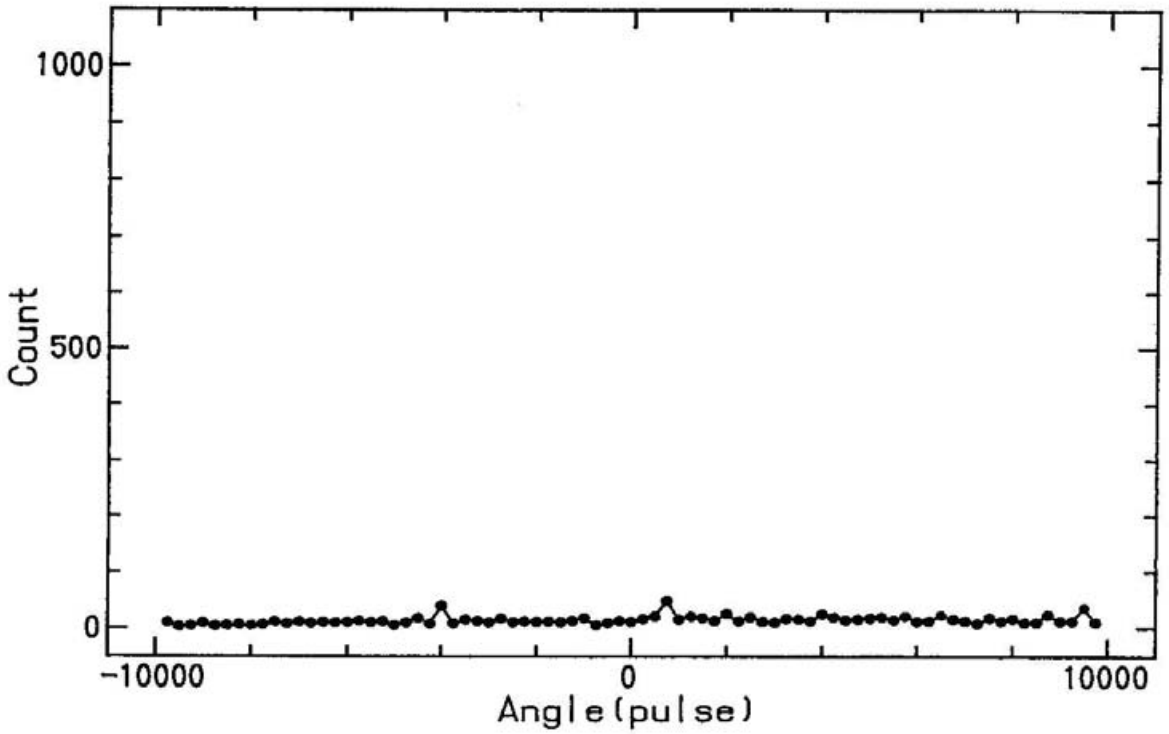

E_1 H = 0 χ = 155°

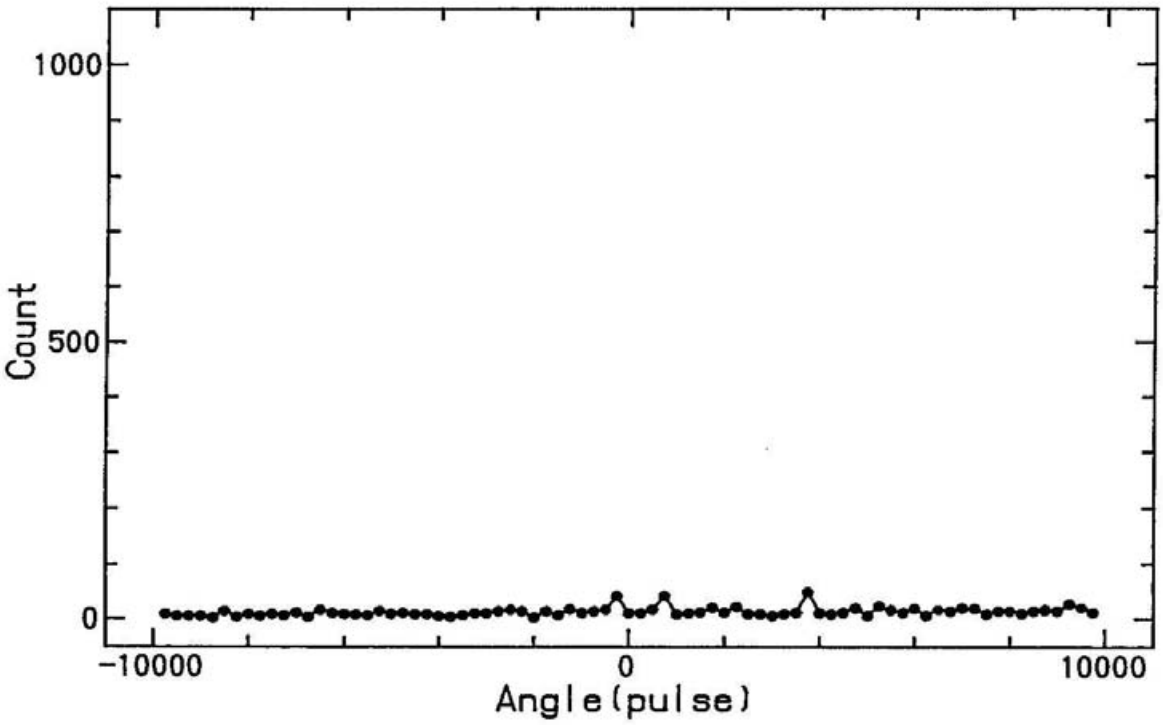

Fig-18

E_1 H = 0 χ = 160°

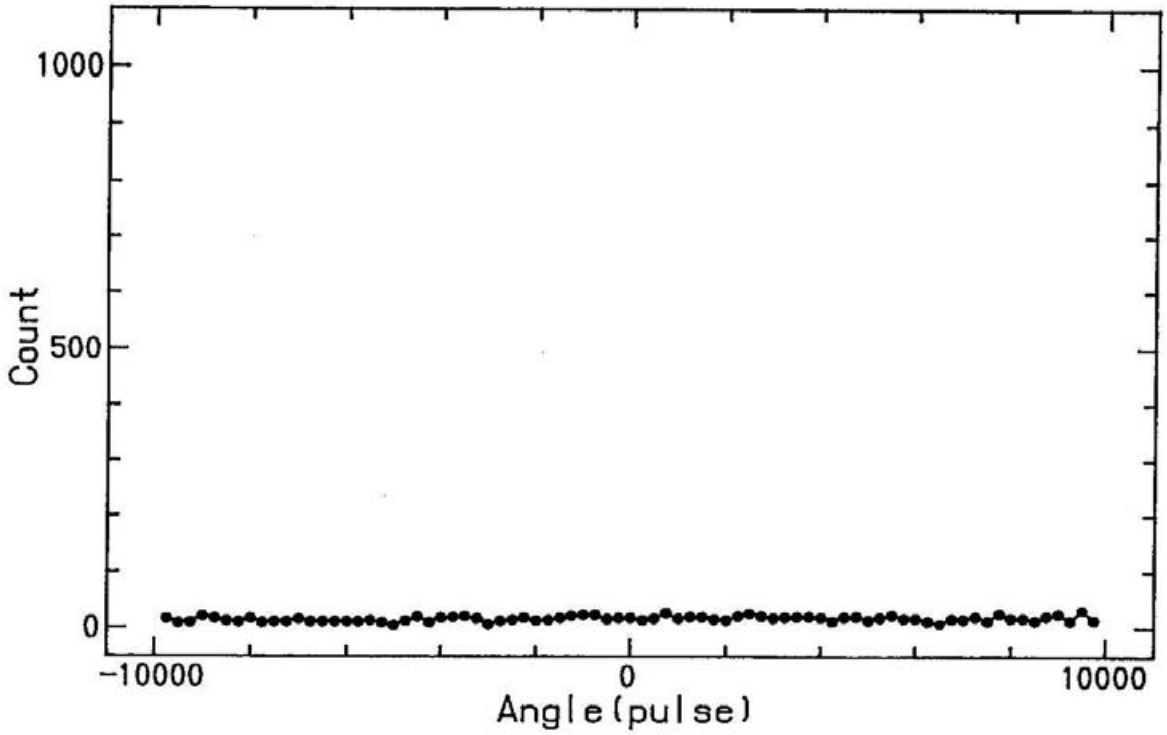

E_1 H = 0 χ = 165°

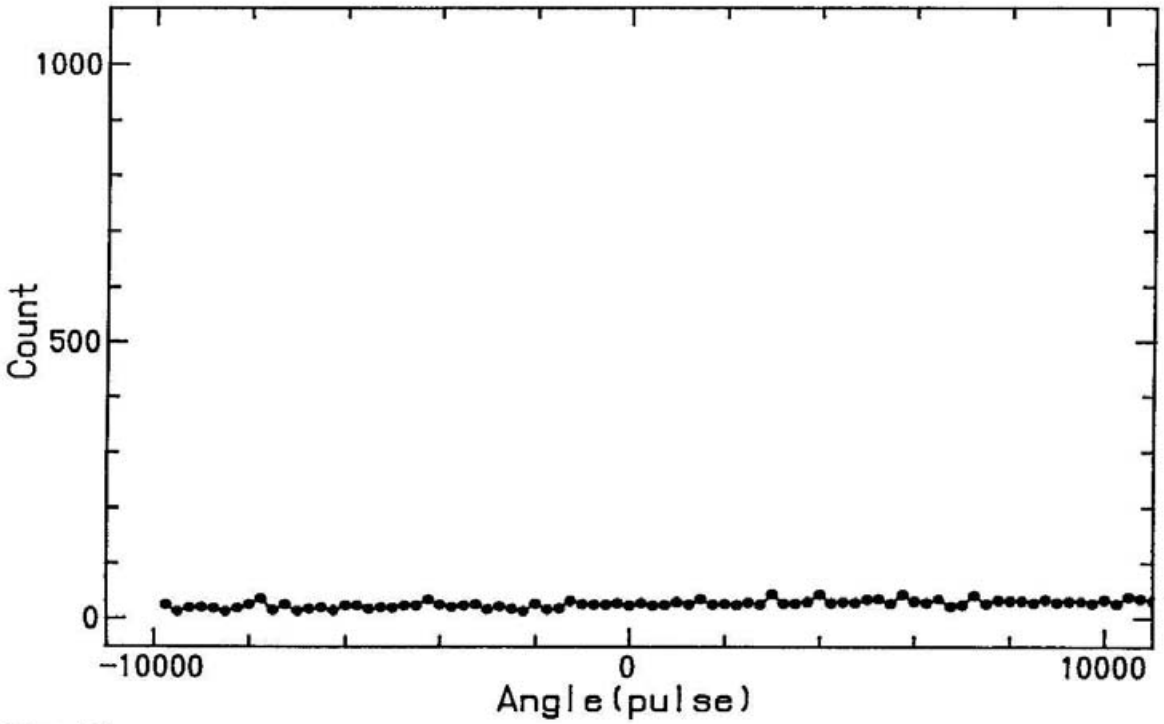

Fig-18

E_1 H = 0 χ = 170°

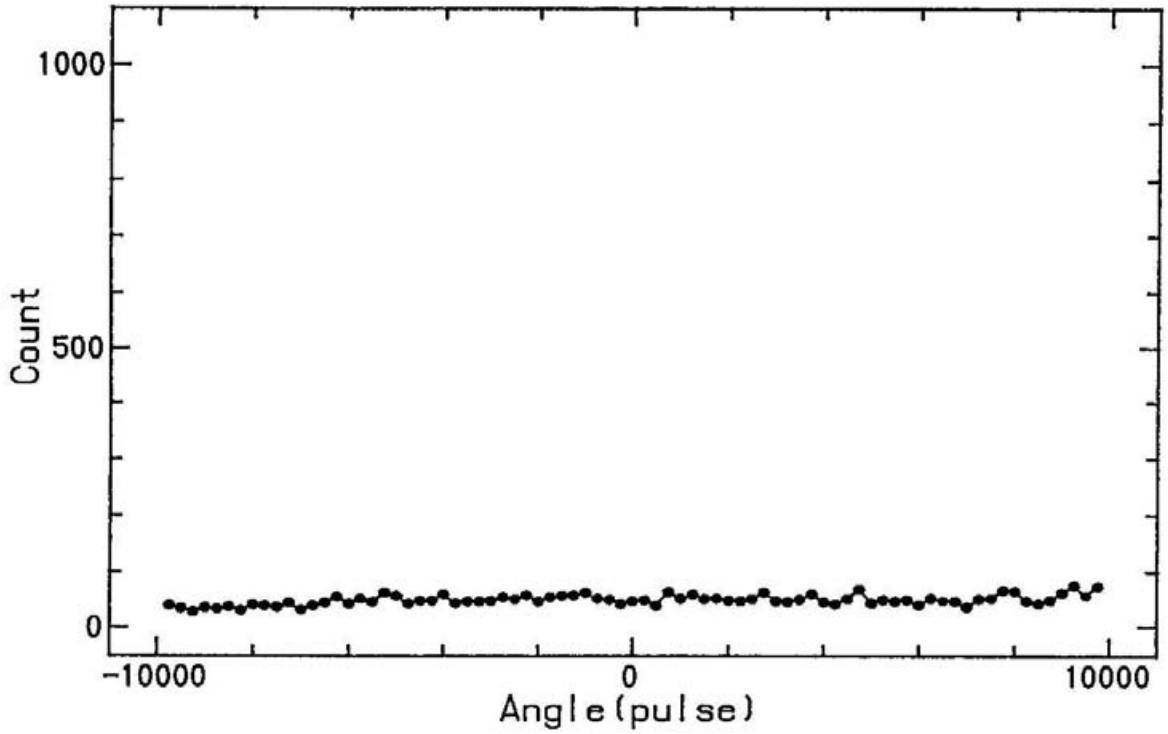

E_1 H = 0 χ = 175°

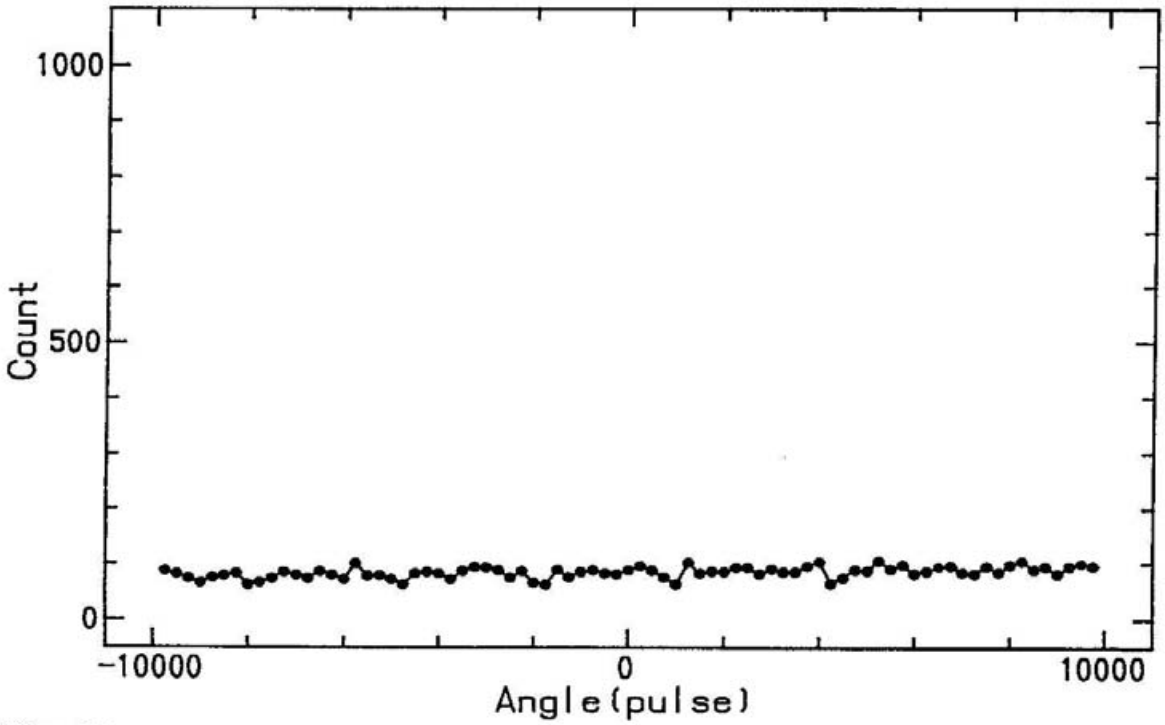

Fig-18

E_1 H = 0 χ = 180°

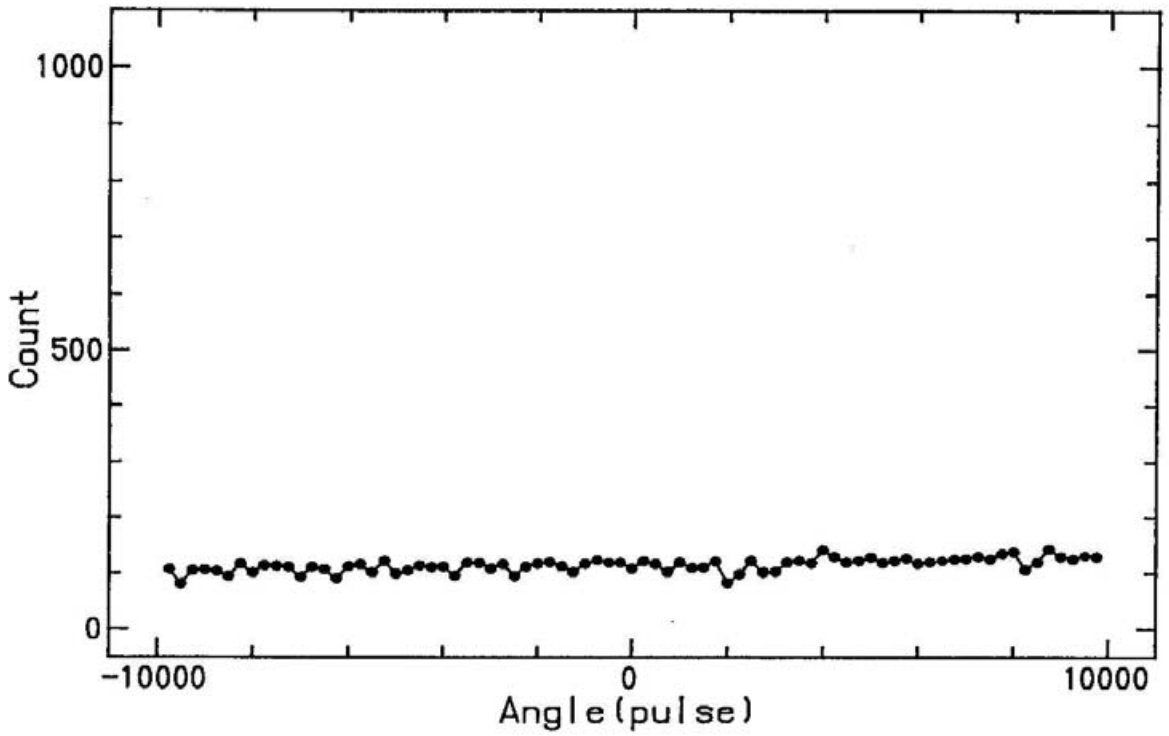

E_1 H = 0 χ = 185°

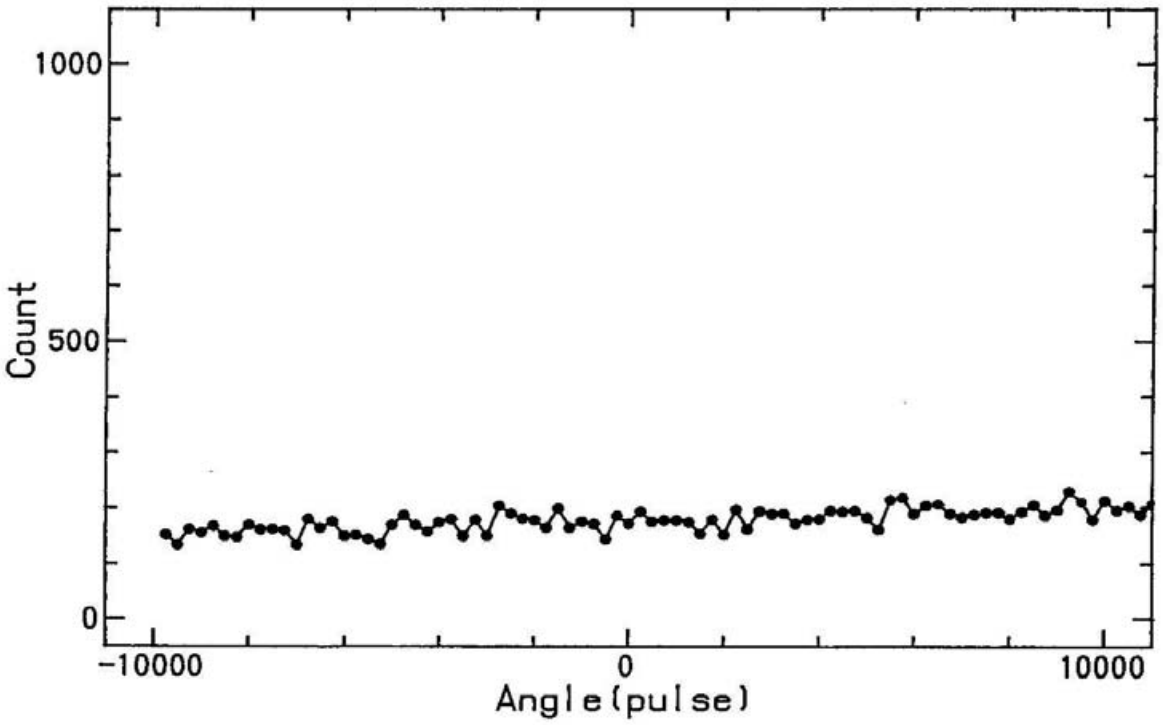

Fig-18

Gd L_2 E_1 H = 0 kG

Azimuthal angle ϕ	Integrated intensity	Back ground noise	Azimuthal angle ϕ	Integrated intensity	Back ground noise
30°		271	110°	11013	
35°			115°	9115	
40°			120°	7580	207
45°			125°	6043	
50°	18450		130°	4712	165
55°	19348	311	135°		
60°	20273		140°		97
65°	20496		145°		
70°	20392		150°		72
75°	20275				
80°	19575				
85°	18566				
90°	16970	202			
95°	15385				
100°	14377				
105°	12892				

Table-1(a)

Table 1 Raw data of the polarization analysis of the scattering X rays.

Gd L_2 E_1 H = 3 kG (↑)

Azimuthal angle ϕ	Integrated intensity	Back ground noise	Azimuthal angle ϕ	Integrated intensity	Back ground noise
30°		299	110°	11128	
35°			115°	9416	
40°			120°	7634	174
45°			125°	5913	
50°	18459		130°	5029	
55°	19297	322	135°		
60°	20395		140°		71
65°	20047		145°		
70°	20461				
75°	19892				
80°	19278				
85°	18361	227			
90°	17436	301			
95°	15760				
100°	14470				
105°	12739	211			

Table-1(b)

Gd L_2 E_1 H = -3 kG (↓)

Azimuthal angle ϕ	Integrated intensity	Back ground noise	Azimuthal angle ϕ	Integrated intensity	Back ground noise
30°		290	105°	12614	189
35°			110°	10756	
40°			115°	9095	
45°			120°	7337	
50°	18783		125°	5815	
55°	19577		130°	4306	
60°	20395		135°		
65°	20756	405			
70°	20393				
75°	20369				
80°	19425				
85°	18257				
90°	16842	302			
95°	15224				
100°	14016	173			

Table-1(c)

Gd L_2 E_2 H = 0 kG

Azimuthal angle ϕ	Integrated intensity	Back ground noise	Azimuthal angle ϕ	Integrated intensity	Back ground noise
45°		361			
50°					
55°					
60°	12446				
65°	12600				
70°	12582	460			
75°	12201				
80°	12153	405			
85°	11519				
90°	11016				
95°	9978				
100°	9387				
105°		302			

Table-1(d)

Gd L_2 E_2 H = 3 KG (↑)

Azimuthal angle ϕ	Integrated intensity	Back ground noise	Azimuthal angle ϕ	Integrated intensity	Back ground noise
40°		458	115°	8806	
45°			120°	7203	239
50°			125°	5676	
55°		353	130°	4177	
60°	19093		135°	2897	97
65°	19399		140°	1739	
70°	19503		145°	1120	
75°	19261	356	150°		101
80°	18550		155°		155
85°	17454				
90°	16426				
95°	15169				
100°	13829				
105°	12238				
110°	10250	264			

Table-1(e)

Gd L_2 E_2 H = -3 kG (↓)

Azimuthal angle ϕ	Integrated intensity	Back ground noise	Azimuthal angle ϕ	Integrated intensity	Back ground noise
40°		355	115°	8765	
45°			120°	7100	
50°			125°	5686	
55°			130°	4077	
60°	19076		135°	2901	
65°	19588		140°	1800	
70°	19534	348	145°	1065	
75°	19034		150°		
80°	18720		155°		
85°	17388		160°		120
90°	16825				
95°	15086				
100°	13633	356			
105°	12038	267			
110°	10380				

Table-1(f)

Gd L_2 E_3 H = 3 kG (↑)

Azimuthal angle ϕ	Integrated intensity	Back ground noise	Azimuthal angle ϕ	Integrated intensity	Back ground noise
35°		282	115°	9633	
40°			120°	7610	
45°			125°	5772	
50°			130°	4059	
55°			135°	2623	
60°	27410		140°	2674	
65°	27556		145°		
70°	26076		150°		120
75°	25534		155°		142
80°	23734				
85°	21993				
90°	19895				
95°	17660				
100°	15953				
105°	13968	203			
110°	11620	221			

Table-1(g)

Gd L_2 E_3 H = -3 kG (↓)

Azimuthal angle ϕ	Integrated intensity	Back ground noise	Azimuthal angle ϕ	Integrated intensity	Back ground noise
30°		241	115°	11346	134
35°			120°	9160	152
40°			125°	7403	
45°			130°	5594	
50°			135°	3866	
55°			140°	2509	
60°	27127		145°		
65°	27038		150°		
70°	26811		155°		
75°	24974		160°		117
80°	23603				
85°	22026	206			
90°	19710				
95°	21700				
100°	17146				
105°	15604				
110°	13675				

Table-1(h)

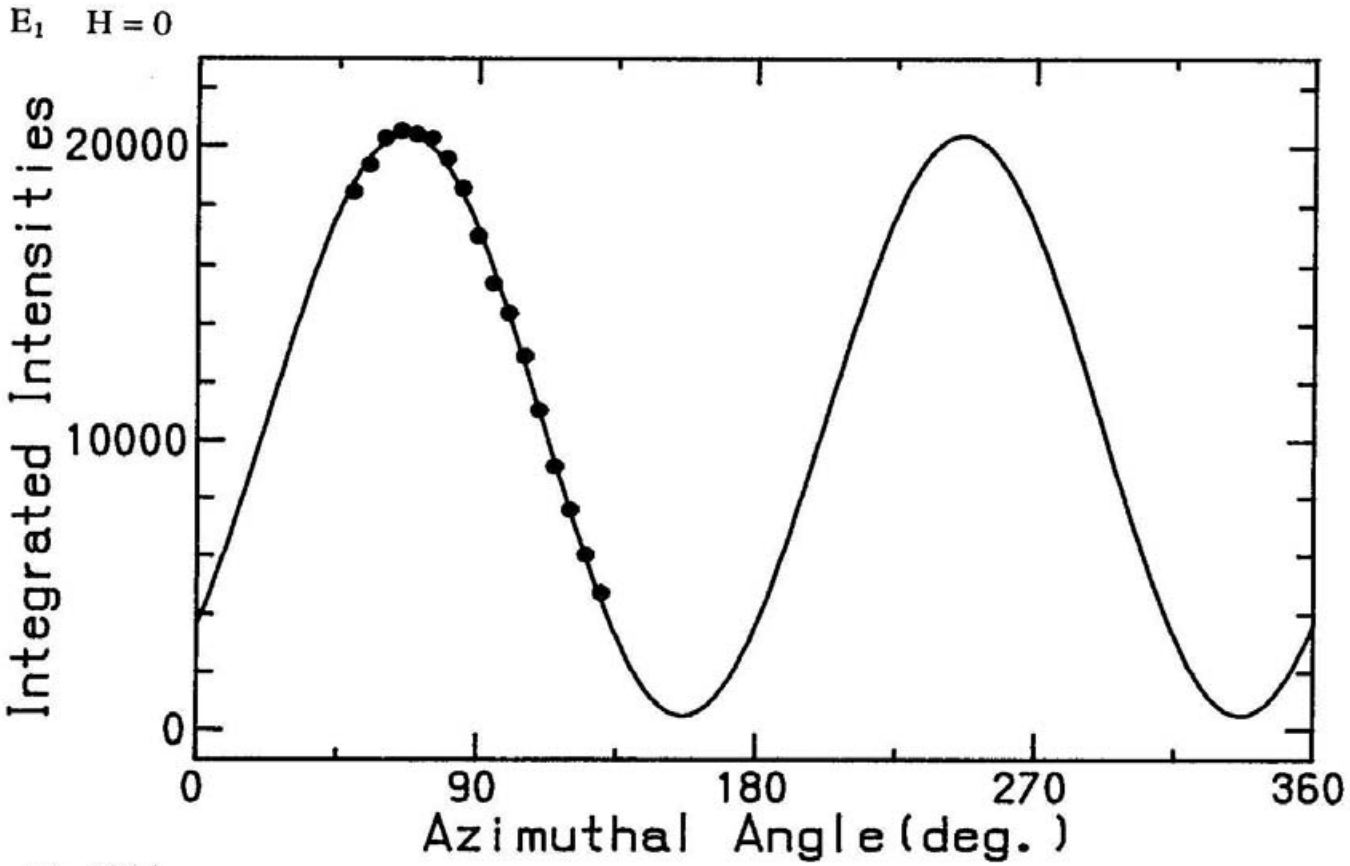

Fig-19(a)

Fig.19 The intensity variation of the scattered X rays.

E_1 H = 3kG

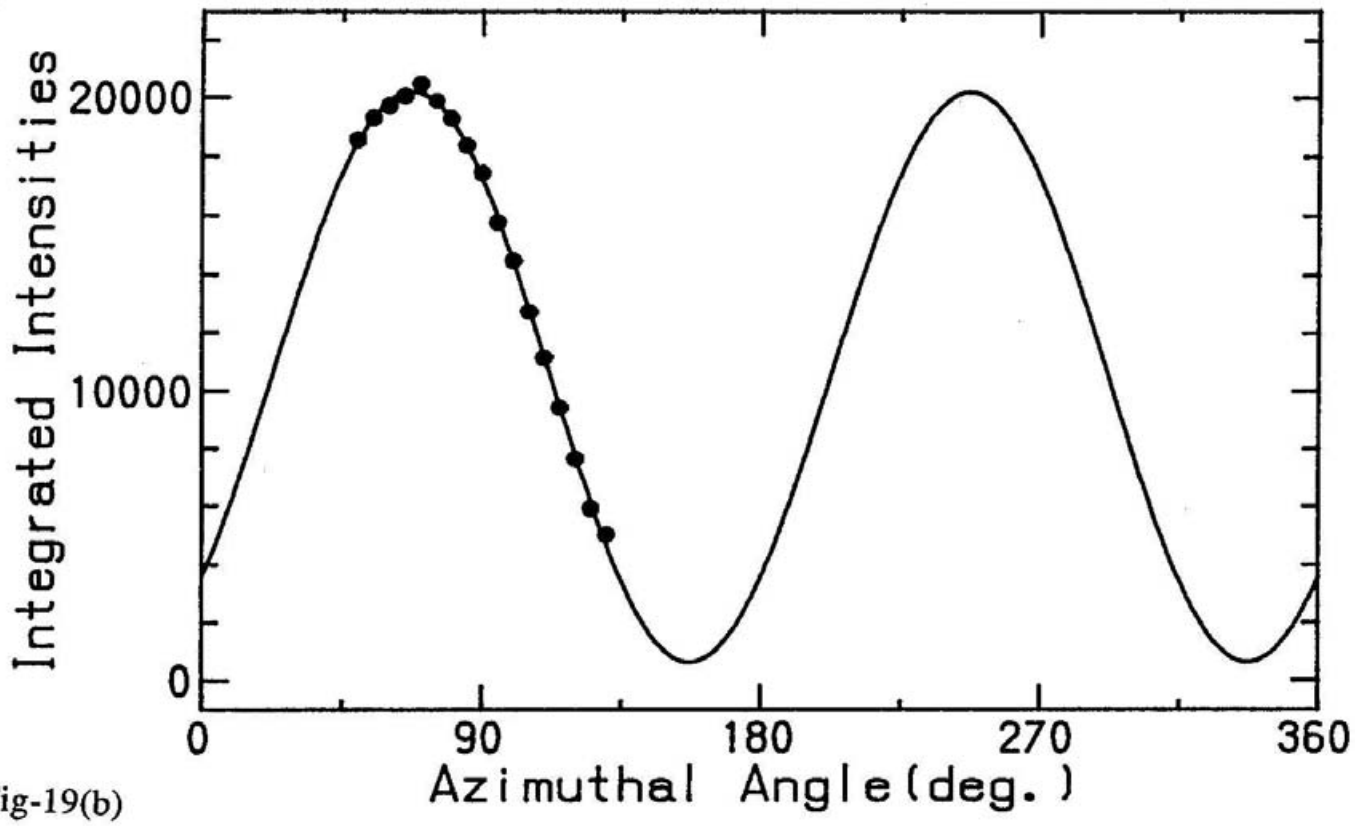

Fig-19(b)

E_1 H = -3kG

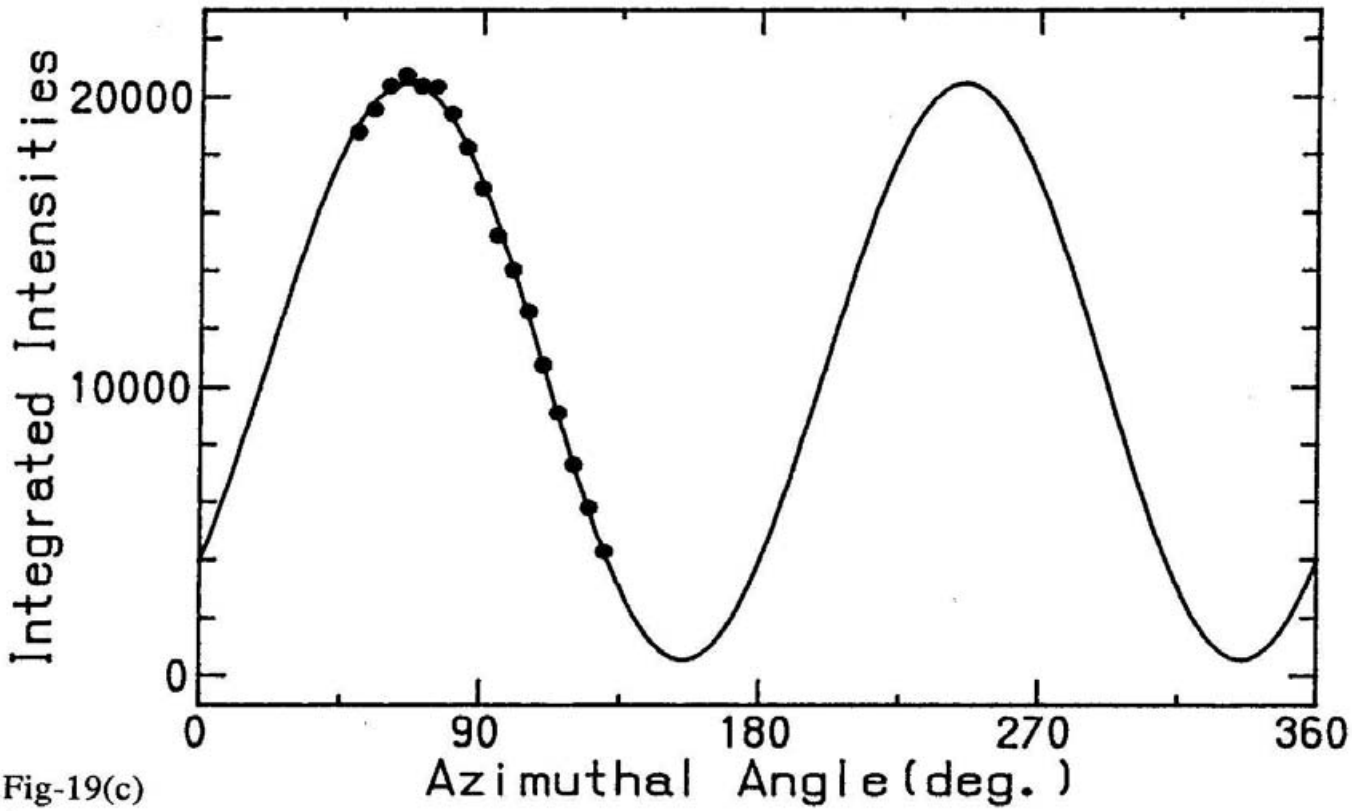

Fig-19(c)

2 H = 3kG

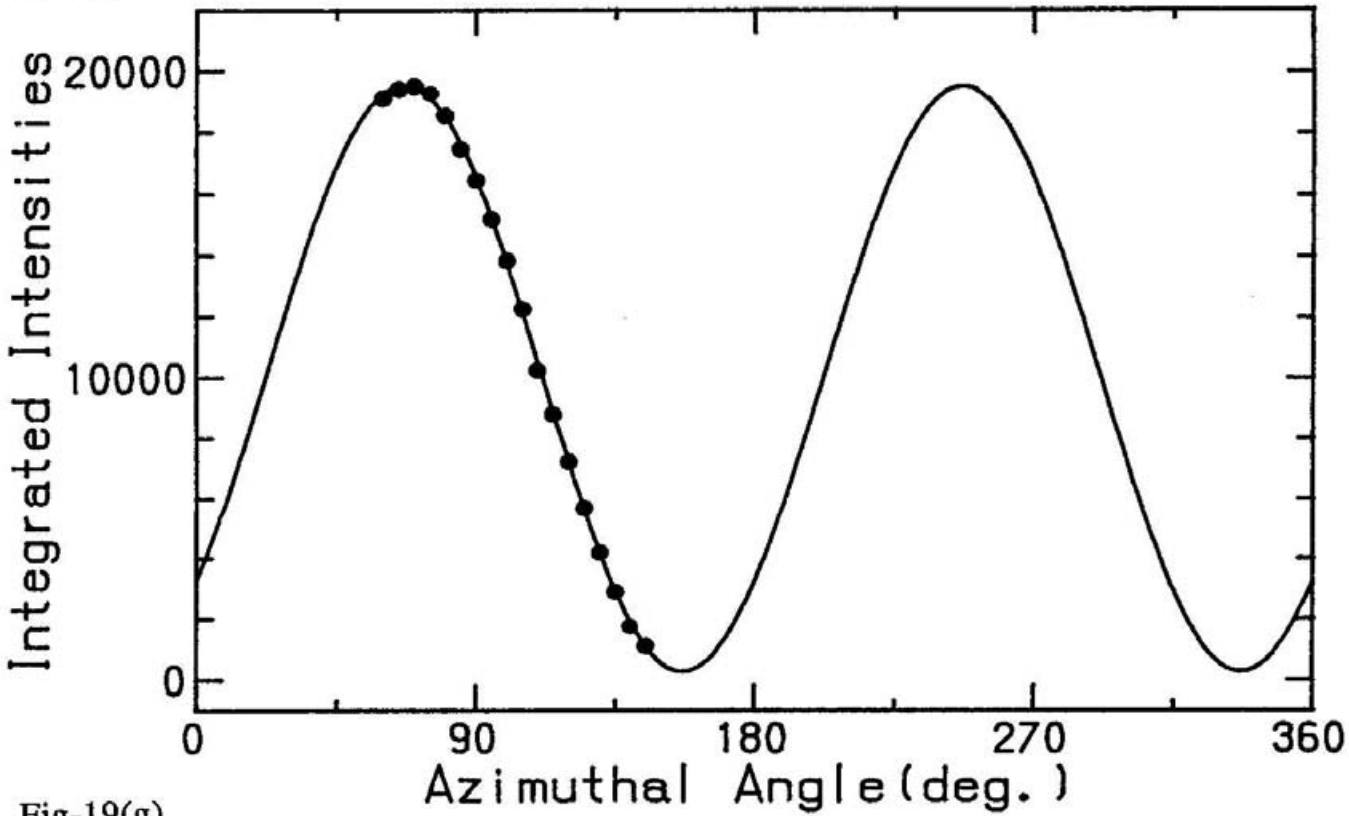

Fig-19(g)

2 H = -3kG

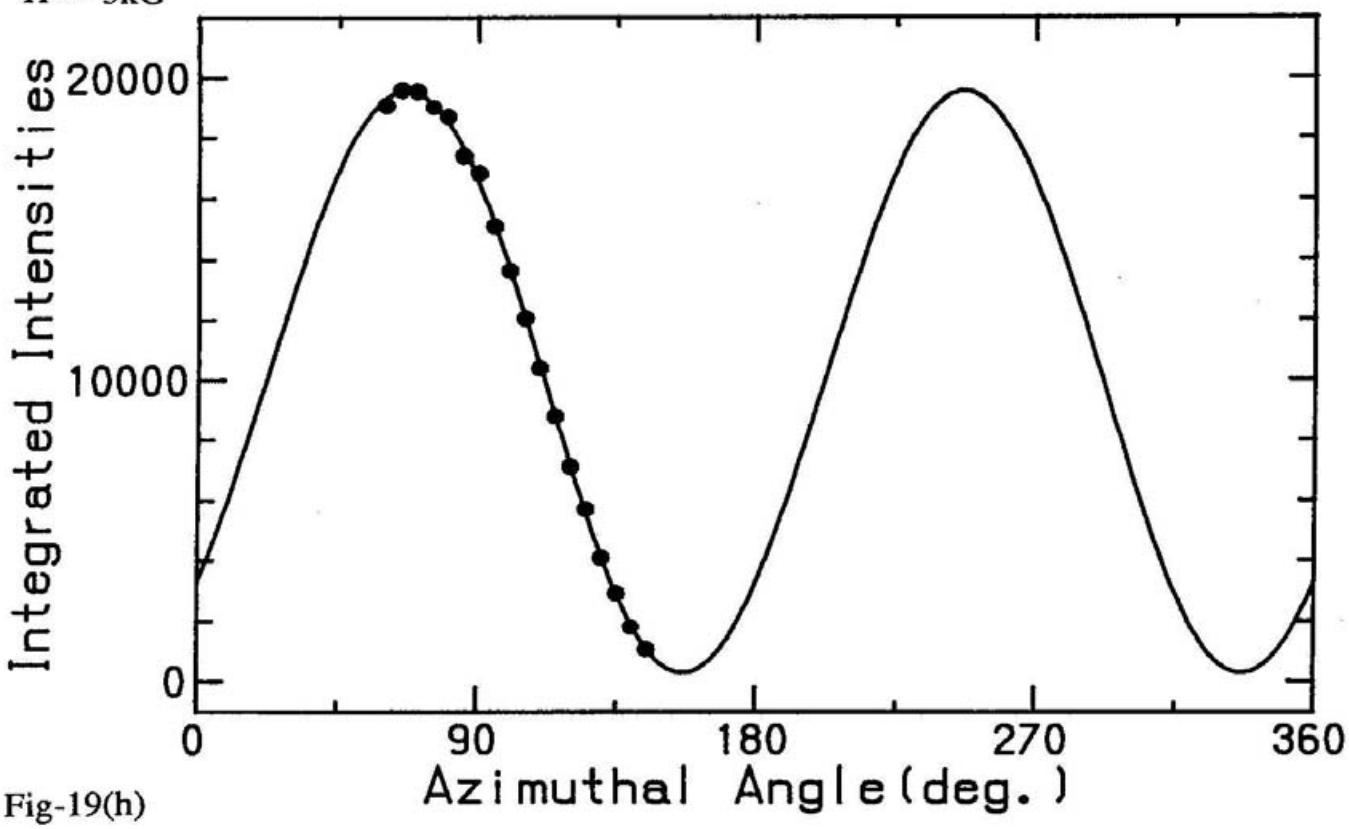

Fig-19(h)

E_3 H = 3kG

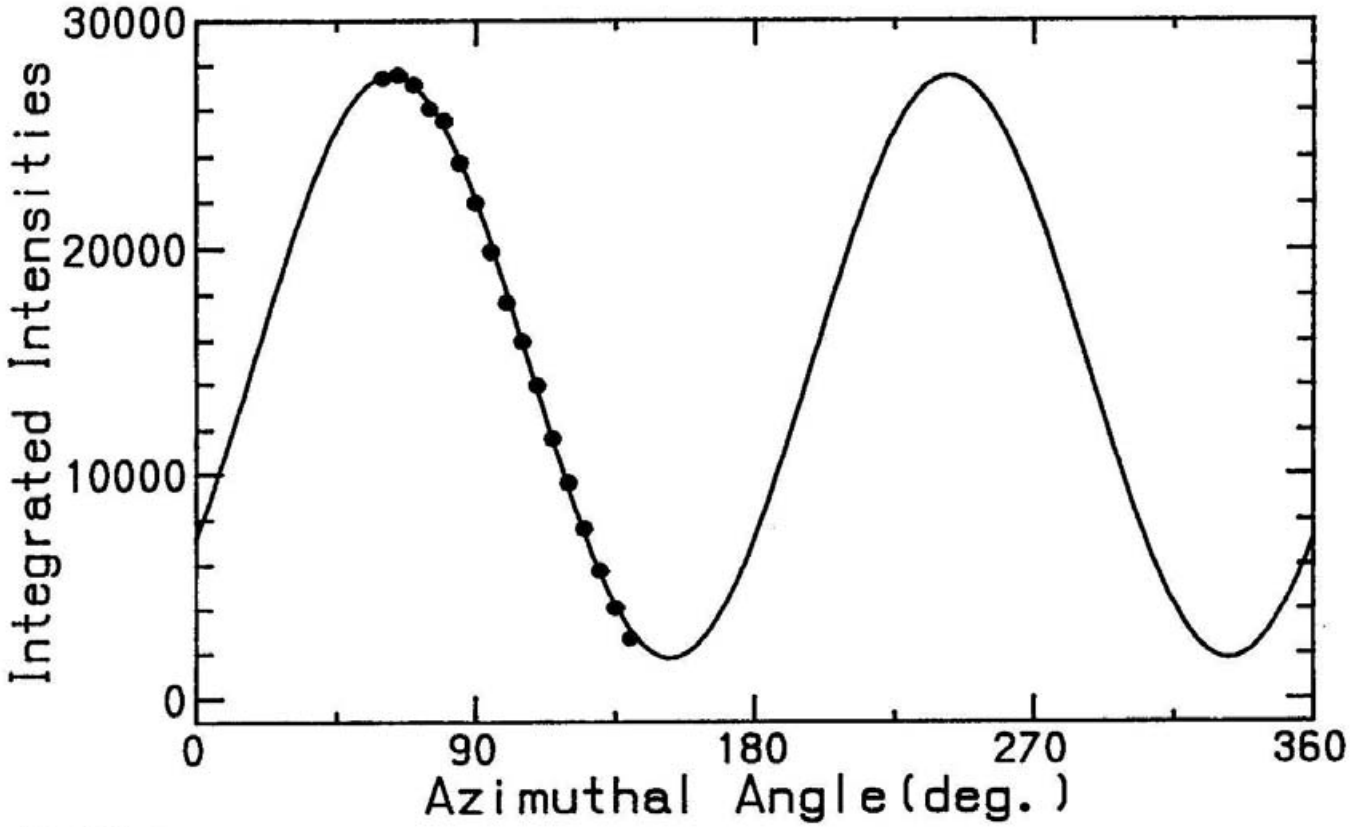

Fig-19(e)

E_3 H = -3kG

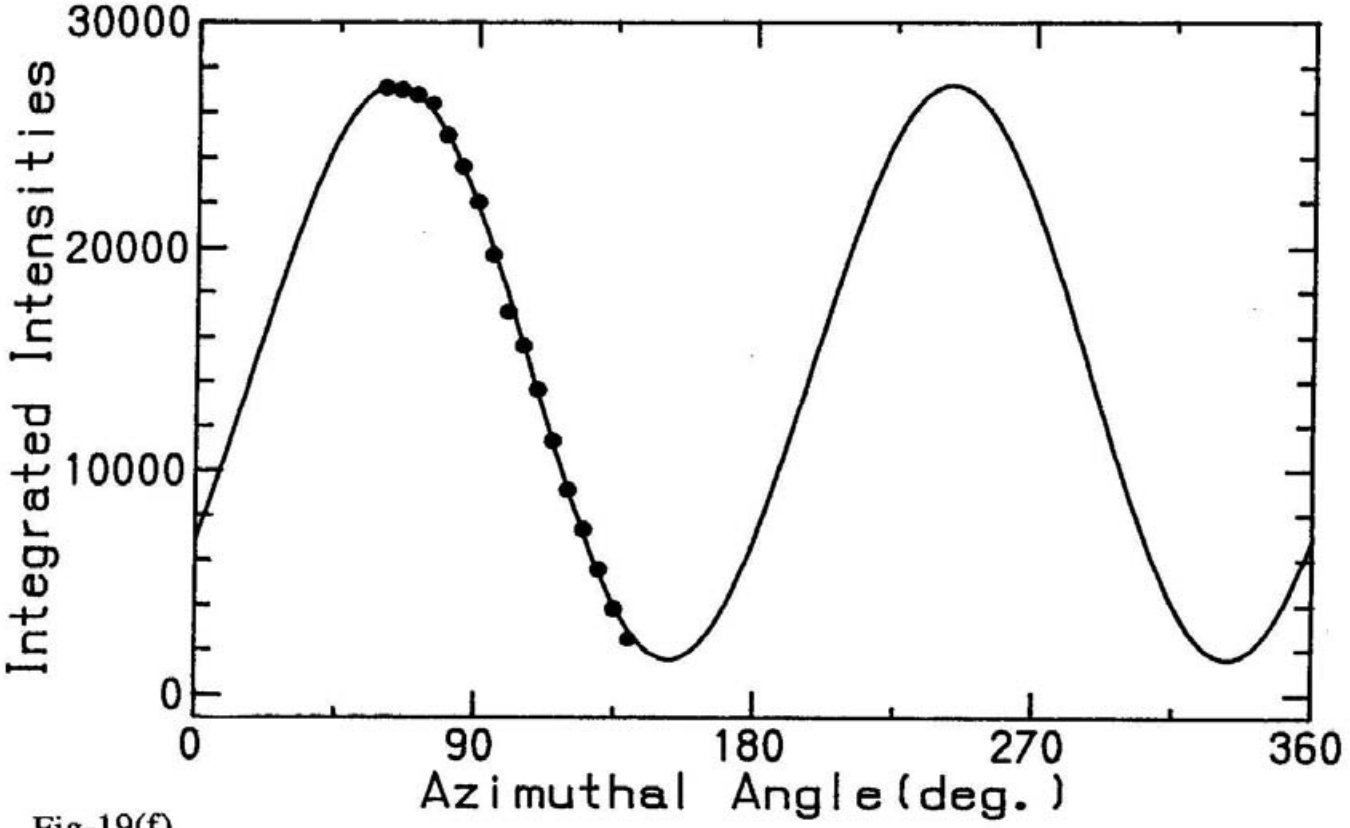

Fig-19(f)

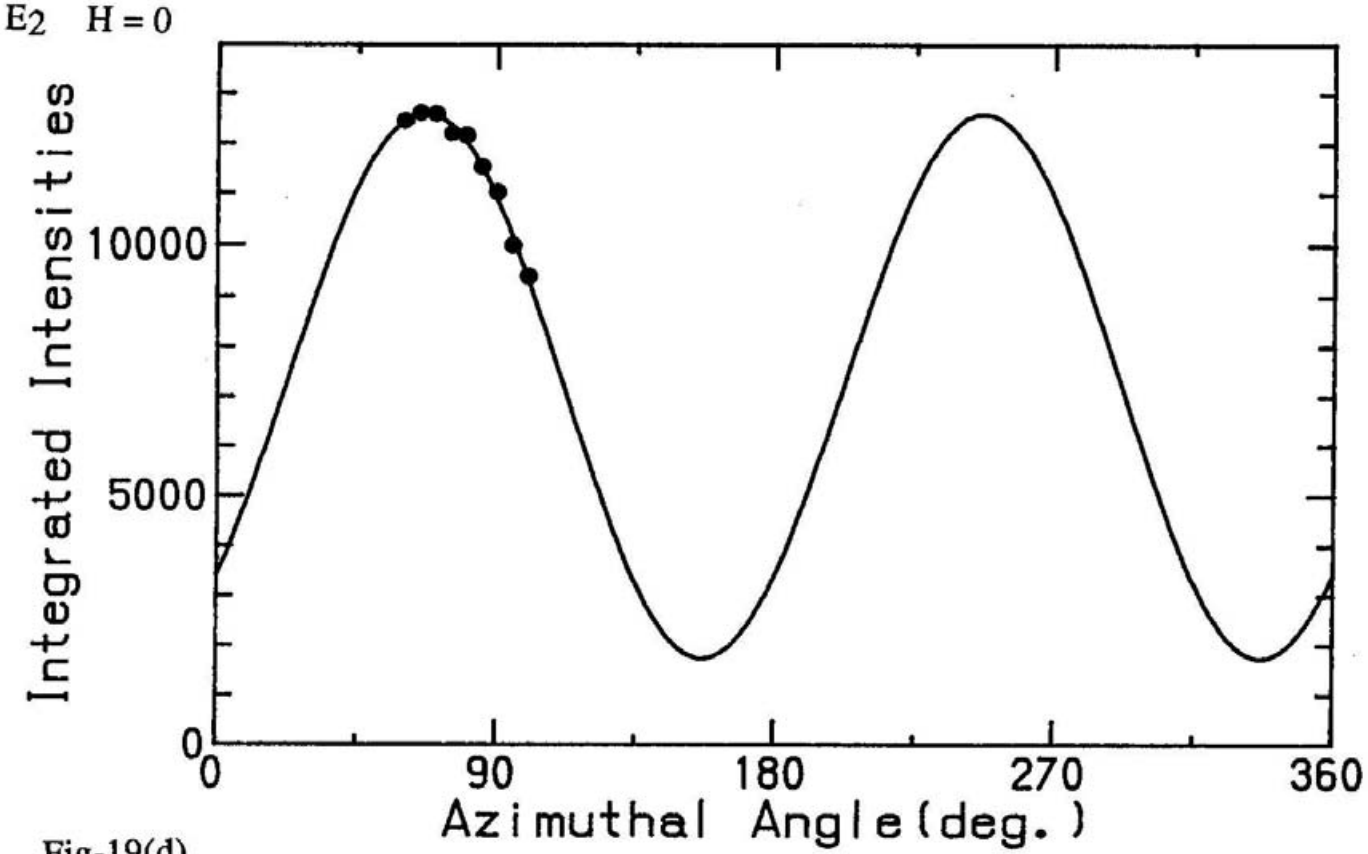
E2 H = 0
Integrated Intensities
10000
5000
0
0
90
180
270
360
Azimuthal Angle(deg.)

Fig-19(d)

Results and Discussion

As shown in Fig.16, the orientation of the plane of polarization of the incident beam was found to be 44.8°. The maximum value of the fitted profile was about 4.9×10^6 counts and the minimum value of the fitted profile was about 1.5×10^4 counts.

The orientation of the major axis of the scattered beam ($\alpha+\Delta\alpha^{\downarrow}$,$\alpha+\Delta\alpha^{\uparrow}$, α) was obtained from the fitted profile from Fig.19(a) to Fig.19(h), as shown in Table 2(a). The rotation ($\Delta\alpha^{\downarrow}$,$\Delta\alpha^{\uparrow}$,$\Delta\alpha$) obtained from the fitted profile is shown in Table 2(b).

The ellipticity ratio was calculated from the maximum and minimum value of the fitted profile, as shown in Table 3.

The observed rotation $\Delta\alpha$ (closed circle) and the estimated rotation due to X-ray magnetic Kerr effect (open circle) is plotted in Fig.20(a) and the fluorescent X-ray spectrum is shown in Fig.20(b). The ordinate in Fig.20(a) denotes the rotation of the major axis, while the ordinate in Fig.20(b) the relative intensity of the fluorescent X rays. The abscissas of both figures denote the energy of the incident X rays, which are measured from the absorption edge.

A channel-cut crystal is used as a polarizer device. Because many Laue-spots are subject to appear, the unwanted components are mixed into the beam to be used as the incident beam. The energy of those unnecessary components are different from that of the primary one by about 140eV, -40eV and -240eV. Among the three the middle component is diffracted by the sample crystal. Its contribution to the total diffracted intensity is estimated about one tenth of that of the primary one. However, there is little or no spin polarization below

	-3 kG ($\alpha+\Delta\alpha^{\downarrow}$)	0 kG (α)	3 kG ($\alpha+\Delta\alpha^{\uparrow}$)
E_1	65.7°	66.7°	67.2°
E_2	66.6°	66.8°	66.8°
E_3	62.8°		62.8°

Table-2(a)

	$\Delta\alpha^{\downarrow}$	$\Delta\alpha^{\uparrow}$	$\Delta\alpha$
E_1	-1.0°	0.5°	1.5° (±0.2)
E_2	-0.2°	0°	0.2° (±0.2)
E_3			0° (±0.3)

Table-2(b)

(a) The orientation of the plane of the polarization (α) and the orientation of the major axis ($\alpha+\Delta\alpha^{\downarrow}$, $\alpha+\Delta\alpha^{\uparrow}$) . (b) The rotation of the major axis.

E_1

H	-3 kG	0 kG	3 kG
max	2.0330×10^4	2.0240×10^4	2.0380×10^4
min	$3.85\ \times10^2$	$3.34\ \times10^2$	$4.53\ \times10^2$
R	0.05±0.01	(0)	0.08±0.01

E_2

Ç	-3 kG	0 kG	3 kG
max	1.9410×10^4	1.728×10^4	1.9370×10^4
min	$1.23\ \times10^2$	$1.11\ \times10^2$	$1.16\ \times10^2$
R	$0.03\ ^{+0.01}_{-0.03}$	(0)	$0.02\ ^{+0.01}_{-0.02}$

E_3

H	-3 kG	0 kG	3 kG
max	2.7110×10^4		2.7350×10^4
min	$1.445\ \times10^3$		$1.670\ \times10^3$
R			

Table-3

The maximum value, the minimum value and the ellipticity ratio of the fitted profile

40eV from the edge. The impure component has only a little influence on the rotation of the major axis.

The value P_L in the equation (19) is about 0.94 at the polarization analysis of the incident beam. The non-polarized component in the SR beams are almost changed into 45 degrees linearly polarized X rays by the polarizer. Then the intensity of the non-polarized component in the incident beam to the sample is 10^{-5} of the linearly polarized one. Therefore we can ignore the intensity of the non-polarized component in the incident beams. The measured polarization ratio is about 3×10^{-3}. This value approximately agrees with the estimation. The measured polarization ratio also agree with the estimation in the case of the polarization analysis at L_2-absorption edge.

As shown in Fig.16, the value of the inclination agrees well with the theoretical estimation. The intensity near the maximum is lower than that of the fitted profile. These data may include the counting loss because of the high counting rate. The experimental data agree well with the fitted profile except for the maximum region. Neglecting the effect of the counting loss, the intensity variation with an azimuthal angle agrees well with the equation (21). The intensity takes the maximum at 45 degrees in azimuthal angle. The minimum value of the intensity is equal to zero. Thus it was confirmed that the 45 degrees linearly polarized X-ray was produced by a polarizer.

In the case of the polarization analysis of L_2-absorption edge, the Bragg angle at the polarizer are about 44.83° at E_1, 44.81° at E_2 and

44.86° at E_3, respectively. The polarization ratio for the two reflections comes up to 10^{-5} so that the incident X rays from the polarizer is the linearly polarized X rays. The accuracy of the measurement in the orientation of the plane of polarization is about 0.2°. The measured rotation of the major axis is 1.5° at E_3. This value is significant.

As shown in Fig. 20, the measured rotation $\Delta\alpha$ agrees with the estimated value at E_1. The measured rotation $\Delta\alpha$ differs from the estimated value at E_2 and E_3. At E_2, the difference is explained if we assume a smaller value of $\{d(Ra) / d\omega\}$.

From the equation (21), the calculated value of the orientation α is about 67.4° at E_1, E_2 and E_3. As shown in Table 2(a), the measured orientation approximately agreed with the calculation at E_1 and E_2. At E_3 , the value of the orientation α is probably 62.8°. The measured orientation α is smaller than that of the calculated one by 4.6°. Below the absorption edge, theoretically, the calculated value of the rotation is expected to be negative. However, the experimental value is positive at E_3. It is well known that the calculated X-ray magnetic circular dichroism(XMCD) of gadolinium at L_2 and L_3-absorption edges is considerably different from the experimental one.[13,14] A similar situation has been found in the measurement of the " flipping ratio "[15]. The disagreement is explainable by a contribution of quadrupole transition. In the similar way the discrepancy observed in the X-ray magnetic Kerr rotation can also be attributed to the quadrupole transition. Because the 4f-vacant band appears below the edge (in the 5d-filled band) at the resonance, the large value of $d(\Delta\rho)/d\omega$ is expected below the edge.

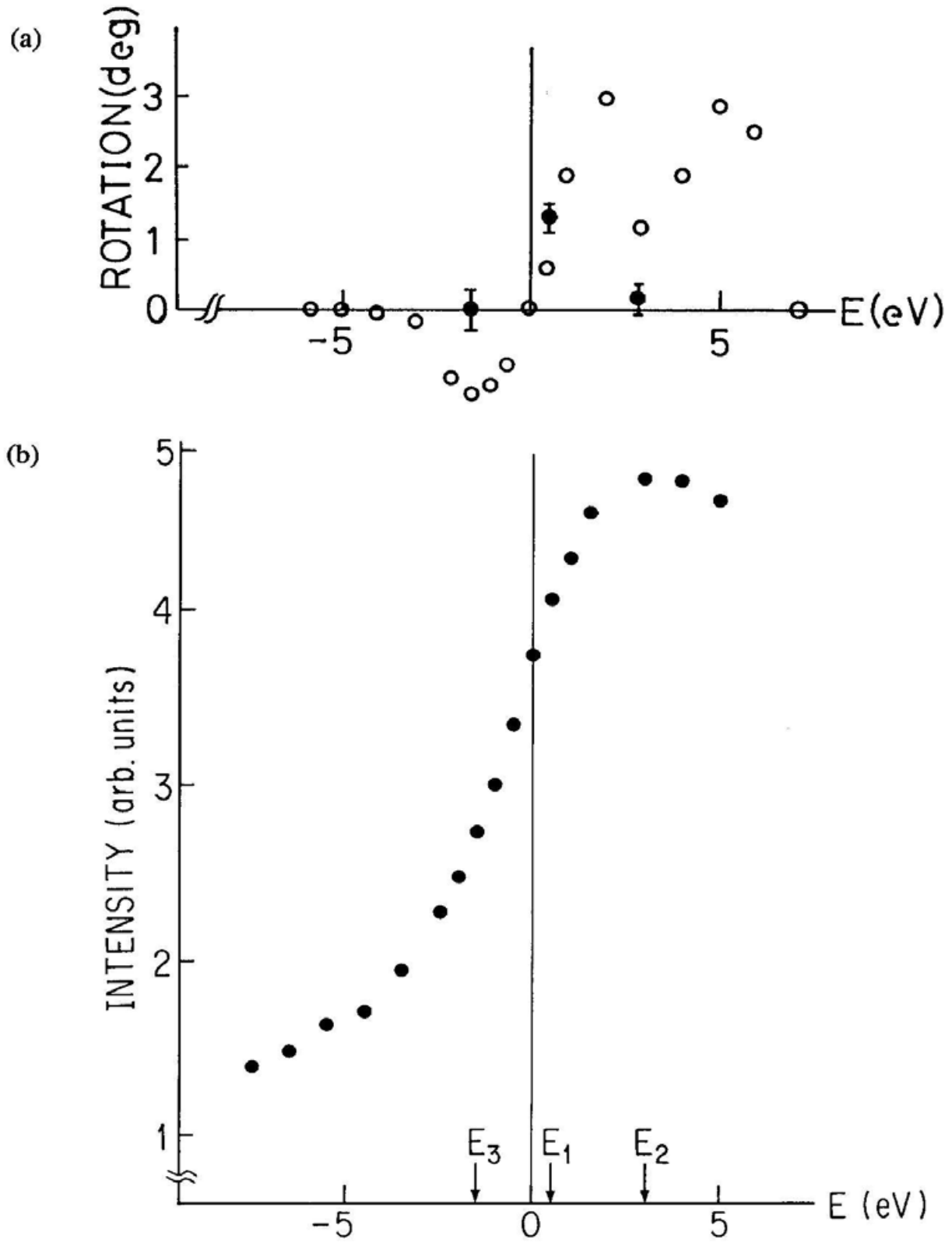

Fig.20 (a)The experimental(⧳) and calculated values(o) of the rotation $\Delta\alpha$. The maximum rotation is estimated about 3 degrees. In the ordinate, the energy 0 means the position of the Fermi energy. (b)Relative intensity of the florescent X rays.

Polarization dependence of the scattering amplitude which includes the contribution of the quadrupole transition is approximated as follows,

$$f \cong (f_0 + f' + if'') \begin{pmatrix} 1 & 0 \\ 0 & \cos 2\theta \end{pmatrix} + f_3 \begin{pmatrix} \cos 2\theta & 0 \\ 0 & 2\cos^2 2\theta - 1 \end{pmatrix},$$

where the complex number f_3 means the scattering amplitude of the quadrupole transition. A contribution of the quadrupole transition is estimated comparable to that of the dipole transition[3]. We estimate the relative magnitude of the quadrupole transition as shown in Fig.21. The abscissa denotes the orientation of plane of the polarization and the ordinate denotes the amplitude ratio of the dipole transition to the quadrupole transition. If we take the assumption that the magnitude of the quadrupole transition is about 30% of that of the dipole transition, the calculated orientation of the plane of polarization agrees well with the measured result.

As shown in Table 2(b) , the magnitude of the measured rotation $|\Delta\alpha^{\uparrow}|$ is not equal to that of the $|\Delta\alpha^{\downarrow}|$. We changed the magnetic field up to zero under the low temperature. It is considered that the value α is inclined to the value $(\alpha + \Delta\alpha^{\uparrow})$ by residual magnetization of the sample.

In the case of the electric scattering ($E=E_2$, $H=0$), the minimum value of the intensity is supposed to be zero. However, it does not become zero in the fitted profile as shown in Table 3. This may be due to contributions of the back ground noises. They have no influence on

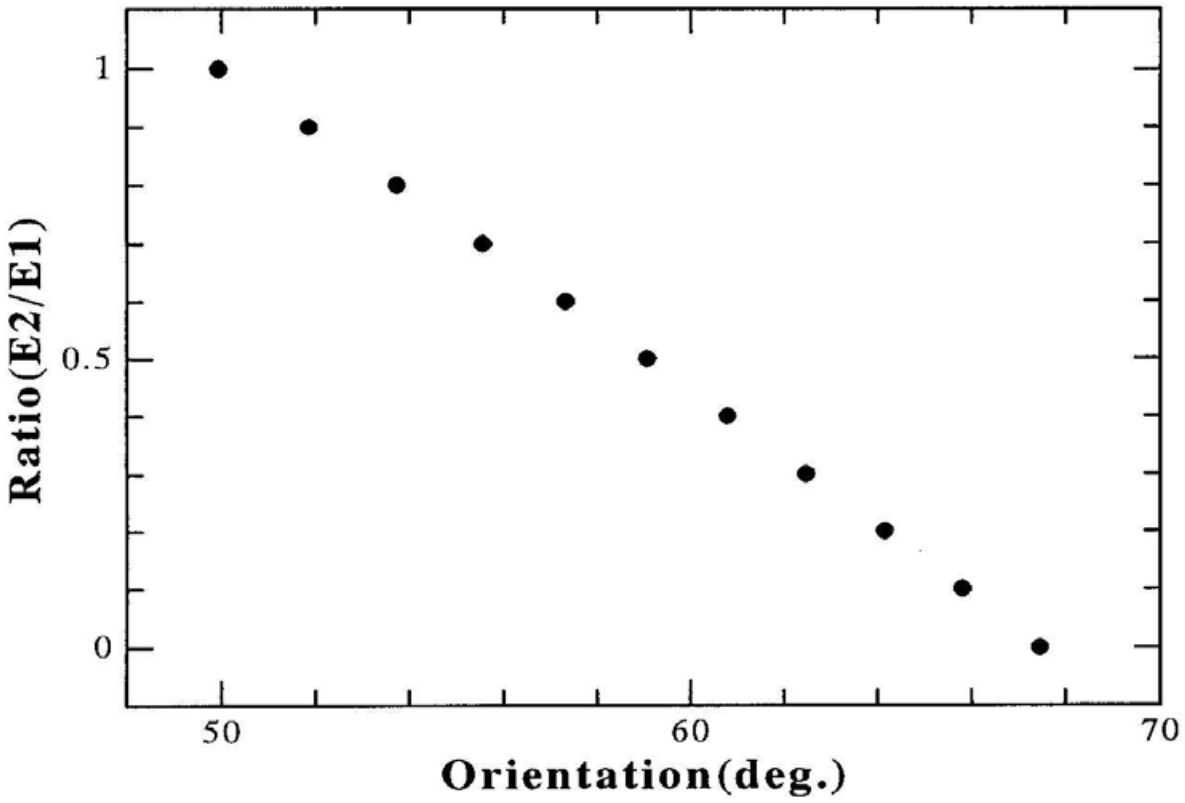

$f_0 = 43.20$

$f' = -14.83$ [16]

$f'' = 8.09$

$2\theta = 65.47°$

Fig. 21 The relative magnitude of the quadrupole transition. The abscissa denotes the orientation of plane of the polarization and the ordinate denotes the amplitude ratio of the quadrupole transition to the dipole transition.

the rotation of the major axis. When we set the minimum value to be zero, then the measured intensity variation agrees well with the theory. The difference in the minimum intensity between the electric scattering and the resonant magnetic scattering (resonant exchange scattering) is considered as an intensity due to the circularly polarized X rays.

In the X-ray magnetic Kerr effect, the rotation $\Delta\alpha$ is large compared to the Faraday rotation. In the X-ray Faraday effect, it is difficult to observe a rotation as large as that of the X-ray magnetic Kerr effect. The amount of the Faraday rotation is proportional to the sample thickness. The intensity of the transmitted X rays become lower above the absorption edge. The X-ray magnetic Kerr effect is applicable to measurement of the sample which needs a strong magnetic field to saturate. It is also applicable to the measurement of a sample which has the large neutron absorption cross section.

As a future plan, it is necessary to confirm the following relation. (1) The maximum rotation $\Delta\alpha$ takes place about 2eV above the edge. The amount of the maximum rotation estimated is a few degrees. (2) The sign of the rotation in the L_2 edge is opposite to that of the L_3 absorption edge.

The polarization ratio (the intensity ratio of the π to σ) of the present data comes up to $10^{-3} \sim 10^{-5}$. In other energy, this value becomes insufficient, because a channel-cut crystal is used in this system as a polarizing device. When we study other absorption edges, we need change the polarizing crystal. Since it is less convenient to use such one, it is efficient to use a tunable polarizer in order to improve the

polarization ratio. Using a double crystal tunable polarizer, we can also suppress higher harmonics and noises.

In the case of the zero magnetic field, the orientation of plane of the polarization is unsettled by the residual magnetization of the sample. If the sample crystal is magnetically saturated up or down, there is nothing to worry about the residual magnetization of the sample. We ought to measure the rotation $\Delta\alpha$ instead of the rotation $\Delta\alpha^{\uparrow}$ and $\Delta\alpha^{\downarrow}$. In the measurement of the rotation $\Delta\alpha$, we slowly change the strong magnetic field up to down or down to up.

Conclusion

(1) The design, the construction and the commissioning of a novel instrument for polarization analysis using 45 degrees linearly polarized incident X rays were successfully performed.

(2) The first successful measurement of X-ray magnetic Kerr rotation at Gd L_2 absorption edge using a Gd single crystal was made at 140K. The phase difference of the fitted profiles between the magnetic field of 3 kG up and down was observed. The amount of the measured X-ray magnetic Kerr rotation is 1.5 degrees with precision of 0.3 degrees.

(3) It has been proved that the information of a differential of spin resolved unoccupied density-of-state of 5d-band can be obtained through the measurement of the X-ray magnetic Kerr rotation.

(4) It is probable that the contribution of the quadrupole transition is not negligibly small at 1.5eV below the L_2-absorption edge, and that value is about 30% that of the dipole transition.

(5) X-ray magnetic Kerr rotation due to the X-ray resonant exchange scattering will be a new method to investigate the spin resolved unoccupied density-of-state for a material which needs a strong magnetic field to saturate.

References

1. F. de Bergevin and M. Brunel: Phys. Lett. **39A**, 141 (1972).
2. K. Namikawa, M. Ando, T. Nakajima and H. Kawata: J. Phys. Soc. Jpn. **54**, 4099 (1985).
3. D. Gibbs, D.R. Harshman, E.D. Isaacs, D.B. McWhan, D. Mills and C. Vettier: Phys. Rev. Lett. **61**, 1241(1988).
4. F. de Bergevin and M. Brunel,: Acta Cryst. A**37** 314(1981).
5. D.P. Siddons, M. Hart, Y. Amemiya and J.B. Hastings: Phys. Rev. Lett. **64**, 1967(1990).
6. K.Namikawa : unpublished
7. J.P. Hannon, G.T. Trammell, M. Blume and D. Gibbs: Phys. Rev. Lett. **61**, 1245 (1988).
8. H. Kitamura: Insertion Device Handbook 1990 Photon Factory KEK Report 89-24 March 1990
9. S. Annaka, K. Kohra and M. Ando: JJAP. **20**, L463 (1981).
10. M. Blume and Doon Gibbs: Phys. Rev. 37, 1779(1988)
11. M. Hart and A.R.D. Rodrigues: Phil. Mag. B**40**, 149 (1979).
12. K. Namikawa :KEK Proceedings (in Japanese) 91-9 Oct. 108 1991
13. G. Shütz, M. Knülle, R. Wienke, W. Wilhelm, W. Wagner, P. Kienle and R. Frahm: Z.Phys. B **73**, 67-75 (1988)
14. H.Ebert, G.Shütz and W.M.Temmerman: Sol. Stat. Com. **76**, 475 (1990)
15. K.Namikawa, M.Ando, H.Kawata, M.Konno and K.Mori unpublished
16. S. Sasaki : KEK Report 88-14 106 (1989)

Acknowledgments

The author expresses my sincere appreciation to Professor Masami Ando (KEK PF and Grad. Univ. for Advanced Studies) for his kind and invaluable guidance, encouragement and helpful suggestions throughout the course of my research work. He heartily thanks Professor Kazumichi Namikawa (Tokyo Gakugei Univ.) for leading him in the theoretical evaluation of the present work and for performing the experimental work to yield a preliminary result.

He would like to thank Mr. Yoshisato Funahashi and Mr. Yasuo Higashi for their collaboration on designing and constructing the apparatus used in the present work. Thanks are also given to Dr. Yoshiyuki Amemiya (KEK PF) and Dr. Tetsuya Ishikawa (Tokyo Univ.) for their advice in the experiment and discussion. Further he thanks Mr. Yasuki Koyama for his assistance on the performance of the experiment.

Finally but not least I deeply thanks Professor Tadasu Suzuki (Sophia Univ.) for giving the author the first opportunity to be involved in this kind of the current research work.

This study has been performed under the approval of PF PAC (No.91-113) and the financial support provided from the Grad. Univ. for Advanced Studies and Japan Scholarship Foundation is also appreciated.